DISSERTATION FOR THE DEGREE OF DOCTOR OF PHILOSOPHY (PHD)

H2A.Z-nucleosomes are stabilized by the superhelicity-dependent DNA binding of the C-terminal tail of the histone variant

by Ibtissem Benhamza

UNIVERSITY OF DEBRECEN
DOCTORAL SCHOOL OF MOLECULAR CELLULAR AND IMMUNE BIOLOGY

DEBRECEN, 2025

DISSERTATION FOR THE DEGREE OF DOCTOR OF PHILOSOPHY (PHD)

H2A.Z-nucleosomes are stabilized by the superhelicity-dependent DNA binding of the C-terminal tail of the histone variant

by Ibtissem Benhamza

Supervisors: Prof. Dr. Gábor Szabó, M.D., Ph.D.
Dr. György Vámosi, PhD.

UNIVERSITY OF DEBRECEN
DOCTORAL SCHOOL OF MOLECULAR CELLULAR AND IMMUNE BIOLOGY

DEBRECEN, 2025

TABLE OF CONTENTS

LIST OF FIGURES

LIST OF ABBREVIATIONS

ACF: Autocorrelation function

ANP32E: Acidic Nuclear Phosphoprotein 32 Family Member E

CCC: Covalently closed circular DNA

CF: Carboxyfluorescein

ChIP: Chromatin immunoprecipitation

CLSM: Confocal laser scanning microscopy (CLSM)

CTCF: CCCTC-binding factor

DDR: DNA damage repair

DSBs: Double-strand breaks

Dox: Doxorubicin

EdU: 5-ethynyl-2′-deoxyuridine

EBr: Ethidium bromide

ESC: Embryonic stem cell

E-MAP: Epistatic MiniArray Profile

eRNAs: enhancer RNAs

FCS: Fluorescence correlation spectroscopy

FRAP: Fluorescence recovery after photobleaching

Hi-C: High-throughput chromosome conformation capture

HMGB: High mobility group box

H4K16Ac: H4K16 acetylation

H3K9me3: Histone H3 lysine 9 trimethylation

H3K27me3: Histone H3 lysine 27 trimethylation

LADs: Lamina-associated domains

LMP: low melting point agarose

LSC: Laser scanning cytometry

MNase: Micrococcal Nuclease

MCC: Manders colocalization coefficient

NCP: Nucleosome core particle

ORC: Origin-recognition complex

PTMs: Posttranslational modifications

PRC2: Polycomb Repressive Complex 2

PWWP2A: PWWP Domain–Containing Protein 2A

QINESIn: Quantitative Imaging of Nuclei after Elution with Salt/Intercalators

RNAP: RNA polymerase

SBECD: Sulfobutyl ether β-cyclodextrin sodium salt

SCR: Scrambled peptide

SmFRET: Single-molecule fluorescence resonance energy transfer

SMC: Structural Maintenance of Chromosomes

TADs: Topologically associating domains

TOPO: Topoisomerases

TSS: Transcription start site

INTRODUCTION

1. DNA packaging and chromatin structure

Research over the past few decades has revolutionized our understanding of chromatin. Initially, the focus was on the packaging and compaction of DNA, resulting in a relatively static picture for long, the sole dynamic event involving chromatin was what Walther Flemming documented on the structural transformation of chromatin during the shift from the interphase nucleus to mitotic chromosomes, referred to as "Karyomitosis" (denoting the threadlike metamorphosis of the nucleus)[1], leading to chromatin condensation and chromosome individualization.

Our understanding of how the functions of chromatin are served by its structural features has changed dramatically in the late 19th century [2 3]. During the first process of compaction, the genome of eukaryotic cells exhibits a multi-scale hierarchical organization, encompassing simple structures to more intricate, higher-order, and non-random configurations. The DNA is folded through a dynamic and precisely regulated process that serves both structural and functional roles including gene expression, DNA replication, DNA damage repair, and maintaining epigenetic memory [4 5]. Some of the key molecules controlling the structural changes involved have been recognized: These include Structural Maintenance of Chromosomes (SMC) complexes, such as cohesin, condensin, opoisomerase IIα, scaffold-associated factors, which together with many other players orchestrate large-scale changes in the organization of chromatin [6 7].

Eukaryotes, from yeast to human, package their DNA double helix, around 2 nm in diameter and over 2 m in length within a nucleus of 10 µm in diameter, which is about five orders of magnitude smaller[8], while prokaryotes do not possess distinct, membrane-enclosed nuclei. The structure of chromatin is established by a basic repeating unit called the nucleosome, including 146 base pairs (bp) of negatively charged DNA coiled around a positively charged octamer of core histones. This first level of compaction leads to ~tenfold DNA compaction. In the classical view, the polynucleosome array is folded into a compact fiber with a diameter of about 30 nm, resulting in a net compaction of around 50 times. Each nucleosome is joined to its neighbors by a brief section of linker DNA (~10–80 bp in length) [9]; the fifth histone, H1, binds to each nucleosome and its neighboring linker to stabilize the 30-nm fiber. The specifics of nucleosome packing within the chromatin fiber, i.e. their solenoid or zig-zag character depends on the average linker length [10

11]. Our understanding of how these fibers are further packed inside the nucleus to generate the highest-order structures (mitotic chromosomes) (Fig. 1) still appears to be incomplete [12 13] .

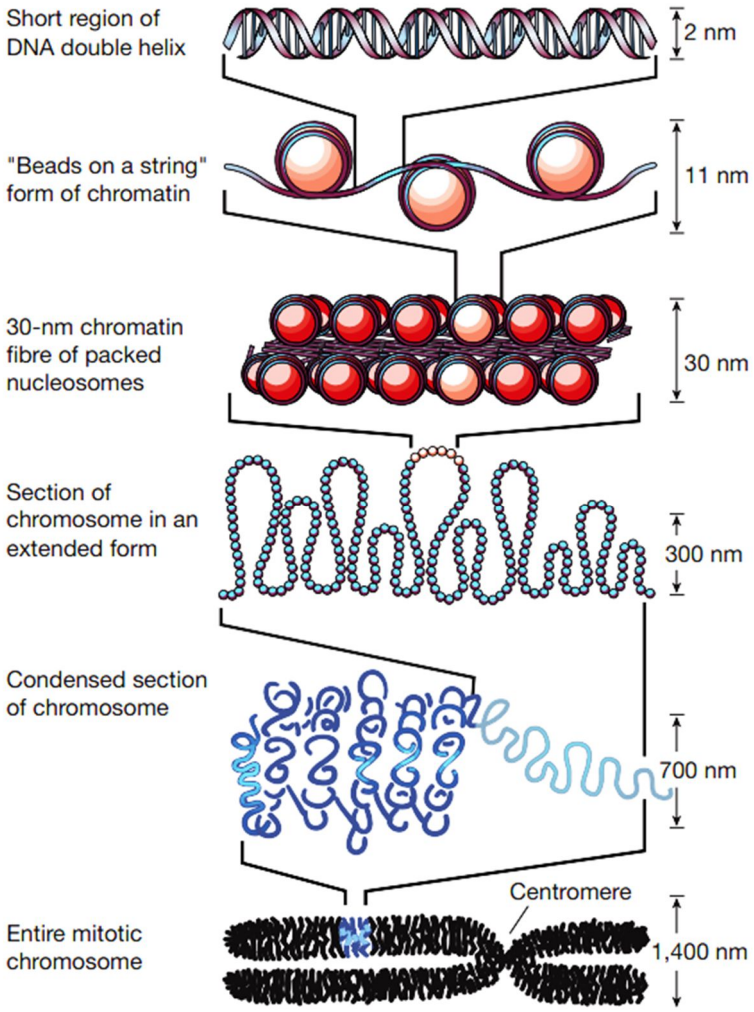

Figure 1: Schematic diagram illustrating the compaction levels of eukaryotic chromatin. The compaction of the chromatin in eukaryotic cells starts with the double helix DNA wrapped around an octamer of histones to form the first unit called nucleosome. Along the chromatin, it forms a beads-on-string structure with an 11nm in diameter. Further compaction of the nucleosome may yield chromatin fibers of ~30nm in diameter. The fibers started to fold and form loops to generate a 300 nm thick extended chromosome, a 700 nm condensed chromosome, and a 1400 nm mitotic chromosome. Figure from [2].

In the interphase nucleus, looping interactions with long-range contacts by the enhancers reaching their target promoters have been detected [14] (Fig. 2C) and several proteins in their maintenance identified. To mention just two factors involved in the maintenance of these high levels of chromatin organization: the "eleven zinc-finger" (ZF) protein CTCF recognizes the DNA motif

CCCTC [15]; the multisubunit protein called Cohesin has a ring-like structure that plays a key role in the folding of chromatin into loops [16 17]. The high-throughput chromosome conformation capture (Hi-C) technique and its various versions also revealed that in interphase, megabase scale domains exist where DNA sequences have a certain probability to interact; these are known as topologically associating domains (TADs) [18] (Fig. 2D). Furthermore, these techniques have revealed chromatin segregation into compartment A, which corresponds to the transcriptionally active euchromatin and compartment B, which comprises transcriptionally repressive heterochromatic domains[19]. Within the B sub-compartment, the lamina-associated domains (LADs) are distinguished, rich in H3K9me2/3 and H3K27me histone marks [5].

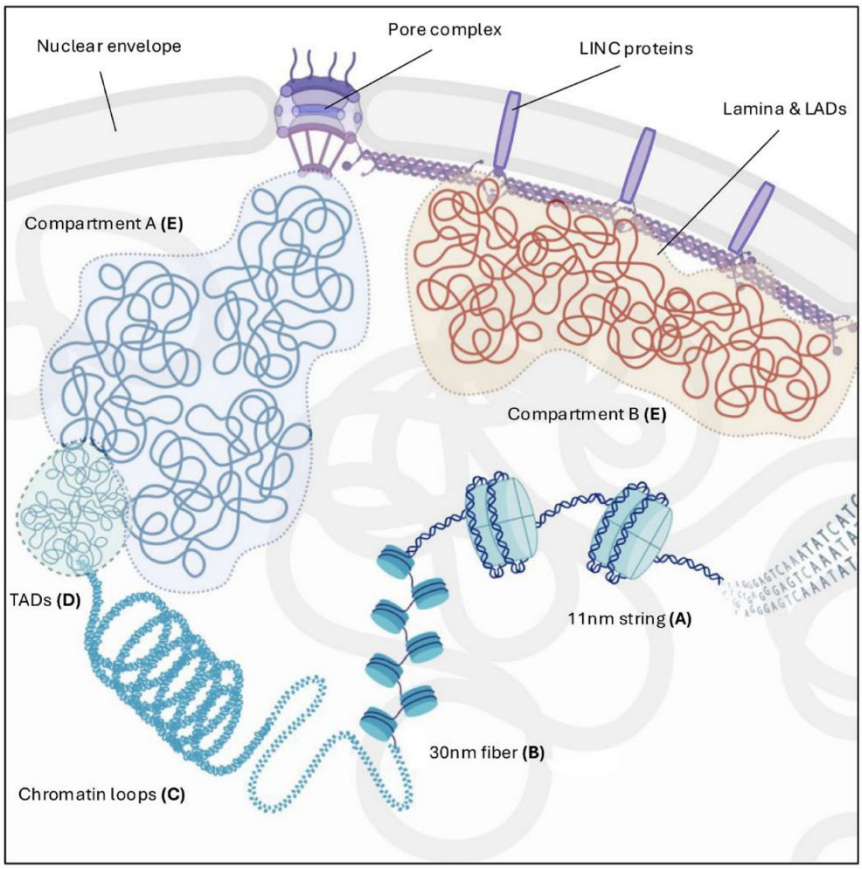

Figure 2: Hierarchical chromatin organization and nuclear compartmentalization in the classical model. This schematic shows the multi-scale structural organization of chromatin within the eukaryotic nucleus. Chromatin fibers initiate an arrangement of 11 nm "beads-on-a-string" **(A)**, wherein DNA wraps around nucleosomes, and can further fold into a 30 nm fiber **(B)**. These fibers create higher-order structures, such as chromatin loops **(C)**, which are organized into Topologically Associating Domains **(D)** i.e. genomic regions that exhibit more frequent

interactions within themselves than with other regions. TADs and loops aggregate into larger nuclear compartments: Compartment A **(E)** is the euchromatin, and Compartment B **(E)** is the heterochromatin. Compartment B often localizes to the nuclear periphery in association with the nuclear lamina and Lamina-Associated Domains (LADs). Nuclear organization is also coordinated by LINC (linker of nucleoskeleton and cytoskeleton) proteins, which link chromatin to the cytoskeleton conveying mechanosensing and to the nuclear pore complexes which regulate transport between the nucleus and cytoplasm. Figure from [5].

2. Nucleosome stability and dynamics

2.1.Structure of the nucleosome core particle

The chromatin structure is established by a repeating fundamental unit called nucleosome [20-22]. The X-ray crystal structure of the nucleosome core particle (NCP) reveals the assembly of the histone protein octamer and the organization of 146 bp of DNA into a superhelix wrapped in 1.65 turns surrounding it. The histone octamer has two copies each of the core histones H2A, H2B, H3, and H4. (Fig. 3) Each core histone contains a conserved motif called the histone-fold, an essential structural component consisting of three alpha helices: α1, α2, and α3. The helices are interconnected by two loops, L1 and L2. The DNA is contacted where the minor groove at 10-bp intervals faces the protein, via its arginine residues, while keeping the major groove accessible to molecular interactions involved in various cellular processes. The path of the DNA superhelix is distorted through bends at several positions. Through channels formed by the minor groove, long unstructured positively charged N-terminal and C-terminal tails protrude out from the nucleosome core, interacting with particular surfaces of a neighboring nucleosome or with nuclear proteins (Fig. 4) [23] and the DNA, both nucleosomal and linker.

The histone tails also mediate nucleosome-nucleosome interactions, resulting in the compact, higher-order structure of chromatin [24]. The interactions between histone tails and nucleosomal DNA determine the thermal stability of mononucleosomes while having no role in the resistance of nucleosomal structure to salt treatment below 700 mM, demonstrating that stability features depend upon the nature of challenging conditions applied in the stability assays [25]. Posttranslational modifications (PTMs) occurring on the tails alter their charge and/or molecular configuration and are recognized by specialized reader proteins. Such modifications appear to influence the accessibility of nucleosomal DNA and the stability of chromatin fibers, although to varying degree [26].

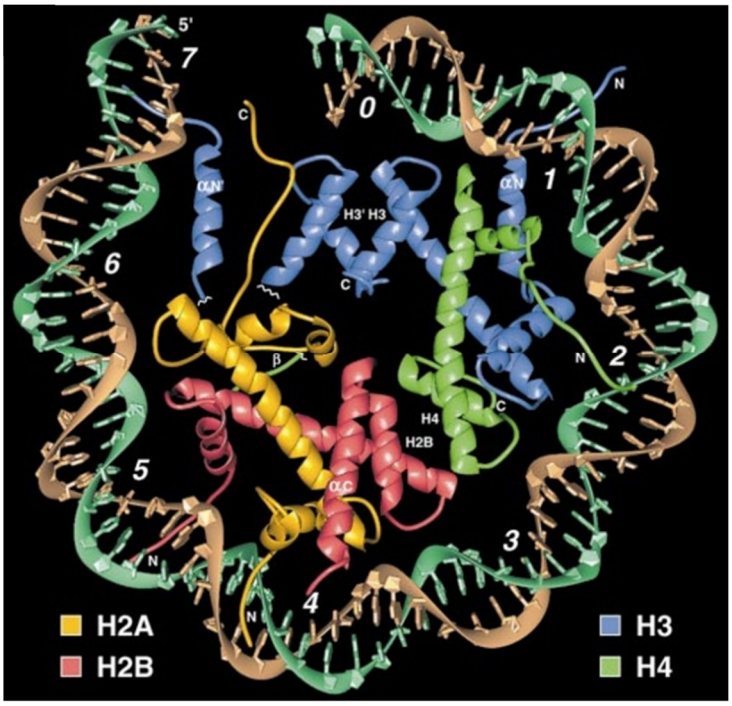

Figure 3: The crystal structure of nucleosome core particle (NCP). The DNA's 146 base-pair phosphodiester backbones are depicted as ribbon traces (brown and turquoise). The eight core histone protein main chains are distinguished by color (blue: H3; green: H4; yellow: H2A; red: H2B). Figure from [27].

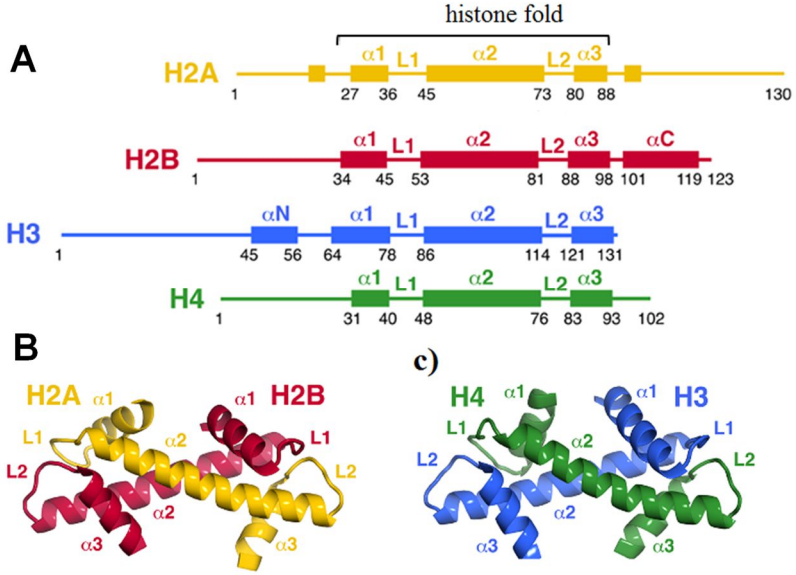

Figure 4: Histone-fold domains and heterodimers. Graphical illustration of the core histone structure and histone fold heterodimers. **(A)** Histone structure illustrating the conserved histone fold including three alpha helices, α1, α2, and α3, interconnected by the L1 and L2 loops. The N-terminal tail of each histone and the C-terminal tail of H2A are depicted as lines on the left and

right of the histone fold, respectively. **(B, C)** Histone fold heterodimers H2A-H2B and H3-H4 showing the adjacent L1 and L2 loops at their ends. Figure from [23].

2.2.Nucleosome stability and nucleosome remodelers

The NCPs interspersed with linker DNA further assemble into higher-order structures stabilized by the linker histone H1 and nucleosome-nucleosome interactions [28 29]. The organization of chromatin is also affected by the association of linker DNA with either linker histone H1 or high mobility group box (HMGB) proteins. H1 molecules possess a core globular domain accompanied by flexible N- and C-terminal tails and play an essential role in the formation of heterochromatin (Fig. 5) [28]. H1 stabilizes nucleosomes by preventing DNA unwrapping, while HMGB may destabilize chromatin through inducing DNA bending [30]. The DNA wrapped around the histone octamer is in general not accessible to regulatory proteins, except for the "pioneer" transcription factors [31]. Accessibility is increased due to nucleosome destabilization, which occurs by several mechanisms, including nucleosome movement (sliding, repositioning), partial or complete removal (eviction). These processes locally influence chromatin structure, a key mechanism by which cells regulate gene expression [2].

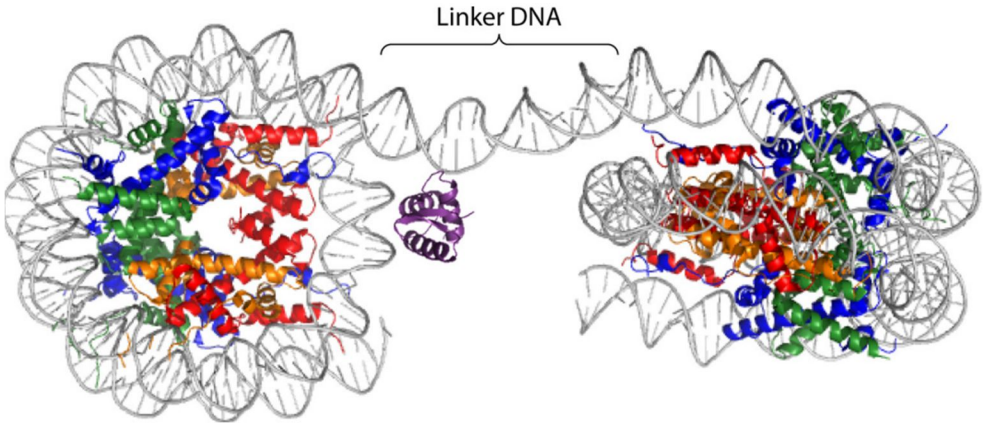

Figure 5: Histone H1 binds to the linker DNA. The globular domain of histone H1 (purple) connects with the nucleosome at the dyad. The dinucleosome architecture is illustrated, with core histone color coding matching that in (Fig. 3). Figure from [32].

Although nucleosomes exhibit considerable stability, generally blocking access to DNA even to low molecular weight intercalator dyes [33], ATP-dependent nucleosome-remodeling factors are able to mobilize nucleosomes, making the overlying DNA accessible for processes such as transcription. These remodelers catalyze various reactions in collaboration with the histone

chaperones, and are involved in the assembly-disassembly and movement of nucleosomes along DNA via a mechanism known as nucleosome sliding [34 35]. These complexes utilize ATP hydrolysis and are classified into four major families (SWI/SNF, ISWI, NuRD/Mi-2/CHD, and INO80) based partly on the unique domains of their shared catalytic ATPase subunit [36 37].

Although nucleosome remodelers possess shared enzymatic mechanisms, specific remodelers demonstrate unique activity in global genome organization. For example, the SWI/SNF complexes mainly catalyze eviction. Other remodelers, such as yeast's ISW1a, ISW1b, Chd1, and the INO80 complexes, accurately position nucleosomes on DNA, creating regularly spaced arrays. Finally, nucleosome editing requires the exchange of canonical histones with histone variants such as H2A.Z within particular nucleosomes, involves the SWR1-complex, (an INO80 sub-family remodeler) in promoting the exchange of H2A-H2B by incorporating H2A.Z-H2B dimers, while INO80 is thought to catalyze the reverse process (Fig. 6).

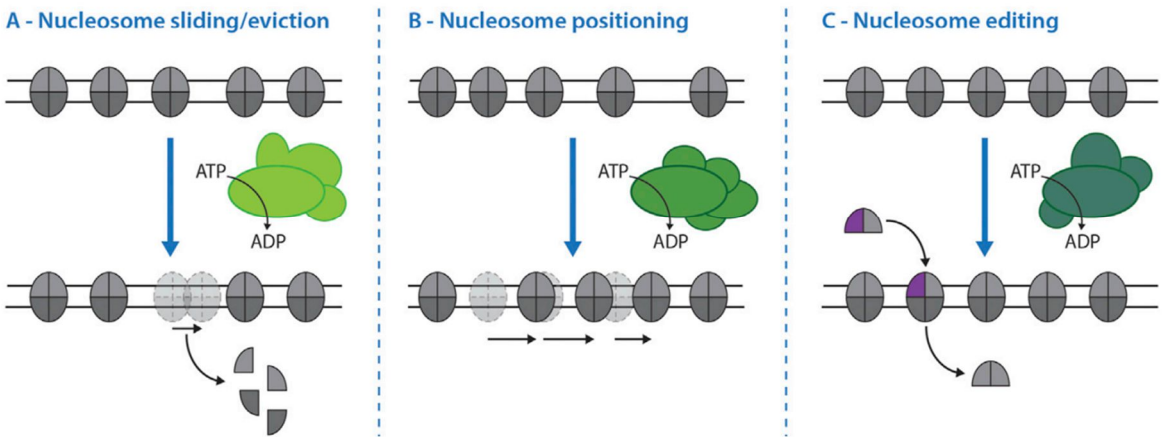

Figure 6: Nucleosome remodeler activities and their effects on chromatin. The activity of various nucleosome remodelers, indicated by shades of green in this illustration, primarily affects nucleosomes in three distinct ways. **(A)** Nucleosome sliding/eviction: remodelers slide nucleosomes, while the SWI/SNF complexes evict them. **(B)** Nucleosome positioning: certain remodelers precisely position nucleosomes on DNA. **(C)** Nucleosome editing: catalyze the exchange of canonical histones with histone variants, like H2A.Z (purple) within the nucleosome, and vice versa. Figure from [38].

2.3.Nucleosome dynamics and gene regulation

Since the nucleosome structure fundamentally limits DNA accessibility to DNA-targeting enzymes like RNA polymerase (RNAP) II and to most transcription factors, nucleosome dynamics is a crucial element in transcriptional machinery [39]. The dynamics of chromatin structure is tightly regulated through multiple mechanisms superimposed on each other, including nucleosome remodeling (see above), covalent histones modification within the nucleosome, or replacement of core histones with histone variants. Certain modifications may directly influence nucleosome stability, like acetylation, while others are recognized by regulatory proteins, or disturb higher-order structures [40].

Posttranslational modifications (PTMs) on histone tails or within the globular core domains, e.g. acetylation, methylation, ubiquitination, and phosphorylation, creates binding sites for particular proteins [41]. The N-terminal tail of histone H4 facilitates inter-nucleosomal interactions, which are essential for the condensation of chromatin. Its acetylation (H4K16Ac) directly decreases these inter-nucleosome interactions involving the tail and a particular charged surface of the nucleosomes, the acidic patch of a neighboring nucleosome [29]. The acidic patch region is primarily formed by the clustering of eight acidic residues on histones — six from H2A (E56, E61, E64, D90, E91, E92) and two from H2B (E102, E110) — which together create a negatively charged binding interface on the nucleosome surface, serving as a critical interaction site for chromatin-associated proteins and neighboring histone tails. H4K16Ac may also regulate gene transcription by modulating the interaction of the acidic patch with non-histone proteins [42]. H3K4me3, H3K27me3, and H3K9me3 are key methylation marks with different functional consequences. H3K4me3 is typically enriched at the promoters of most active genes and has been associated with open chromatin and transcriptional activity [43]. H3K27me3, attached by the Polycomb Repressive Complex 2 (PRC2), marks repressed genes contributing to the formation of facultative heterochromatin [44]. H3K9me3 is mostly located in constitutive heterochromatin, particularly in the pericentromeric regions of the chromosomes, where it promotes stable gene silencing and repression of transposable elements by the recruitment of HP1 proteins [45]. These modifications establish a histone code that precisely ensures accurate gene regulation during key cellular processes.

In addition to modifications, core histones can also be replaced with histone variants, with functional effects [46]. For instance, H2A.Z non-randomly replaces H2A contributing to transcriptional regulation by decreasing nucleosome stability at transcription start sites (TSS) as suggested by the enhancement of nucleosomal DNA mobility [47]. H2AX is phosphorylated during DNA break repair in long stretches of chromatin surrounding the lesion [48]. H3.3 gets incorporated into the chromatin of non-dividing cells at the promoters of active genes, often together with H2A.Z [49].

2.4.Methods to study nucleosome stability

Diverse biophysical and biochemical methods have been developed to study the structure and stability of nucleosomes. *In vitro* techniques are generally performed on purified nucleosomes or reconstituted chromatin in test tubes, among those: **thermal denaturation assay** which measures their resistance to thermal stress thought to reflect the strength of histone-DNA interactions [50]; **salt-induced dissociation assay** is used to determine the NaCl concentration required for nucleosome disassembly, interfering with the electrostatic interactions involved in their assembly [51 52]; **the Micrococcal Nuclease (MNase) digestion assay** evaluates the accessibility of DNA wound around the histone octamer, where less stable nucleosomes have increased sensitivity to enzymatic digestion, hence representing the relative accessibility and stability of nucleosomes. [53]; **single-molecule force spectroscopy techniques**, such as optical and magnetic tweezers, along with single-molecule fluorescence resonance energy transfer (smFRET), provide insights on the mechanical stability of individual nucleosomes and precisely measure the force necessary for their unspooling and disassembly pathways, and additionally allowing real-time monitoring of nucleosome unwrapping and rewrapping [54 55].

Conversely, *in vivo* or *in situ* approaches aim to investigate nucleosome stability within the native cellular conditions inside living cells, or intact nuclei under near-native conditions. This involves **chromatin immunoprecipitation (ChIP)-based approaches** which detect histone occupancy at specific genomic loci, and live-cell imaging methodologies such as following the mobility of photoactivated labeled histones by **Fluorescence Recovery After Photobleaching (FRAP)** [56].

Our group has developed a versatile and robust quantitative imaging-based method using salt/intercalator elution performed on agarose-embedded nuclei, allowing the study of nucleosome

stability within intact nuclei [57]. In this *in-situ* method named **Quantitative Imaging of Nuclei after Elution with Salt/Intercalators (QINESIn)** nucleosome stability is assessed by treating chromatin, prepared by the treatment of the agarose-embedded live cells with nonionic detergents, with different concentrations of salt or intercalator agents, leading to a differential effect on nucleosome stability depending on their histone composition and PTMs marking the nucleosomes. When histones are eluted from nucleosomes using salt, mainly the electrostatic interactions keeping the nucleosome together are challenged, measuring what will be alluded to as intrinsic stability. In contrast, exposure to DNA binding intercalators is used to assess DNA superhelicity-dependent stability features. Intercalators destabilize nucleosomes by extending and unwinding the DNA double-helix [58]. The retained, chromatin-bound histones are detected within individual nuclei using histone type- or PTM-specific antibodies, followed by automated quantitative imaging by laser scanning cytometry (LSC).

3. DNA supercoiling and chromatin topology

As mentioned before, nucleosomes typically function as barriers for polymerases and other enzymes involved in DNA-based cell biological processes [59]. Nevertheless, they are dynamic and are influenced by different factors such as thermal fluctuations [60], DNA supercoiling [61], PTMs of histones [62], the activity of chromatin remodelers [63 64], and linker histones [65], possibly among many other factors. These mechanisms regulate nucleosome stability and, consequently, chromatin structure, also in the sense that they influence the stacking of nucleosomes in chromatin fibers creating an additional barrier for the drivers of disassembly, hence influencing gene regulation [66].

Among these factors the contribution of DNA supercoiling to the regulation of gene expression is probably the least understood. Supercoiling refers to the over- or under-twisting of the right-handed DNA double helix in relation to its standard 10.4 bp per helical repeat (turn) [67]. This occurs to the nucleosomal DNA during the formation of the nucleosomal structure itself in S phase, constraining negative supercoiling [66], while the internucleosomal linker DNA regions get over- or underwound in processes such as replication and transcription. During transcription, RNAP creates high torsional stress, generating positive supercoils ahead and negative supercoils behind, yielding net overall supercoiling levels depending on the selective elimination of positive or negative supercoils by topoisomerases based on their preferences [68]. The positive torsion is

thought to destabilize nucleosomes ahead of the RNA polymerase, whereas the negative torsion behind facilitate nucleosome reassembly (Fig. 7A).

In order to get deeper insight into the physical response of chromatin fibers to torsional stress especially that induced by transcription, researchers have used advanced single-molecule techniques such as magnetic tweezers, which twist and stretch reconstituted chromatin fibers *in vitro*. This approach allows precise measurement of fiber extension as a function of applied turns, mimicking the mechanical constraints exerted during transcription (Fig. 7B, C).

This torsional stress is regulated and relieved *in vivo* by specialized enzymes called topoisomerases (TOPOs), which transiently create single or double stranded DNA breaks, preventing excessive supercoiling that could prevent progression of transcription or replication [69]. Understanding the effects of twist generated by DNA-processing enzymes requires considering the higher-order structure of chromatin. Single-molecule force- and torque-spectroscopy studies have been extended from single nucleosomes to the detailed analyses of the dynamics and unfolding of nucleosome arrays. Such studies have led to the direct confirmation of the earlier assumptions based on indirect evidence that every second nucleosome interacts more closely in the chromatin fiber, forming a zig-zag configuration [70]. These high-resolution techniques also enable investigation of dynamics at the sub-nucleosomal level, revealing the steps leading to the dismantling of the nucleosomes under torsional stress [71].

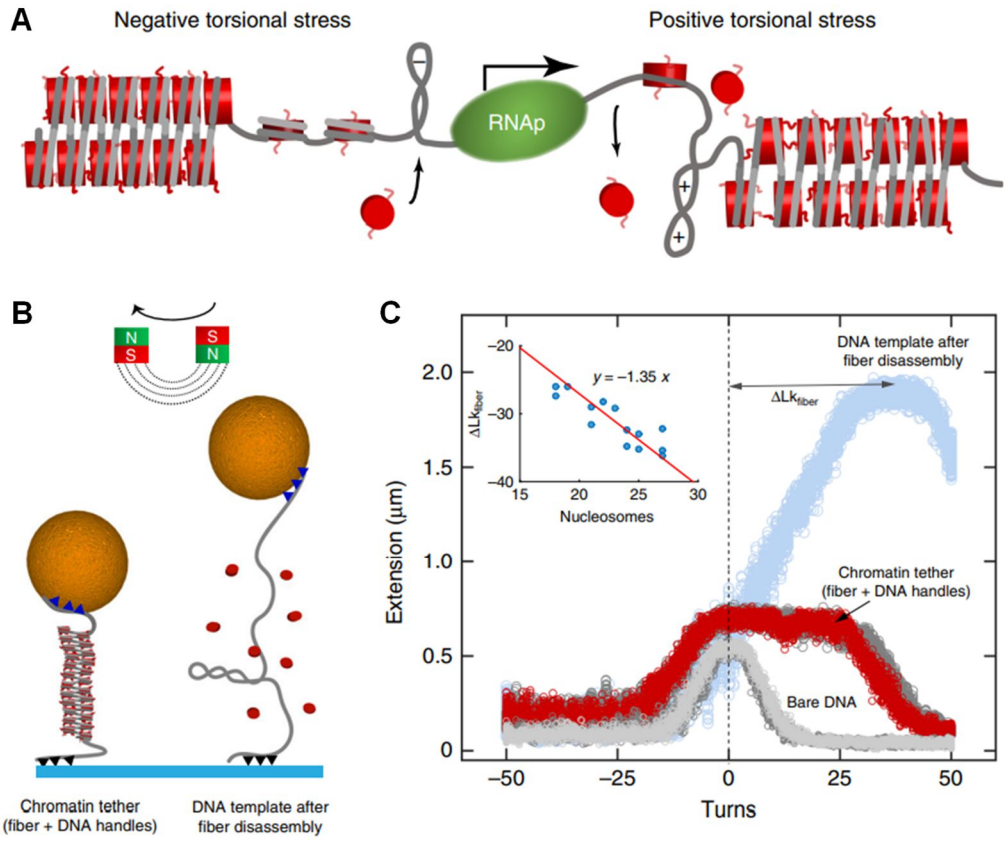

Figure 7: Applying torsional stress to reconstituted chromatin fibers mimics *in vivo* supercoiling dynamics. (A) Schematic illustration showing that RNA polymerase (RNAP) generates positive supercoils ahead and negative supercoils behind the transcription fork, leading to nucleosome destabilization or reassembly. **(B)** Schematic representation of single-molecule magnetic tweezers used to apply tension and torsion to chromatin fibers with ~30 nucleosomes (red) flanked by ~2 kb DNA handles for tethering to a paramagnetic bead (gold) and glass slide (blue) via biotin and digoxigenin (triangles). **(C)** Magnet rotation induces positive or negative turns. Figure from [66].

In the B-DNA form, the most common right-handed double helix under physiological conditions, linear DNA consisting of N bp (total length), exhibits a natural coiling of the two complementary strands around each other once every 10.4 base pairs, as mentioned above, referred to as the helical repeat (h) [67]. When the two ends of such a linear DNA are joined (ligated) to form a relaxed, covalently closed circular (CCC) DNA molecule, the structure becomes topologically constrained, meaning that the DNA strands are now permanently intertwined. In this case, separation of these strands can only occur if one or both strands are enzymatically cleaved, allowing rotational movement "swiveling" around the other. The total number of times (crossings) one strand wraps

around the other in this closed conformation is defined as the linking number (Lk), which is always an integer due to the chemical orientation of DNA ends (3' to 5') that can be ligated. Lk can only be changed by inducing a break in one or both DNA strands via e.g. TOPOs. When the circular DNA molecule is in a relaxed state, where it's h = 10.4 bp/turn, the corresponding Lk is defined as Lk_0. If the linear double helix was twisted around its axis prior to ligating its ends, the resulting circular DNA will have a Lk that deviates from Lk_0, and this deviation is denoted as ΔLk, where ($\Delta Lk = Lk - Lk_0$). Such molecules are described as superhelical or supercoiled. A positive ΔLk indicates right-handed (overwound) supercoiling, while a negative ΔLk indicates left-handed (underwound) twisting. To measure the degree of supercoiling independently of DNA molecule length, the superhelical density (σ) is used, calculated as ($\sigma = \Delta Lk / Lk_0$) [72].

The Lk denotes a fundamental geometrical parameter composed of two distinct elements: twist (Tw) and writhe (Wr). Consequently, any change in Lk is distributed between these two components, as defined by the formula ($\Delta Lk = \Delta Tw + \Delta Wr$). Tw represents the number of times one DNA strand winds around the other within the DNA double helix, whereas Wr denotes the number of times the entire DNA double helix winds around its own axis (coiling). A relaxed covalently closed circular (CCC) DNA molecule possesses no writhe; therefore, its Lk calculated as $Lk_o = Tw$, and is directly derived from the formula N/h, where N represents the DNA length in bp and h signifies the helical repeat length in bp. Writhing configurations that freely form in space are termed "plectonemic" which is characterized by the intertwining of the DNA double helix and an apical loop, whereas those that are constrained by wrapping around nucleosomes are termed "toroids" (Fig. 8), [73].

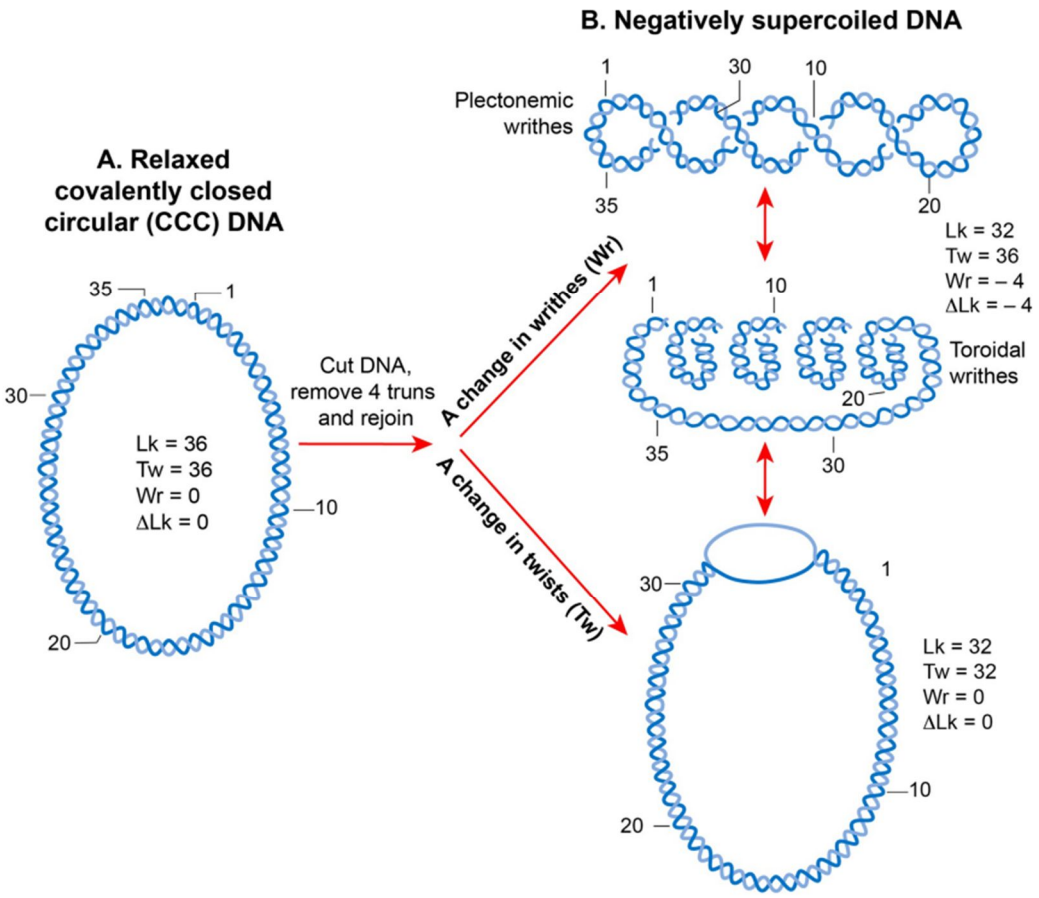

Figure 8: DNA supercoiling and topological parameters. **(A)** Relaxed CCC-DNA molecule was generated by the ligation of the two ends of a linear B-DNA. **(B)** A torsional stress was induced when the CCC-DNA was cleaved and subjected to four left-handed, resulting in a negative supercoiled DNA (the only shown) characterized by a decrease in the number of twists or writhe or both, which is showed as right-handed plectonemic writhes (top panel), left-handed toroidal writhes (middle panel), or local strand separation (bottom panel). Figure from [74].

The topology of DNA influences its physical and biological properties, thus impacting fundamental cell processes such as gene expression, replication, the structure and segregation of chromosomes. In both prokaryotes and eukaryotes DNA topology is precisely regulated, and the degree of supercoiling in specific genomic regions may vary according to physiological conditions [75]. Topological features, including underwinding, overwinding, intramolecular knotting, and intermolecular tangling, affect DNA processes. Additionally, TOPOs modulate DNA topology by generating transient breaks in the double helix, thereby maintaining genomic stability [76].

The genome's topological state is determined during replication, as newly synthesized DNA is immediately assembled into nucleosomes [77], establishing a superhelical density of approximately -0.06 [73], which is modulated upon processive enzymatic processes so as to generate extra positive or negative supercoiling in the internucleosomal linker and nucleosome-free DNA regions. Topological changes induced by RNAP during transcription are eventually due to blocked DNA rotation caused by viscous drag associated with its length [78] or by anchorage to components of the nuclear matrix. This results in positive supercoils ahead and negative ones behind the RNAP, as described by the twin supercoiling domain model [68]. Similar process occurs during replication, with positive supercoils forming ahead of the replication fork and negative supercoils within the continuously synthesized nascent leading strand [79].
An accumulation of these topological modification can stop transcription which directly impacts gene expression [80] and perhaps also impair genome integrity. To prevent this issue, TOPOs function to relax the extra supercoiling. In eukaryotic cells there are two main types, Topoisomerase I (TOPO I) and Topoisomerase II (TOPO II). The TOPO I can cleave a single strand of DNA double helix, whereas TOPO II can cleave both strands; in order to relax both positive and negative supercoiling [78].

Supercoiling influences the three-dimensional organization of chromatin, enabling or influencing long-range interactions between distant genomic elements such as enhancers and promoters [81]. It also alters the DNA geometry, which affects its interaction with regulatory and structural proteins, thereby modulating transcription [73].

4. The H2A.Z histone variant

4.1.Structural features of H2A.Z variant

The H2A.Z histone variant has two isoforms, H2A.Z.1 and H2A.Z.2.1, which differ only by three amino acids and are encoded by separate genes [82 83]. Alternative splicing of H2A.Z.2.1 creates a different version known as H2A.Z.2.2, which is shorter than H2A.Z.1 or H2A.Z.2 by 14 amino acids. This hypervariant conspicuously destabilizes nucleosomes compared to H2A.Z.1 or H2A [84] (Fig. 9). H2A.Z exhibits approximately 60% amino acid sequence identity to the canonical H2A [85].

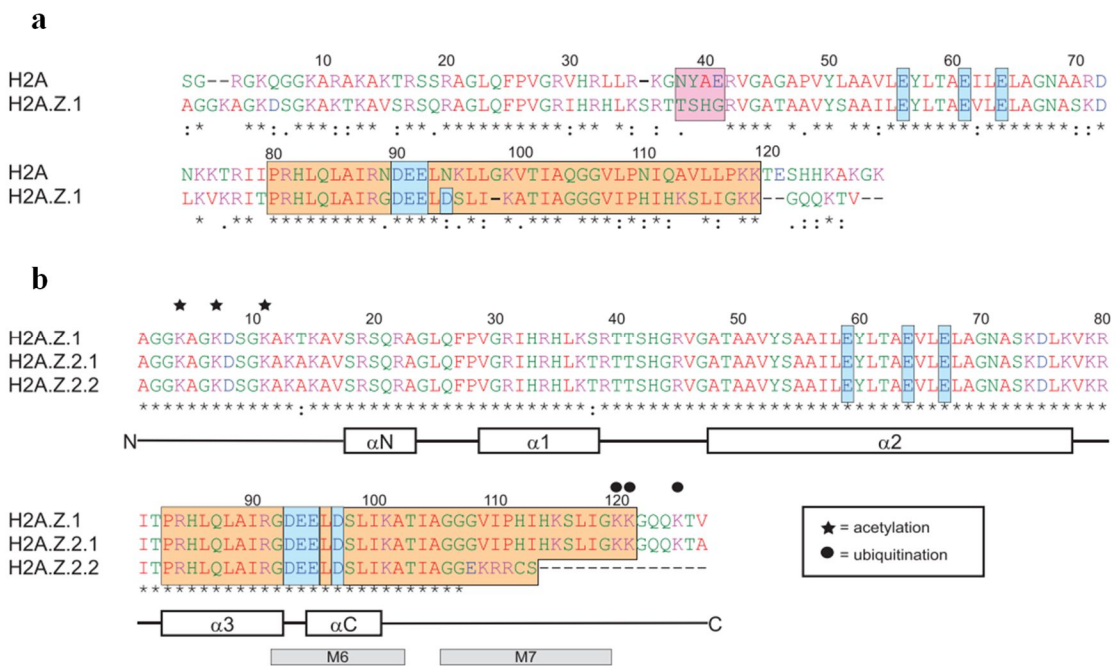

Figure 9: Amino acid sequences of human H2A and its variant, H2A.Z. (a) Alignment of human H2A and H2A.Z.1. **(b)** Alignment of human H2A.Z.1 with its isoforms, H2A.Z.2.1 and H2A.Z.2.2. The amino acids are color-coded based on their properties (red for small/hydrophobic, blue for acidic, magenta for basic, and green for hydroxyl/sulfhydryl/amine/glycine groups). Figure from [86].

As mentioned before, the nucleosomal structure is in general repressive for transcription, replication, and repair. Hence, eukaryotic cells regulate these processes by de- repression through the destabilization or mobilization of particular nucleosomes. [87]. Beside the canonical H2A, several variants exist, including H2A.X, H2A.Bbd, MacroH2A, and H2A.Z, with varying functions and stability features [86 88]. In the case of H2A.Z, there appears to be no consensus in the field whether the presence of H2A.Z in nucleosomes increases [89-91] or decreases [92-94] nucleosome stability. Regardless of remaining controversies, the observations suggesting a destabilizing role appear to have received more attention. For instance, the presence of H2A.Z destabilizes local nucleosome structure in embryonic stem cells, resulting in reduced nucleosome occupancy and enhanced chromatin accessibility, especially at promoters and enhancers [95], has received over 200 citations in PubMed. In concert with this finding, the presence of ANP32E, a chaperone that binds the C-terminal tail of H2A.Z, prevents H2A.Z deposition and consequential appearance of wide ATAC-Seq positive promoter regions throughout the genome of mouse fibroblasts [96]. Recent findings from MNase-X-ChIP-seq experiments indicate reduced

unwrapping of the +1 nucleosomes containing also another variant, H3.3 following H2A.Z depletion [97], confirming earlier data on H2A.Z/H3.3-containing unstable nucleosomes at the TSS of transcriptionally active promoters [94]. On the other hand, recent cryo-EM studies of H3.3/H2A.Z-containing nucleosomes could confirm the destabilizing effect of H2A.Z only [49]. However, such studies may be too myopic: investigating nucleosomes in their chromatin context using a differential MNase digestion method has indicated that H2A.Z nucleosomes located upstream or downstream of the TSS exhibit a much higher resistance to MNase compared to those at the TSS [98]. Moreover, H2A.Z-containing nucleosomes are also present in transcriptionally repressed facultative [99] and constitutive heterochromatin [100], which likely possesses different stability characteristics from those of the euchromatic regions, suggesting that the different findings may also reflect the possible intranuclear heterogeneity of H2A.Z nucleosomes.

The stability of H2A.Z containing nucleosomes may also be modulated by the H2A.Z1, Z2 isotype composition, the PTMs that mark H2A.Z, and the presence or absence of the C-terminus binding reader protein PWWP2A [86 101], which facilitates the recruitment of the deacetylase subcomplex M1HR to H2A.Z-containing chromatin, resulting in modifications in histone acetylation levels [102]. These factors may all modulate the stability of H2A.Z nucleosomes.

In human cells, the incorporation of H2A.Z into chromatin is mediated by the action of ATP-dependent chromatin remodeling complexes, primarily Tip60/p400 and SRCAP, while its removal or eviction is facilitated by the histone chaperone ANP32E [103] and the INO80 remodeling complex [104]. Additionally, members of the ISWI and CHD chromatin remodelers have also been implicated in the regulation of H2A.Z dynamics under replication-independent conditions [105 106]. These remodeling activities operate alongside, and potentially modulate, the intrinsic and DNA superhelicity-dependent stability characteristics of H2A.Z-containing nucleosomes.

4.2.H2A.Z functions in health and disease

The diverse functions of this histone variant appear to depend on several factors: organismal context (H2A.Z differs between species, e.g., its knockout is lethal in mice but not in yeast) [107 108], nucleosome composition (how many and which of the isotypes are incorporated into a nucleosome), protein interactome (whether transcriptional activators or repressors are recruited), genomic location (its presence at promoters, enhancers or heterochromatin), and H2A.Z PTMs

(for instance, acetylated H2A.Z is often linked to active transcription, while ubiquitination is associated with gene repression). With all this complexity, H2A.Z is an essential player in the regulation of transcription, DNA replication, DNA repair, and 3D chromatin structure, and it is implicated particularly in embryonic development, cellular differentiation, neurodevelopment, and brain function [109-111].

Role in gene transcription: H2A.Z appears to be an essential factor in RNAPII initiation and pause release as well as re-loading of certain pre-initiation complex components [112 113]. RNAPII pauses 20–60 bp downstream from the TSS in early elongation, the release from this paused state being a key regulatory step in gene expression [114]. The first (+1) nucleosome is considered a major barrier for transcription *in vivo* [113 115]. The role of H2A.Z in pause release appears to be complex: although the presence of the variant seemed to anticorrelate with height of the barrier for RNAP II in one report [116], it was also found that H2A.Z.1 depletion results in faster release of RNAPII pausing towards elongation and increases nascent RNA [112] and H2A.Z at the TSS correlates with paused RNAPII [113]. In addition to the absence or presence of the variant in nucleosomes of strategic significance, H2A.Z-binding proteins can also influence transcription. For instance, PWWP2A binds H2A.Z and promotes transcription at highly expressed genes [101]; on the other hand, its depletion reduces NuRD recruitment and histone deacetylation [102].

Role at enhancers and 3D chromatin remodelling: The characteristics of H2A.Z nucleosomes also influence chromatin dynamics at enhancers. Enhancers activate transcription by delivering regulatory proteins to promoters, thereby stimulating the preinitiation complex (PIC) formation and the transition to elongation. H2A.Z and H2A.Zac (acetylation) are present at poised and active enhancers, facilitating the formation of nucleosome-depleted regions (NDRs) that allow the binding of transcription factors and chromatin remodelers [95 117-119]. H2A.Z is essential for the transcription of enhancer RNAs (eRNAs) [117 118]. Nevertheless, active intragenic enhancers in expressed genes can lack H2A.Z or H2A.Zac [120].

Role in DNA replication: H2A.Z indirectly controls the cell cycle by regulating the induction of cyclin genes [121 122], and its overexpression promotes the upregulation of cell cycle genes and cell proliferation [123 124]. Recent studies also link H2A.Z directly to DNA replication. A genome-wide study in mouse ESCs showed that H2A.Z regulates initiation of early replication

origins [125]: H2A.Z binds SUV420H1, promoting H4K20me2 deposition needed for origin-recognition complex (ORC) recruitment.

Role in DNA repair: The loading of H2A.Z and its removal are strictly regulated during DNA damage repair (DDR). Initially, the remodeling enzyme p400 places H2A.Z into nucleosomes at DNA double-strand breaks (DSBs) to promote chromatin opening [126], facilitating the entry of various chromatin modifying activities required for repair. The accumulation of H2A.Z is transient; the chaperone ANP32E removes it from nucleosomes within 10 minutes post-DNA damage [127]. Thus, regulated H2A.Z dynamics is an important player in the repair of DNA breaks.

Role in development and cell differentiation: H2A.Z is crucial for epigenetic reprogramming in early mammalian embryonic development, as its absence in mouse embryos prevents stem cell lineage formation [107 128]. In mESC self-renewal and differentiation, H2A.Z acts as a "general facilitator" for chromatin access [95].

Role in neurodevelopment and brain function: H2A.Z is a key regulator of neurodevelopment and brain function, linked to neurological disorders like schizophrenia [129] and fetal alcohol spectrum disorder [130]. Brain-specific H2A.Z.1 depletion impairs neurogenesis [131] and gliogenesis [132]. H2A.Z also plays a role in learning and memory: ANP32E depletion increases H2A.Z in chromatin, impairing dendritic branching [133].

4.3. The C-terminal H2A.Z tail

In *Schizosaccharomyces pombe* (fission yeast), as in *Saccharomyces cerevisiae* (budding yeast), H2A.Z is loaded into chromatin by the Swr1C complex at promoters of low expressing genes, highlighting a conserved deposition mechanism across eukaryotes. However *S. pombe* Swr1C has an additional subunit, Msc1, which prevents mislocalization of H2A.Z to centromeric and subtelomeric regions [134]. In *S. cerevisiae*, the HTZ1 (also known as HTA3) gene encodes the H2A.Z variant, a member of the H2A gene family. Although HTZ1 is not essential in budding yeast, its disruption leads to slow growth and increased sensitivity to formamide, indicating a significant functional role. Comparison using the plasmid shuffle technique revealed that the major H2A genes (HTA1 and HTA2**)** and HTZ1 cannot substitute for each other's essential functions.

This demonstrates that H2A.Z has a function distinct from that of the major H2As. Moreover, the H2A.Z gene from *Tetrahymena thermophila* (a protozoan) can rescue the HTZ1 deletion phenotype, confirming that H2A.Z functions are evolutionary highly conserved across distant eukaryotes. [108].

The comparison of the H2A.Z histone variant across eukaryotic species is shown in Table 1, which summarizes the conservation and divergence of H2A.Z across species, highlighting the high sequence conservation within mammals and the greater divergence observed in lower eukaryotes, particularly in the C-terminal docking domain, while core functional regions remain preserved. This level of conservation is indicative of a common evolutionary origin and the retention of conserved core regions essential for function. Importantly, the evolutionary conservation of H2A.Z across diverse species indicates a preserved structural and functional role throughout evolution and further highlights its fundamental role in chromatin organization and gene regulation.

NCBI RefSeq ID	Species	Protein name (H2A.Z)	Gene name	Length (AA)	% Identity to human H2A.Z.1	C-terminal docking domain sequence	% Identity to human C-terminal
NP_002097.1	Human *(Homo sapiens)*	H2A.Z.1	H2AFZ	128	-	**IHKSLIGKKGQQKT**V	-
NP_036544.1	Human *(Homo sapiens)*	H2A.Z.2.1	H2AFV	128	97.7 %	**IHKSLIGKKGQQKT**A	93.3 %
NP_619541.1	Human *(Homo sapiens)*	H2A.Z.2.2	H2AFV	114	83.6 %	C-terminal truncated	-
NP_058030.1	Mouse *(Mus musculus)*	H2A.Z.1	H2afz	128	100 %	**IHKSLIGKKGQQKT**V	100 %
NP_084214.1	Mouse *(Mus musculus)*	H2A.Z.2	H2afv	128	97.7 %	**IHKSLIGKKGQQKT**A	93.3 %
NP_014631.1	Yeast *(Saccharomyces cerevisiae)*	Htz1	HTZ1	134	65.2 %	NKAL**L**LKVEKKGSKK	6.7 %
NP_500569.1	*Caenorhabditis elegans*	Htz-1	htz-1	140	78.6 %	APVPGKPGAPG**Q**GPQ	6.7 %
NP_175683.1	Plant (*Arabidopsis thaliana*)	HTA8, **HTA9**, HTA11	*HTA8*, ***HTA9***, *HTA11*	134	70.8 %	**I**PHIHKSLINKSAKE	6.7 %

Table 1: Comparative overview of H2A.Z histone variant across species. This table shows the conservation and divergence of the H2A.Z variant across different eukaryotic species, emphasizing the C-terminal docking region. Human H2A.Z.1 and H2A.Z.2.1 are almost identical, as differ by only three amino acids. Mouse H2A.Z.1 is 100 % identical to human H2A.Z.1, while mouse H2A.Z.2 closely resembles human H2A.Z.2.1. The human H2A.Z.2.2 isoform is shorter, however its shared region remains highly conserved. These observations highlight the strong conservation of H2A.Z within mammals, suggesting its critical and conserved roles. In contrast, H2A.Z exhibits more sequence divergence in lower Eukaryotes including yeast,

nematodes, and plants, where the percentage identity decreases, but remaining considerable. This level of conservation is still indicative of a common evolutionary origin and conserved core regions.

H2A.Z possesses subtle differences in specific regions that likely underlie its distinct identity and functions [135 136]. One notable structural divergence is the L1 loop, where two H2A.Z molecules within the nucleosome can interact. However, a major structural and functional divergence resides in the C-terminal "docking domain" which shows less than 40% amino acid identity with H2A and has been identified as providing an interaction surface for H3/H4 and likely serves as a binding platform for nucleosome remodeling activities [135 136]. Research, including a high-throughput technique for detecting epistasis (where the effect of one gene depends on the presence or absence of another gene) by systematically mapping genetic interactions, called E-MAP (Epistatic MiniArray Profile) analysis [137] in *S. cerevisiae*, demonstrates the critical role of the C-terminal region in cellular growth under genetic stress (when certain genes are compromised). The finding that the H2A.Z (1–114) truncation, which excludes the last 20 amino acid segment, compromises vital H2A.Z functions in genotoxic stress resistance, heterochromatin restriction, GAL1 gene activation, and chromatin anchoring underscores the functional importance of this domain [136]. These findings indicate that the functional effects of the H2A.Z C-terminal tail arise from specific molecular interactions mediated by this region. Among its molecular partners, the histone chaperone ANP32E specifically recognizes the H2A.Z–H2B dimer through interaction with the C-terminal H2A.Z tail, facilitating its eviction from chromatin [138], similarly to the Chz1 chaperone of *S. cerevisiae* [139] . In human cells, H2A.Z incorporation into chromatin is primarily mediated by Tip60/p400 and SRCAP complexes, while its removal by ANP32E is strictly regulated during DDR [103 126]. Moreover, ANP32E prevents H2A.Z deposition at promoter regions throughout the genome of mouse fibroblasts [96], underscoring the functional significance of molecular interactions involving the C-terminal tail in gene regulation and genome stability.

A previous study identified H2A.Z.2.2**,** an alternatively spliced variant of H2A.Z.2.1 that is shorter than any of the H2A.Z isoforms by 14 amino acids, lacking its C-terminus. This hypervariant markedly destabilizes nucleosomes compared to those containing H2A.Z.1 or canonical H2A [84 86]. The destabilized state of these nucleosomes lacking the C-terminal H2A.Z tail suggests that nucleosome stability might be tail-dependent and crucial for nucleosome stability and dynamics. Thus, the C-terminal H2A.Z tail appears to be a key determinant of H2A.Z nucleosome stability

and may provide a means to modulate chromatin structure and function through interactions involving this region. To investigate the tail's role in nucleosome stability and identify the molecular interactions involved, we employed QINESIn, a nucleosome stability assay developed in our lab [57]. The chromatin of the agarose-embedded nuclei used in the assay is devoid of loosely bound proteins like H1 and HMGB1 [140], small molecules like polyamines or nucleotides including ATP [57 141], thus its state may represent the most basic conformational features of the nucleosomes the activity of chromatin modifying enzymes act upon.

AIMS AND OBJECTIVES

1. To establish a cyclodextrin-based method for introducing a synthetic tail peptide resembling the C-terminal tail of H2A.Z into live HeLa and melanoma cells.

2. To confirm the C-terminal tail-dependent stability of H2A.Z-containing nucleosomes using an independent approach, intercalator elution, that challenges nucleosome integrity by inducing torsional stress.

3. To further validate tail-dependence of the stability of the H2A.Z-nucleosomes using a different intercalator that allows the simultaneous measurement of its binding to the DNA and its effect on nucleosomes.

4. To determine, using fluorescence correlation spectroscopy (FCS), if the binding of the tail peptide to DNA is superhelicity-dependent by comparing its binding to supercoiled and relaxed plasmid DNA.

5. To assess whether the absence of the C-terminal H2A.Z tail affects the biological behavior of cells.

MATERIALS AND METHODS

Peptides

Peptides representing the C-terminus of H2A.Z (C9) were synthesized and fluorescently labeled with 5(6)-carboxyfluorescein (CF) yielding the peptide H-GKKGQQKTV-Ahx-K(CF)-OH (CF-C9) as described in [142]. As a negative control, a scrambled peptide (SCR) was created, consisting of the same residues as C9 but arranged in a different order as described in the same publication.

Plasmid

The plasmid DNA (pCMV-EGFP-4X, 4479 bp), provided by Dr. Katalin Tóth (DKFZ, Heidelberg), used for assessing the DNA-binding of CF-C9 and CF-SCR by fluorescence correlation spectroscopy (FCS) analysis, was introduced into *Escherichia coli* DH5α by heat shock and selected on LB agar plates containing 100 µg/ml kanamycin.

Cell culture

HeLa cells, provided by Dr. Hiroshi Kimura (Yokohama, Japan) [143], and MEL1617 cells (from Coriell Institute for Medical Research) were cultured in DMEM supplemented with 10% FCS, 2 mM L-glutamine, 100 µg/ml streptomycin, 100 U/ml penicillin. WM35 cells (from Coriell Institute for Medical Research) were cultured in RPMI supplemented with 10% FCS, 2 mM L-glutamine, 100 µg/ml streptomycin, 100 U/ml penicillin. Concerning DT40 chicken B cells, H2A.Z.1 expressing DKO DT40 cells (DKO/Z1), and DKO DT40 expressing C-terminally truncated H2A.Z.1 (DKO/ΔC), were provided by Dr. Masahiko Harata (Sendai, Japan) https://pubmed.ncbi.nlm.nih.gov/26833946/. These cells were cultured in DMEM supplemented with 2% chicken serum, 8% fetal calf serum (FCS), 2 mM L-glutamine, 100 µg/ml streptomycin, and 100 U/ml penicillin at 38.9°C in 5% CO_2 atmosphere.

Introduction of peptides into live cells

500,000 HeLa or MEL1617 melanoma cells were seeded in a 35 mm cell culture Petri dish and grown overnight before peptide treatment. The formation of cyclodextrin/peptide complex required a mixture of 30 µM peptide and 300 µM SBECD (Sulfobutylether-β-Cyclodextrin;

CycloLab, Budapest, Hungary) diluted in colorless, serum-free RPMI1640, followed by a 1 h incubation at room temperature (RT). 2 ml SBECD/peptide complex were given to the cells and incubated for 2 h at 37°C in 5% CO_2 atmosphere. Following incubation, the cells were washed once with complete RPMI medium and subsequently cultured overnight prior to agarose embedding.

Cell cycle analyses

DKO/Z1 and DKO/ΔC cells, cultured in 6-well plates at 250,000 cells/well density were harvested by centrifugation at 1500 rpm for 5 minutes at RT, then the cell pellets were washed with ice-cold PBS and fixed with 500 µl of 70% ethanol added gradually to reduce clumping. After fixation on ice for 1 hour, the cells were washed twice with ice-cold PBS and treated with RNaseA (100 µg/ml) at RT for 30 minutes, followed by staining with propidium iodide (PI, 5 µg/ml) on ice for 10 minutes. The stained samples were washed with PBS, resuspended in 200 µl of PBS, and analyzed using a Novocyte flow cytometer. Data were processed using the FCS Express 6 software.

EdU cell proliferation assay

The manufacturer's protocol for the Invitrogen Click-iT™ Plus EdU Flow Cytometry Assay Kit (#C10632) was followed. Briefly, DKO/Z1 and DKO/ΔC cells were seeded in 6-well plates with complete media and cultured for 4, 24, or 48 hours. EdU was applied drop-wise to each well, followed by 1-hour incubation at 37°C. The cells were then washed with 1% BSA/PBS, fixed, washed again, and resuspended in 100 µl permeabilization buffer for 15 minutes. The reaction cocktail was added to the samples in a volume of 495 µl and incubated at room temperature in the dark for 30 minutes. Finally, the cells were washed, treated with RNase A, stained with PI and analyzed as above.

Embedding live cells into low melting point agarose and permeabilization

Embedding of cells into 8-well microscopic chambers (Ibidi, Martinsried, Germany) coated with 1% (m/V) low melting point (LMP) agarose was as described earlier [57]. Briefly, after washing with 500 µl ice-cold PBS/EDTA 3 times for 3 minutes each, the cells were permeabilized by

treatment with 500 µl of ice-cold 1% (V/V) Triton X-100 dissolved in PBS/EDTA (5 mM EDTA in PBS) twice for 10 minutes each.

Treatment of the embedded nuclei with salt (histone eviction by salt)

After permeabilization, nuclei were washed with 500 µl ice cold PBS/EDTA 3 times for 3 min and were treated with different concentrations of NaCl on ice. Nuclei were incubated with 500 µl of ice cold salt for 1 hour. After this treatment, nuclei were washed with 500 µl ice cold PBS/EDTA 3 times for 3 min. Since NaCl was diluted in PBS/ EDTA, the salt concentrations indicated on the X axes of the graphs in the relevant figures show the total NaCl concentrations together with NaCl present in the PBS buffer. For the analysis of the elution curves SigmaPlot 12.0 software was applied.

Treatment of the embedded nuclei with intercalators, immunostaining

After permeabilization, nuclei were washed 5 times with 500 µl ice cold PBS/EDTA for 3 minutes each. Ethidium bromide (EBr) treatment was performed using concentrations ranging from 0 to 100 µg/ml in PBS/EDTA containing 750 mM salt for 1 hour on ice followed by washing 3 times with 500 µl ice cold PBS/EDTA for 10 minutes each. H2A.Z was stained by overnight incubation at 4°C with the primary antibody (anti-H2A.Z Rabbit Polyclonal Antibody, Abcam ab97966; anti-H2A Rabbit Polyclonal Antibody, Abcam ab18255; anti-H2A.X Rabbit Polyclonal Antibody, Abcam ab20669; anti-H3 Rabbit Polyclonal Antibody, Abcam ab1791; anti-H3K27me3 mouse monoclonal antibody and H3K9me3 mouse monoclonal antibody, both provided by Prof. Hiroshi Kimura, as described in [142], diluted 1:800 in 1% BSA in PBS/EDTA. After 4 sequential washes (quick, 10, 30, and 60 minutes) with 500 µl ice cold PBS/EDTA, nuclei were incubated at 4°C in the dark with a secondary antibody (Alexa Fluor 488 Goat Anti-Rabbit, Invitrogen A11008 or Alexa Fluor 647 Goat Anti-Mouse, Invitrogen 21235) diluted 1:800 in 1% BSA in PBS/EDTA. When Doxorubicin (Dox) https://www.drugs.com/monograph/doxorubicin.html, or Biotin-labeled Doxorubicin (Dox-Biotin) was used as an intercalator, the washed nuclei were incubated with 200 µl of 1 µM Dox-Biotin dissolved in PBS/EDTA (from Zutao Yu, Cambridge University, UK) for 2 hours on ice in the dark, followed by 3 washes with 500 µl ice cold PBS/EDTA (10 minutes each). Samples were stained overnight at 4°C in the dark with 150 µl of the primary antibody

(mouse anti-biotin, Sigma B7653), and after 4 washes (as above), were incubated with the secondary antibody (Alexa Fluor 647 goat anti-mouse, Invitrogen A21235) under the same conditions.

Samples were fixed in 200 µl of 1% formaldehyde overnight at 4°C in the dark. The next day, formaldehyde was removed, and the samples were washed 3 times with 500 µl ice cold PBS/EDTA for 5 minutes each before staining with 12.5 µg/ml propidium iodide (PI) for 1 hour on ice. After 3 additional washes with 500 µl ice cold PBS/EDTA for 3 minutes each, fluorescence intensity distributions were recorded in an iCys Laser Scanning Cytometer (LSC). The data were analyzed using the iCys0.7 software, and statistical analyses were performed in GraphPad Prism V8.2.1.

Nickase treatment of nuclei

Cells were embedded into agarose and permeabilized as described above. The frequent cutter Nt.CviPII nickase (recognition site: CCD; New England Biolabs Inc., Ipswich, Massachusetts, USA) was applied after the washing steps following permeabilization. Before digestion, the samples were equilibrated with nickase buffer (10 mM Tris-HCl pH 8.0, 50 mM NaCl, 10 mM $MgCl_2$, 1 mg/ml BSA) by washing 3 times with 500 µl of the buffer solutions. Nickase treatment was performed in 300 µl nickase buffer for 30 min at 37°C, using the enzyme at a final concentration of 0.5 U/ml. After enzymatic treatment, the samples were washed with 500 µl ice cold PBS/EDTA 3 times, for 3 min.

Fluorescence correlation spectroscopy (FCS)

The native plasmid DNA was either nicked or linearized using 1 U of Nb.BsmI (ER2051) or 1 U of EcoRI (ER0275), respectively, in a 20 µl reaction volume, for 1 hour at 37˚C. Both enzymes were from Thermo Scientific, Waltham, Massachusetts, USA. Equal amounts of supercoiled, nicked and linearized plasmid DNA were mixed and loaded into wells of a 1% agarose gel. The bands were cut from the gel and the DNA was isolated and purified using a Promega kit (Wizard® Plus SV Minipreps DNA Purification Systems, A1460).

In FCS, the fluorescence intensity fluctuations of molecules diffusing across the sub-femtoliter detection volume illuminated by a focused laser beam is measured in a confocal arrangement. The

temporal autocorrelation function (ACF) of the fluorescence intensity gives information about the mobility, absolute concentration and aggregation state as well as the photophysical properties of the molecules [144]. FCS was used to assess the binding of CF-C9 and CF-SCR peptides to superhelical or relaxed plasmid DNA (pCMV-EGFP-4X) based on the FCS-derived mobility of the peptides/peptide-DNA complexes.

For sample preparation, all solutions were kept on ice. A freshly prepared 1 M stock of the antioxidant vitamin C was made by dissolving 176 mg of vitamin C powder in 1 ml of deionized water and vortexing until fully dissolved. For calibration, 20 nM of Alexa Fluor 488 (A488) was made from a 10 µM stock, which was centrifuged at 14,000 rpm for 10 min at 4°C, then dissolved in ice-cold TE buffer (10 mM Tris, 0.1 mM EDTA, pH 7.4). 400 nM of the carboxyfluorescein labeled C9 peptides CF-C9 and CF-SCR (scrambled) were made from 2 mM stock, which were diluted stepwise in ice-cold PBS under thorough vortexing, then centrifuged at 14,000 rpm for 10 min at 4°C. A base solution was prepared by mixing 3.992 ml of TE buffer (pH 7.4, 4 µl of 1 M vitamin C (1 mM), and 4 µl of 10% NP-40 detergent (0.01%). FITC (control) were measured by FCS at a final concentration of 20 nM (in 10 mM Tris-EDTA buffer, pH 7.4), while the peptides CF-C9 and CF-SCR were added at 40 nM in PBS. The peptides were either measured alone or in combination with 10 µg/ml plasmid DNA (pCMV-EGFP-4X) in a supercoiled form or relaxed by nickase using Nb.BsmI (Thermo Scientific ER2051, Waltham, Massachusetts, USA.). FCS measurements were performed using 8-well microscopic chambered cover slips (Ibidi, Martinsried, Germany) with a sample volume of 200 µl at room temperature (22.5°C), using a Carl Zeiss LSM 880 confocal microscope (Carl Zeiss, Jena, Germany), equipped with a 60× water immersion objective and a photon counting detector. Fluorescence of the CF-tagged peptide was excited by the 488 nm laser line and its emission was detected between 500–550 nm.

Evaluation of raw FCS data

FCS measurements consisted of 5 × 20 s runs, and each sample was measured at least 3 times at each condition. FCS data were evaluated by using the QuickFit3 software ((JW. Krieger, J. Langowski (2015): QuickFit 3.0 (status: beta, compiled: compiled: Jan 5, 2015, SVN: 3695): A data evaluation application for biophysics, [web page] http://www.dkfz.de/Macromol/quickfit/ [Accessed on Jan 5, 2015]).). Autocorrelation functions from each run were inspected, and those

displaying artefacts due to large fluctuations caused by aggregates were excluded. The remaining runs were averaged, and the resulting correlation curve was fitted to different models using a simulated annealing algorithm with box constraints weighted by the standard deviations of the runs. We tested normal (free Brownian) and anomalous diffusion models with a two-component normal diffusion model for measurements of Plasmid + CF-C9 (or CF-SCR) and a one-component model for the CF-C9 (or CF-SCR) alone to fit ACFs.

Each model included a triplet term:

$$G(\tau) = \frac{1-T+Te^{-\tau/\tau_{tr}}}{1-T} G_{diff}(\tau) \quad (1)$$

where,

$$G_{diff}^{normal}(\tau) = \frac{1}{N}\left[\rho_1 \left(1+\frac{\tau}{\tau_1}\right)^{-1}\left(1+\frac{\tau}{S^2\tau_1}\right)^{-1/2} + \rho_2 \left(1+\frac{\tau}{\tau_2}\right)^{-1}\left(1+\frac{\tau}{S^2\tau_2}\right)^{-1/2}\right] \quad (2)$$

N denotes the average number of diffusing fluorescent molecules present in the detection volume, τ is the lag time, T is the equilibrium mole fraction of fluorophores in triplet state, and τ_{tr} is the triplet correlation time [145 146].

In the model, we assumed one or two distinct diffusing species: a fast population with a fraction of ρ_1, a diffusion time of τ_1 and a slow one with a fraction of ρ_2 and a diffusion time of τ_2; ρ_2 equals 1-ρ_1. S is the ratio of the axial and longitudinal diameters of the ellipsoid-shaped confocal detection volume, defined by the properties of the microscope. S was determined before each measurement by fitting the ACFs of the 20 nM fluorescein dye (FITC) solution (in 10 mM Tris-EDTA buffer, pH 7.4).

The diffusion coefficients of the fast and slow components were calculated by:

$$D_i = {\omega_{xy}}^2/4\tau_i \quad (3)$$

where ω_{xy} is the lateral radius of the detection volume. ω_{xy} was calculated from the measured diffusion time of 20 nM fluorescein solution dye as follows:

$$\omega_{xy} = \sqrt{4D\tau_D} \quad (4)$$

where τ_D is the diffusion time of the dye, and D is its diffusion coefficient taken from the literature (425 μm^2/second at 25°C) [147].

Confocal laser scanning microscopy

Confocal images were taken using Nikon A1 laser scanning confocal microscope (Nikon, Tokyo, Japan), equipped with a Plan Apo 60 × NA 1.27 water immersion objective. Alexa 488 was excited by the 488 nm laser. Alexa 647 and PI were excited by the 633 nm and 543 nm lasers, respectively. Images were analyzed using Fiji ImageJ.

Laser scanning cytometry (LSC)

Automated microscopy imaging was done using an iCys laser scanning cytometer (Research Imaging Cytometer; CompuCyte, Westwood, Massachusetts, USA). The instrument is based on an Olympus IX-71 inverted microscope equipped with four lasers, photodiodes (detecting light loss and scatter) and four photomultiplier tubes (PMTs). The 488 nm Argon ion laser was used to excite Alexa 488 and PI and the 633 nm HeNe laser was applied in the case of Alexa 633. Fluorescence signals were collected via an UPlan FI 20× NA 0.5 objective. Alexa 488 fluorescence was detected through a 530/30 nm bandpass filter, while Alexa 647 and PI were detected through a 650/LP filter. Data analysis was performed using the iCys 7.0 software, and graphs were prepared using SigmaPlot 11.0.

Statistical Analysis

The data from each experiment are shown as the mean and standard deviation (SD) of $n \geq 3$ biologically independent experiments. Data were plotted in SigmaPlot 11.0 and statistical analyses were performed with GraphPad Prism V8.2.1 using one-way ANOVA or unpaired Student's t-tests, as indicated in the figure legends. Statistical significance of difference was denoted as *, $p < 0.05$; **, $p < 0.01$; ***, $p < 0.001$; and ****, $p < 0.0001$.

RESULTS

1. Epigenetic modulation via the C-terminal tail of H2A.Z variant

Our studies focused on exploring the role of the C-terminal H2A.Z tail in determining the stability of H2A.Z-containing nucleosomes. We thought that we could take advantage of QINESIn, the nucleosome stability assay developed in our lab [57] to study the role of the tail in determining the stability of these nucleosomes, benefiting also from a collaboration with Prof. Harata's lab (Sendai, Japan) who provided us with a DT40 cell line pair expressing either human H2A.Z1 (DKO/Z1) or its C-terminally truncated version (DKO/ΔC) [148].

In QINESIn (see Introduction), histones remaining in the nuclei after treatment with increasing NaCl concentrations (or intercalators, used as described in the next chapter) were detected by immunofluorescence or directly in the case of histones tagged with fluorescent proteins, followed by automated quantitative imaging with a laser scanning microscope (LSC). In the salt elution assay, salt ions (Na^+, Cl^-) perturb electrostatic forces and weaken the interactions responsible for nucleosome integrity. Elevated salt concentrations disrupt not only DNA-histone interactions, but also those acting among the histones themselves, as well as interactions between the two DNA strands (by affecting the equilibrium between double-stranded and denatured states), thereby influencing nucleosome stability. At moderate salt concentrations, this leads to the dissociation of the peripheral H2A-H2B dimers, while the central H3-H4 tetramer remains associated with DNA. At high NaCl concentrations, even the H3-H4 tetramer is disrupted, ultimately resulting in full nucleosome disassembly. The dissociated nucleosomal components diffuse out from the nuclei embedded into agarose. The Triton X100 treatment used to prepare permeabilized nuclei is expected to remove the cytoplasm and the nuclear envelope, leaving the nuclear pores and the nuclear lamina intact, representing barrier to diffusion above 20 nm particles. This approach allows us to evaluate how DNA unwrapping and histone dissociation occur in specific nucleosomes.

1.1. The intrinsic stability of H2A.Z-nucleosomes is C-terminus- dependent

When comparing the salt elution profiles of various histone proteins, including H2A, H2A.X, H2A.Z and H3-GFP within HeLa nuclei, it was observed that H2A.Z demonstrates an unusually stable association with chromatin (Fig. 10A), exhibiting salt elution profiles similar to those of H3

or H4, as compared with canonical H2A or H2A.X, across all phases of the cell cycle (Fig. 10B). Surprisingly, a higher salt concentration was necessary to elute H2A.Z compared to H2A, which was coeluted with histone H3 (Fig. 10A, B). Furthermore, in the salt elution curves shown in figure 10A, almost 10% of H2A.Z remains in the nucleus even with exposure to the maximum salt concentration. As detailed above, spurred mainly by the destabilized nature of the H2A.Z.2.2 isoform, experiments were performed utilizing DT40 cells expressing human H2A.Z.1 with a deletion of the last 9 amino acids at the C-terminus (between residues 119–128) (Fig. 10C) in a double H2A.Z.1, H2A.Z.2 knockout (DKO) background [148] (The same experimental system was used in the intercalator elution studies described in chapter 2). The H2A.Z nucleosomes of DKO/ΔC cells were less stable compared to those of the control DKO/Z1 cells (Fig. 10D). Notably, the intranuclear localization pattern of H2A.Z nucleosomes was significantly influenced by the C-terminus (Fig. 10E, F). In the DKO/ΔC cells, the localization of H2A.Z, as identified by ZAbA antibody, changed from peripheral to a more dispersed pattern within a similar DKO background (Fig. 10E). Interestingly, the distribution of H3K9me3-marked nucleosomes was also altered, as evidenced by the decreased degree of colocalization between H2A.Z and H3K9me3 in DKO/ΔC nuclei relative to DKO/Z1 nuclei (Fig. 10F). Based on their salt elution features, three categories of H2A.Z-containing nucleosomes could be distinguished: the unusually salt-stable nucleosomes associated with peripheral heterochromatin, termed H2A.Z^{hc}, the more centrally positioned and dispersed H2A.Z-nucleosomes exhibiting stability characteristics akin to canonical nucleosomes resembling euchromatin, termed H2A.Z^{eu} and a third category, H2A.Z^{lmn} that appears to be tightly associated with the nuclear lamina and is referred to as H2A.Z^{lmn}, based on the immunofluorescence staining of nuclear halos ([142]; data not shown).

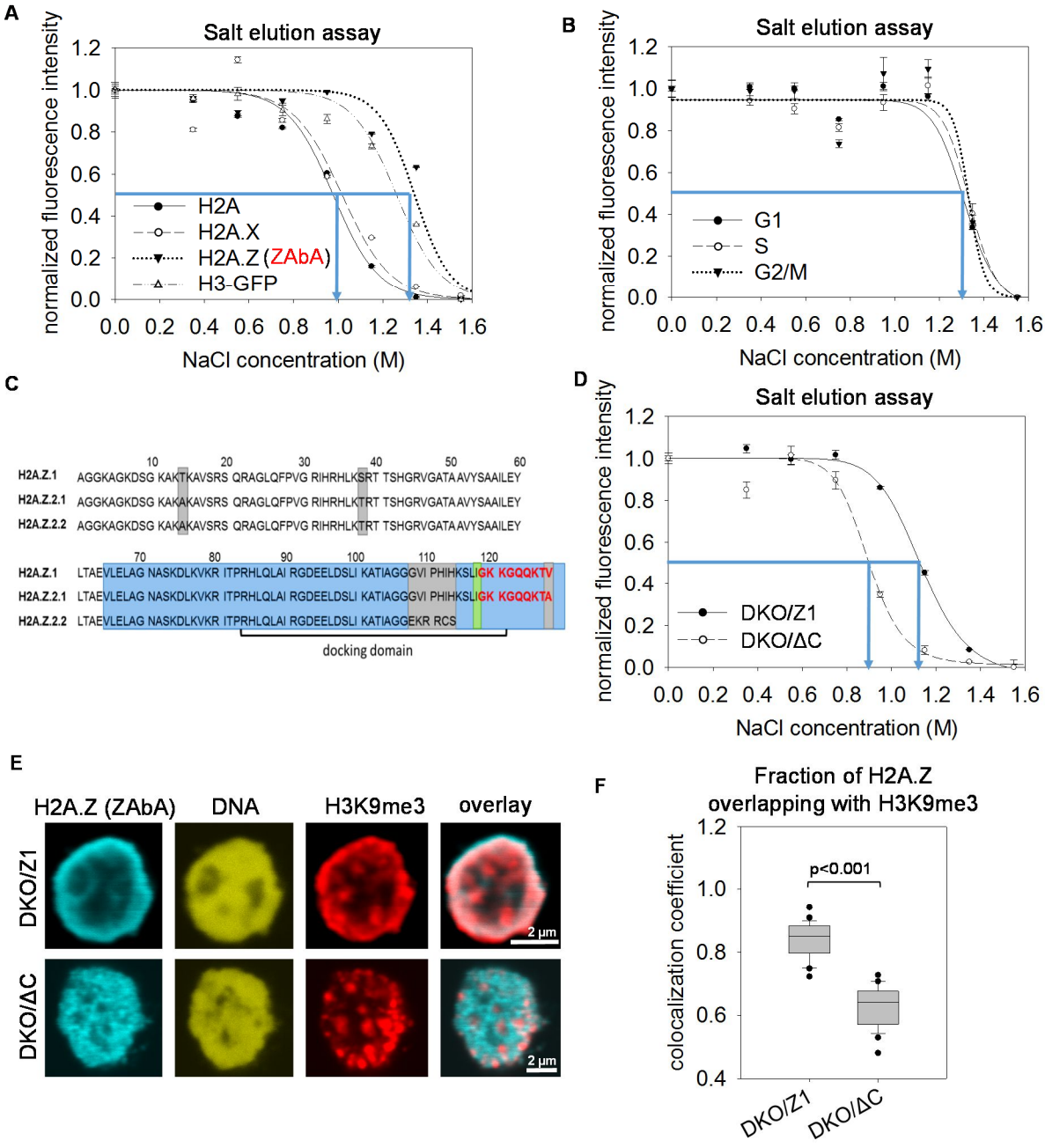

Figure 10: Role of the H2A.Z C-terminus in nucleosome stability and nuclear localization. **(A)** Comparison of the salt elution patterns determined by the QINESIn for H2A, H2A.X, H2A.Z, and H3-GFP (used as an internal control) in HeLa nuclei. **(B)** Salt elution profile of H2A.Z identified by ZAbA antibody in HeLa nuclei across the cell cycle. **(C)** Amino acid sequences of human H2A.Z.1, H2A.Z.2.1, and H2A.Z.2.2. Grey boxes highlight sequences that are different among H2A.Z isoforms. Blue Square indicates the C-terminal epitope recognized by ZAbA starting with amino acid (aa) 65, comprising the H2A.Z docking domain and the C-terminal unstructured tail. The 9 aa long deletion in the H2A.Z ΔC is shown in red font. **(D)** Salt elution

profiles of H2A.Z nucleosomes in DKO/ΔC and DKO/Z1 nuclei. The elution curves in all panels correspond to G1 phase nuclei gated according to their DNA fluorescence intensity distribution, with the error bars indicating the SEM of about 600 nuclei analyzed by LSC. The blue arrows on the elution curves signify EC50 values. **(E)** CLSM images illustrating the nuclear localization of H2A.Z detected by ZAbA, and H3K9me3 co-labeled with H2A.Z in both nuclei. **(F)** Represent the colocalization analysis of H2A.Z and H3K9me3 in DKO/ΔC and DKO/ Z1 nuclei, using the Manders colocalization coefficient (MCC) to quantify the fraction of H2A.Z overlapping with H3K9me3 from 25 nuclei [142].

These observations were made on isolated nuclei, using the salt elution format of QINESIn, i.e. exposing chromatin to challenging conditions that are non-physiological and the simultaneous eviction of H2A.Z and H3 left us with the impression that H2A.Z may be bound to H3. Further experiments revealed that the chromatin of DKO/ΔC nuclei is more sensitive to different nucleases and their nucleosomes are unstable relative to those of the DKO/Z1 nuclei through the spectacles of salt elution ([142]; data not shown). Based on the above observations a synthetic peptide corresponding to the last 9 amino acids of the H2A.Z C-terminus was tested as to its possible effects on nuclear architecture and nucleosome stability when added to agarose-embedded HeLa nuclei expressing normal H2A.Z1. In these experiments all the features of the DKO/ΔC DT40 nuclei were recapitulated ([142]; data not shown). My role in the project was to establish a cyclodextrin-based procedure for the introduction of the peptide into live cells, and to further investigate the role of the C-terminus in determining nucleosomal stability using the other format of the QINESIn assay, intercalator elution.

1.2. The effects of C9 peptide introduced into live cells

The destabilized state of the nucleosomes containing C-terminally truncated H2A.Z and their altered intranuclear localization suggested that these characteristics are a direct result of molecular interactions involving this specific tail region. To further explore this, the synthetic peptide (C9) corresponding to the last nine amino acids of the C-terminus (Fig. 10C) was added to HeLa nuclei and also introduced into live HeLa and Melanoma (MEL1617) cells under conditions that did not significantly affect cell viability (Fig. 11).

I first assessed the cytotoxicity of the cyclodextrin derivative sulfobutyl ether β-cyclodextrin sodium salt (SBECD), commonly used in pharmaceuticals to enhance the solubility of poorly

water-soluble drugs [149], in both HeLa and MEL1617 cells. Cell viability was measured using the Alamar Blue assay, which evaluates cellular metabolic activity by quantifying the reduction of a non-fluorescent dye (resazurin) into a highly fluorescent product (resorufin), providing a reliable estimation of the number of viable cells in the measured well [150]. In HeLa cells, the exposure to SBECD did not reduce the viability at any of the tested incubation time points compared to the SBECD-untreated controls, as indicated by stable absorbance values across increasing concentrations up to 300 μM (Fig. 11A). Similar results were obtained for MEL1617 cells (Fig.11C). To further evaluate the cytotoxic threshold, cells were treated with increasing SBECD concentrations and cell numbers were quantified by direct cell counting. In both HeLa (Fig. 11B) and MEL1617 cells (Fig. 11D), a clear dose-dependent reduction in cell number was observed, indicating that SBECD exerts cytotoxic effects at concentrations above 300 μM. These data establish 300 μM as the upper safe concentration for SBECD use in peptide delivery. Next, I investigated the kinetics of peptide uptake in HeLa cells using flow cytometry, measuring cell-associated total fluorescence of the C9 peptide labeled with carboxyfluorescein (CF) following its co-incubation with SBECD at RT for varying time points to allow the formation of peptide-SBECD complexes. The peptide was mixed with the cyclodextrin at a molar ratio of 1:10 to ensure that all the SBECD molecules become loaded with the peptide. The flow cytometric data showed that both CF-C9 and CF-C6 (containing only the last 6 amino acids of the C-terminal tail) exhibited time-dependent uptake by the cells. Notably, fluorescence intensity increased over time, reaching a maximum at 2 h (Fig. 11E, F), indicating progressive cellular uptake of the peptide-SBECD complexes. Peptide localization was visualized in HeLa cells using confocal microscopy. Both CF-C6 and CF-C9, were observed in the nuclei of HeLa cells after fixation with 1% formaldehyde, CF-C9 showing a higher accumulation (Fig. 11G). These observations confirmed that SBECD facilitates efficient cellular uptake and nuclear delivery of the peptides.

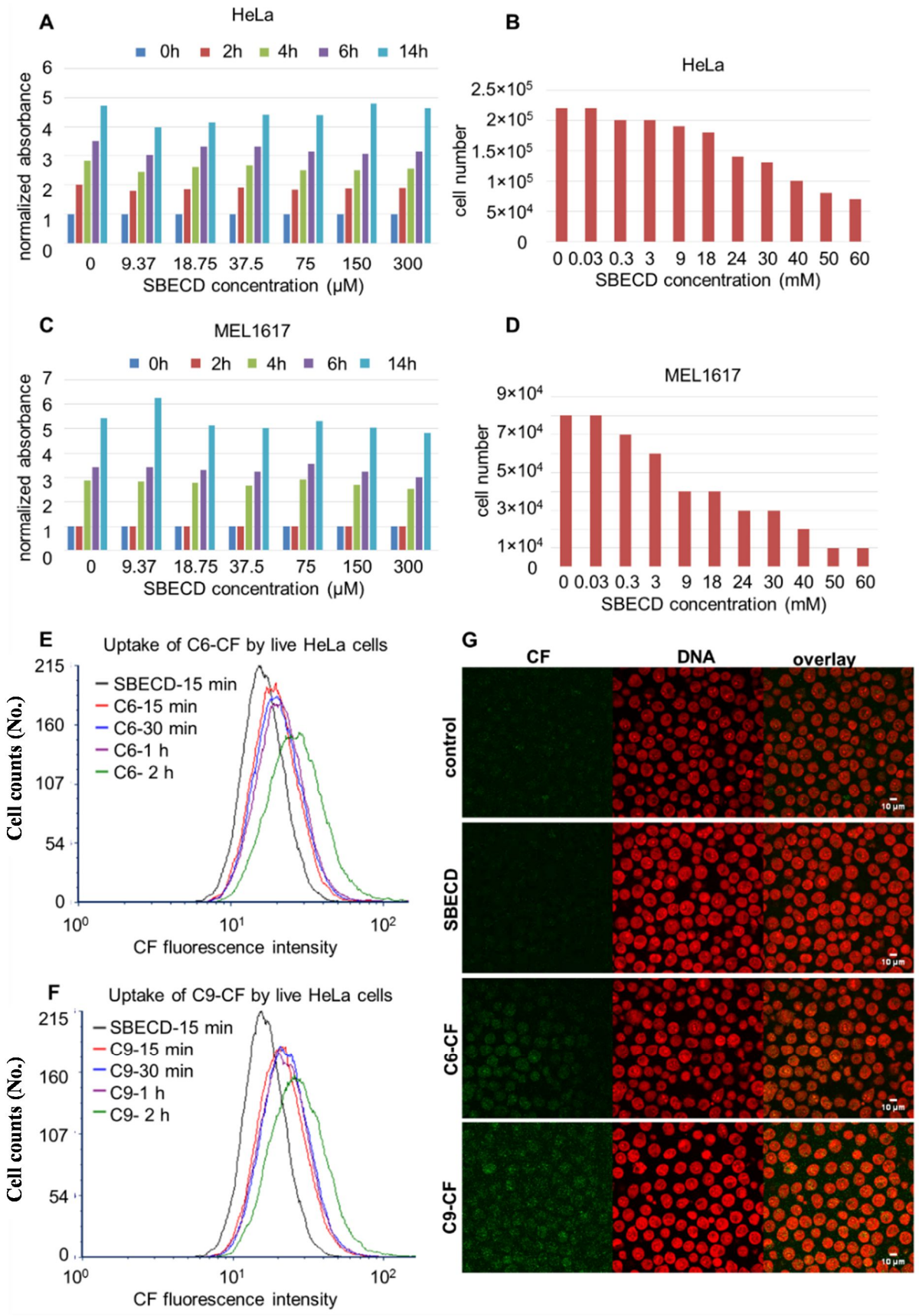
A
HeLa
0h 2h 4h 6h 14h
normalized absorbance
0 1 2 3 4 5 6
0 9.37 18.75 37.5 75 150 300
SBECD concentration (μM)
B
HeLa
cell number
0 5×10^4 1×10^5 1.5×10^5 2×10^5 2.5×10^5
0 0.03 0.3 3 9 18 24 30 40 50 60
SBECD concentration (mM)
C
MEL1617
0h 2h 4h 6h 14h
normalized absorbance
0 1 2 3 4 5 6 7
0 9.37 18.75 37.5 75 150 300
SBECD concentration (μM)
D
MEL1617
cell number
0 1×10^4 3×10^4 5×10^4 7×10^4 9×10^4
0 0.03 0.3 3 9 18 24 30 40 50 60
SBECD concentration (mM)
E
Uptake of C6-CF by live HeLa cells
SBECD-15 min
C6-15 min
C6-30 min
C6-1 h
C6- 2 h
Cell counts (No.)
0 54 107 160 215
10^0 10^1 10^2
CF fluorescence intensity
F
Uptake of C9-CF by live HeLa cells
SBECD-15 min
C9-15 min
C9-30 min
C9-1 h
C9- 2 h
Cell counts (No.)
0 54 107 160 215
10^0 10^1 10^2
CF fluorescence intensity
G
CF
DNA
overlay
control
SBECD
C6-CF
C9-CF
10 μm

Figure 11: Demonstration of peptide delivery while maintaining cell viability in HeLa and melanoma cells. (A) Titration of cyclodextrin derivative SBECD concentration in the micromolar range in HeLa cells measuring cell viability by the Alamar Blue assay. **(B)** Titration of SBECD concentration in HeLa cells in the millimolar range quantifying cell number by cell counting (the values were normalized to 0 time). **(C, D)** SBECD titration performed using melanoma cells (MEL1617), as in panel (A) and (B), respectively. **(E, F)** Kinetics of carboxyfluorescein-C6 **(E)** or carboxyfluorescein-C9 **(F)** uptake by live HeLa cells analysed using flow cytometry. Complex formation was prepared using 300 μM SBECD and 30 μM peptide. **(G)** CLSM images that visualize the accumulation of fluorescent peptides in the nucleus of HeLa cells, after fixation with 1% formaldehyde.

The confocal microscopy images of Fig. 12 showed intracellular accumulation of CF-C9 following treatment with either 30 μM or 90 μM peptide concentrations (Fig. 12A). The fluorescence signal was present in the nucleus, indicating efficient cellular uptake and nuclear localization of the peptide. The CF-C9 accumulation slightly increased with higher peptide concentration, suggesting a dose-dependent internalization. Flow cytometric analysis further confirmed these observations (Fig. 12B). Cells treated with the SBECD/CF-C9 complex exhibited an upward shift in the size-fluorescence scattergrams compared to untreated controls, consistent with peptide uptake. The fluorescence signal was slightly higher in cells exposed to 90 μM CF-C9 than those treated with 30 μM, in accordance with the microscopy data. However, since the difference was minimal, subsequent experiments were conducted using 30 μM CF-C9 for practical reasons. Similarly to the cyclodextrin alone, the SBECD/C9 complexes did not decrease cell viability at the SBECD concentration used neither in HeLa (Fig. 12C) nor in MEL1617 (Fig. 12D) cell lines. These results demonstrate that the peptide delivery system is well tolerated under the tested conditions and does not exert cytotoxic effects on either cell line.

Collectively, these findings define a functional concentration range of 300 μM SBECD and 30 μM C9 that maintains cell viability and demonstrates the capacity to mediate efficient peptide uptake and nuclear delivery in both HeLa and melanoma cells.

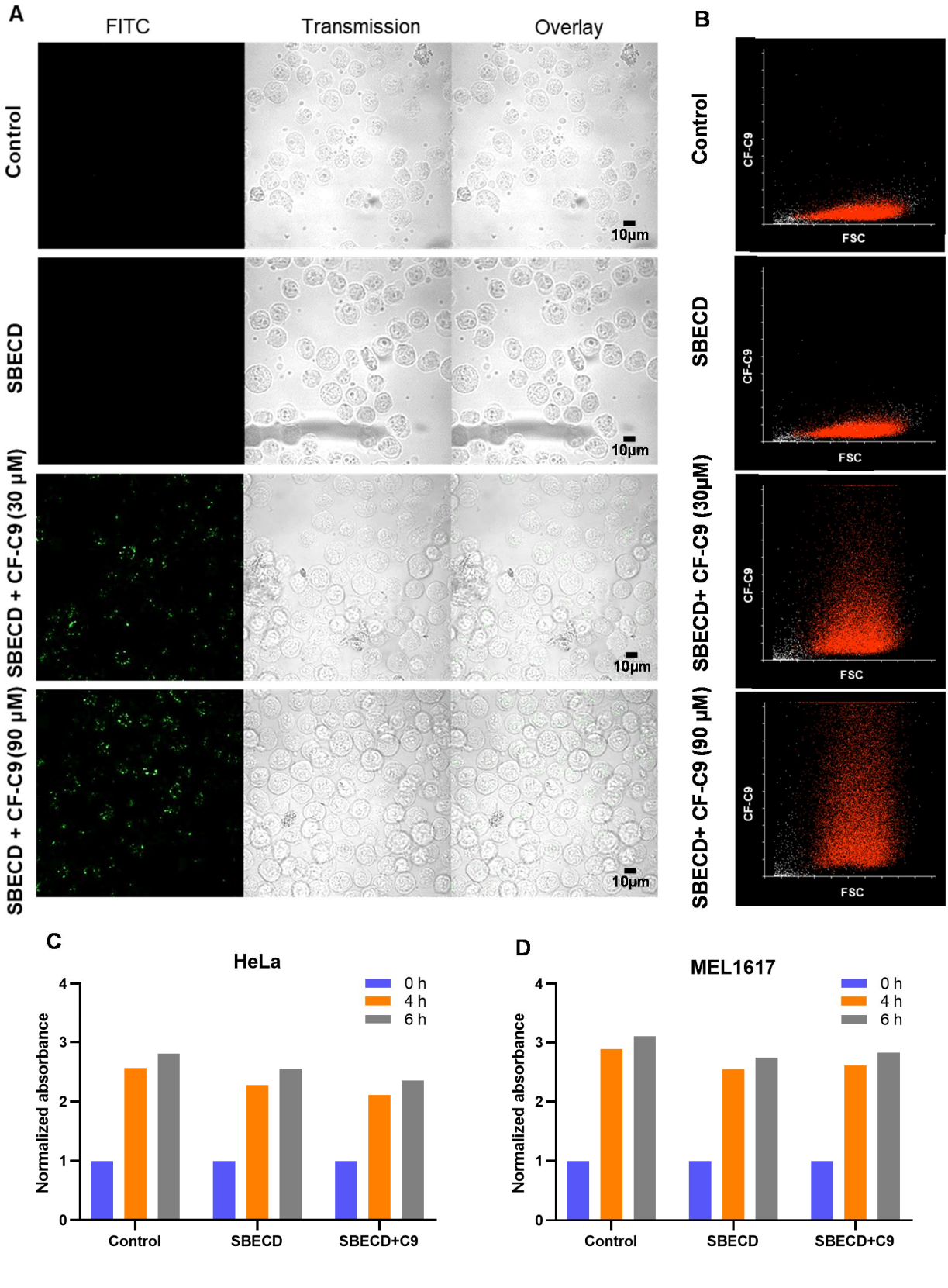
A
FITC
Transmission
Overlay
Control
SBECD
SBECD + CF-C9 (30 μM)
SBECD + CF-C9 (90 μM)
10μm
B
Control
SBECD
SBECD+ CF-C9 (30μM)
SBECD+ CF-C9 (90 μM)
CF-C9
FSC
C
HeLa
Normalized absorbance
0 h
4 h
6 h
Control
SBECD
SBECD+C9
D
MEL1617
Normalized absorbance
0 h
4 h
6 h
Control
SBECD
SBECD+C9

Figure 12. Titration of C9 peptide and its effect on HeLa and melanoma cell viability. (A) CLSM images showing the intracellular accumulation of fluorescently labeled C9 (CF-C9) in HeLa cells treated with the complex SBECD + 30 μM or 90 μM peptide. Cells were fixed with 1% formaldehyde prior to imaging. **(B)** Flow cytometric analysis of CF-C9 uptake in live HeLa cells. Complexes were prepared using 300 μM SBECD and C9 at concentrations of 30 μM or 90 μM. **(C, D)** Cell viability measurements of untreated cells, cells treated with SBECD alone, or with SBECD/C9 complexes (30 μM of C9), assessed using the Alamar Blue assay in **(C)** HeLa and **(D)** MEL1617 cell lines. The indicated time points correspond to the incubation time with the Alamar Blue reagent. Absorbance values were normalized to the 0-hour time point.

After a single dose of C9 peptide delivered via SBECD (Fig. 13A), several changes were detected in the nuclei of HeLa cells within one day. Peripheral H2A.Z-containing heterochromatin was reorganized relative to H3K9me3 (Fig. 13B, C). Comparable although less obvious alterations were observed in the nuclei of two melanoma cell lines (WM35 and MEL1617), emphasizing the specific effect of the C9 peptide compared to the control peptide, SCR (see Materials and Methods) (Fig. 13D, E). In addition, other data detected a decrease in nucleosome stability and an increase in nuclease (e.g. nickase) sensitivity upon C9 treatment ([142]; data not shown). Overall, the findings made possible by the successful introduction of the peptide to live cells recapitulated the effects detected when C9 was added to agarose-embedded nuclei and both reminded of the differences observed between the nuclear architecture and nucleosome stability features of the DKO/ΔC-DKO/Z1 DT40 cell pair, in support of the complex role of the C-terminal H2A.Z tail in determining nuclear architecture and the stability of the H2A.Z-nucleosomes *in vivo* as well as providing an experimental tool to modulate chromatin structure and function.

We were intrigued to further investigate whether the stability of nucleosomes appears to be tail-dependent also when assessed in more physiological conditions. To address this, an alternative approach is to challenge nucleosome structure by altering the superhelicity of the DNA wrapped around them, as well as interconnecting them**,** rather than perturbing ionic and hydrogen bonds with salt. This approach proved to be sensitive to somewhat different aspects of nucleosome stability as compared with the salt elution [57] and provides an independent means to assess nucleosome stability. Alterations in DNA superhelicity do occur *in vivo* during processive enzymatic activities in the nucleus like transcription, suggesting that differences in nucleosome stability revealed by this assay may have direct biological significance.

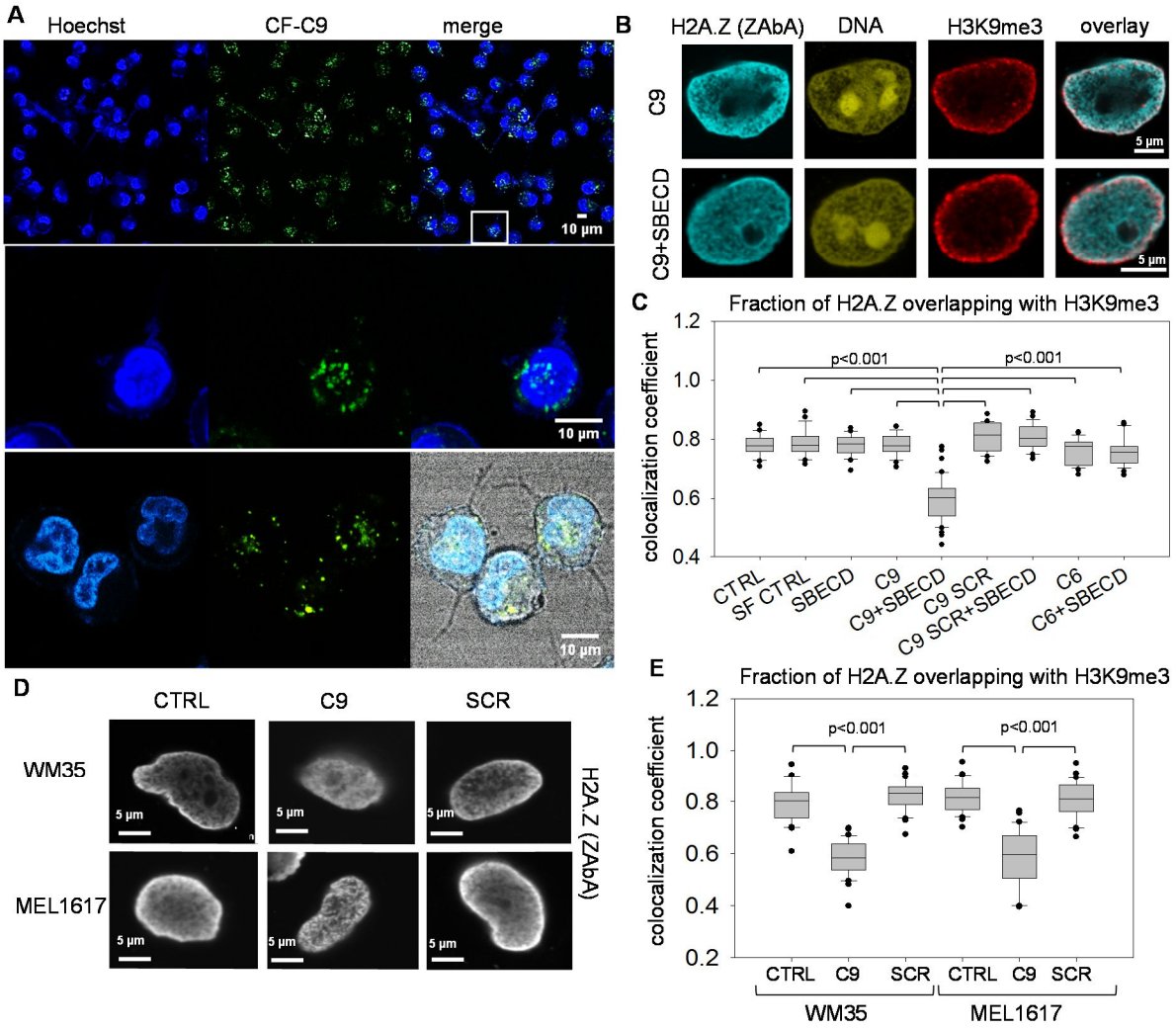

Figure 13: Localization and effects of C9 after being introduced into live HeLa and melanoma cells by SBECD. (A) CLSM image showing the localization of CF-C9 in live HeLa cells after 2 h treatment with (CF-C9+SBECD) complex followed by overnight culture. Inset image of top image is shown below. The third image is from a different field includes a bright-field to clearly show that the peptide was introduced to live, intact cells **(B)** CLSM images of nuclei co-labeled with H2A.Z and H3K9me3 after the introduction of C9 into live HeLa cells alone or with SBECD. **(C)** Colocalization of H2A.Z and H3K9me3 in HeLa cells untreated or treated with C9, or SCR peptides alone or with SBECD. The MCC values representing the fraction of H2A.Z overlapping with H3K9me3 calculated for the nuclei of in panel B. **(D)** CLSM images of nuclei showing H2A.Z rearrangement untreated or after the introduction of C9 or SCR into live WM35 and MEL1617 cells. **(E)** Colocalization of H2A.Z and H3K9me3 in WM35 and MEL1617 cells treated with C9, SCR or left untreated (CTRL). MCC values representing the fraction of H2A.Z overlapping with H3K9me3 are shown. Box-and-whisker plots were created from the data of 30 nuclei [142].

2. Superhelicity-dependent DNA binding of the H2A.Z C-terminal tail stabilizes nucleosomes containing this variant

2.1. Characterization of H2A.Z nucleosome stability by intercalator-induced histone elution

We employed an assay that differs from salt elution and affects nucleosomal structure by modulating DNA superhelicity. We used different intercalating agents that unwind the DNA double-helix, including ethidium bromide (EBr), a widely used DNA-binding probe becoming fluorescent (being shielded from quenching by water when intercalated between the base-pairs of the DNA; [151]) upon binding to DNA, and doxorubicin (Dox), a well-known antibiotic and anticancer drug [57]. The latter is fluorescent by itself but the quantum efficiency decreases upon DNA binding [152], unlike for EBr, therefore its biotinylated derivative [153] was applied in our experiments, made available for us by Dr. Zutao Yu (Cambridge, UK). These intercalators unwind and extend the DNA without directly perturbing ionic or hydrogen bonds [154]. This structural perturbation alters the wrapping of DNA around the histone core, leading to histone eviction that reflects nucleosome stability under conditions in which intercalator-induced DNA unwinding mimics the local changes occurring during physiological processes such as transcription.

In our initial experiments, ethidium bromide (EBr) was applied. EBr is able to evict nucleosomes only in the presence of at least 750 mM NaCl solution, based on the titration described in our group's previous publication [57]. Up to this salt concentration, the core histones stay almost 100% chromatin-bound, yet the H2A-H2B dimers become loosely attached to nucleosome core and begin to dissociate as EBr concentration increases, as shown in Fig. 14. A large subpopulation of H2A.Z was retained in the nuclei unlike the H2A, H2A.X (Fig. 14A), or H3 nucleosomes (Fig. 14B), suggesting that the H2A.Z nucleosomes are relatively resistant to the changes of superhelicity evoked by the intercalator. In the confocal images of the samples from Fig. 14A and B, the localization of the EBr-resistant H2A.Z nucleosomes has changed characteristically, the dispersed distribution of H2A.Z in the untreated (control) HeLa nuclei (Fig. 14C) was transformed into a perinuclear-perinucleolar topography after treatment with 100 μg/ml EBr (Fig. 14D). The H2A.Z nucleosomes behaved differently when compared to others in the EBr elution assay regardless of the cell cycle phases as well as the H2A.Z isotypes in HeLa cells ([142]; data not shown).

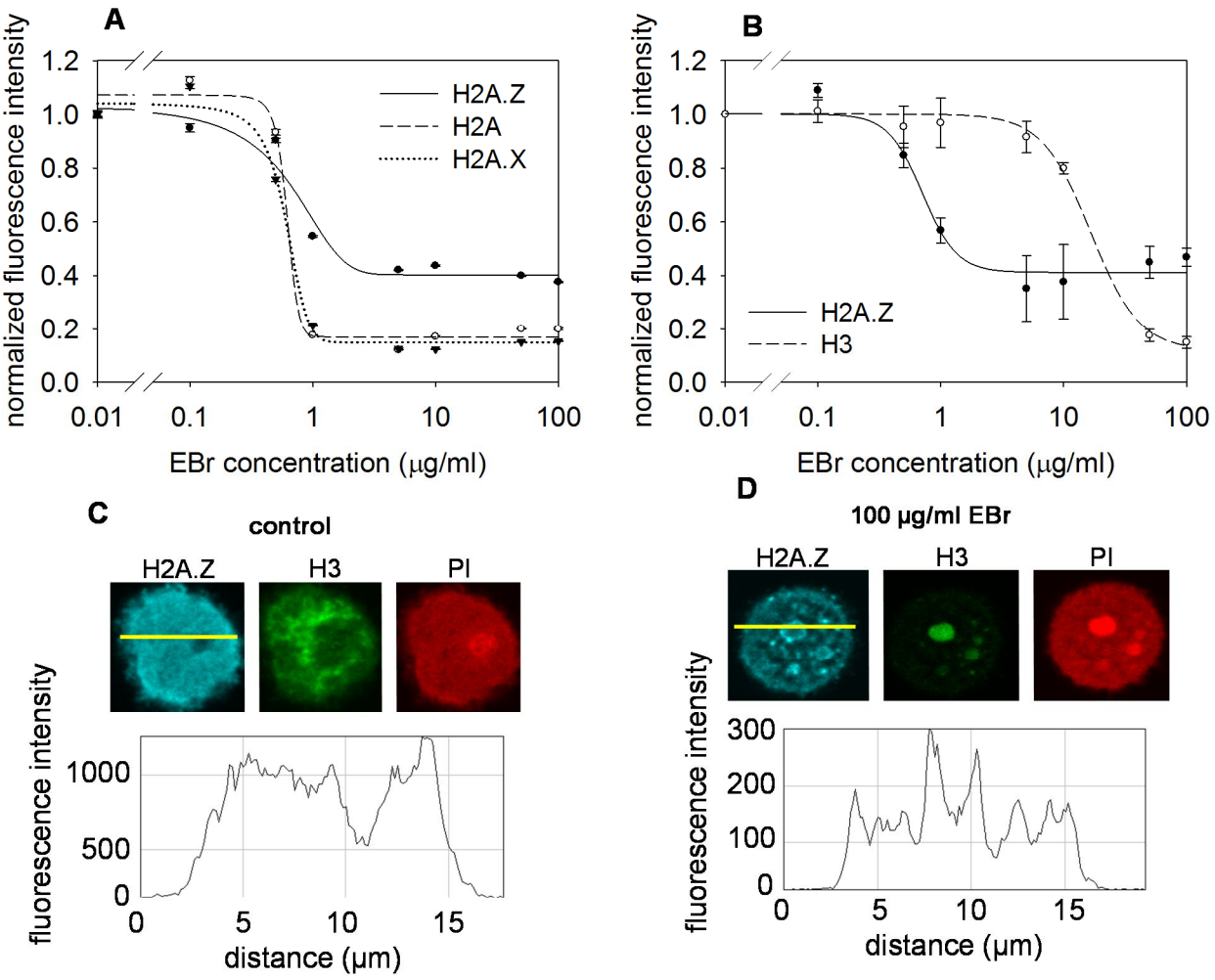

Figure 14. *In situ* investigation of H2A.Z nucleosome stability via treatment of nuclei with the intercalator EBr. **(A)** Comparison of the intercalator elution profiles of H2A, H2A.X, and H2A.Z in HeLa nuclei, utilizing EBr in the presence of 750 mM NaCl measured by QINESIn aproach. **(B)** Comparison of the EBr elution curves of H2A.Z and GFP-tagged H3, utilized as an internal control in HeLa cell nuclei, assessed by QINESIn. The curves respresent the mean of the histone amount in ~600 G1 phase nuclei gated according to their DNA content. **(C, D).**CLSM images and line-scans illustrating the distribution of H2A.Z and H3 within untreated **(C)** and EBr-treated (100 µg/ml) HeLa nuclei **(D)**, in the presence of 750 mM NaCl for both.

Conversely to the salt elution data shown in (Fig. 10A), where H2A.Z and H3 exhibited similar behavior, approximately 50% of all detected H2A.Z has dissociated while H3 remained associated with chromatin. At higher intercalator (EBr) concentrations, most of the H3 was eluted, whereas H2A.Z remained in HeLa nuclei (Fig. 14B) suggesting that H2A.Z is not bound to bulk H3. The above results showing the resistance of H2A.Z-containing nucleosomes to EBr and their nuclear

distribution (Fig. 14D), suggest that it might be localized at the heterochromatin, what was confirmed in similar experiments focusing on facultative and constitutive heterochromatin ([142]; data not shown).

To investigate whether the sensitivity of H2A.Z-containing nucleosomes to EBr, is C-terminus dependent, I performed experiments using the two DT40 cell lines (DKO/Z1 expressing the full-length H2A.Z1, and the DKO/ΔC expressing its C-terminal truncated version). The data demonstrated a strong and clear dependence on the histone variant's C-terminal tail, as the intercalator sensitivity of the H2A.Z-containing nucleosomes differed significantly between the two cell lines (Fig. 15A, B). When the agarose-embedded nuclei of these cells were pretreated with 0.5 U/ml nickase prior to EBr treatment, we found that upon DNA relaxation by nickase treatment, the EBr elution profile of H2A.Z nucleosomes (DKO/Z1-nicked) was shifted to the left compared to the untreated nucleosomes (DKO/Z1), signifying destabilization. Furthermore, the DKO/Z1-nicked sample exhibited a behavior similar to those lacking their C-terminal tail (DKO/ΔC) in the EBr elution (Fig. 15C), indicating that the effect of the DNA nicking and the C-terminal tail truncation are similar in terms of intercalator sensitivity. These finding highlights the critical role of the C-terminal tail in modulating the sensitivity of H2A.Z-nucleosomes in the assay based on intercalator elution and raise the possibility that DNA superhelicity might be also a key factor in the stability of the H2A.Z-nucleosomes.

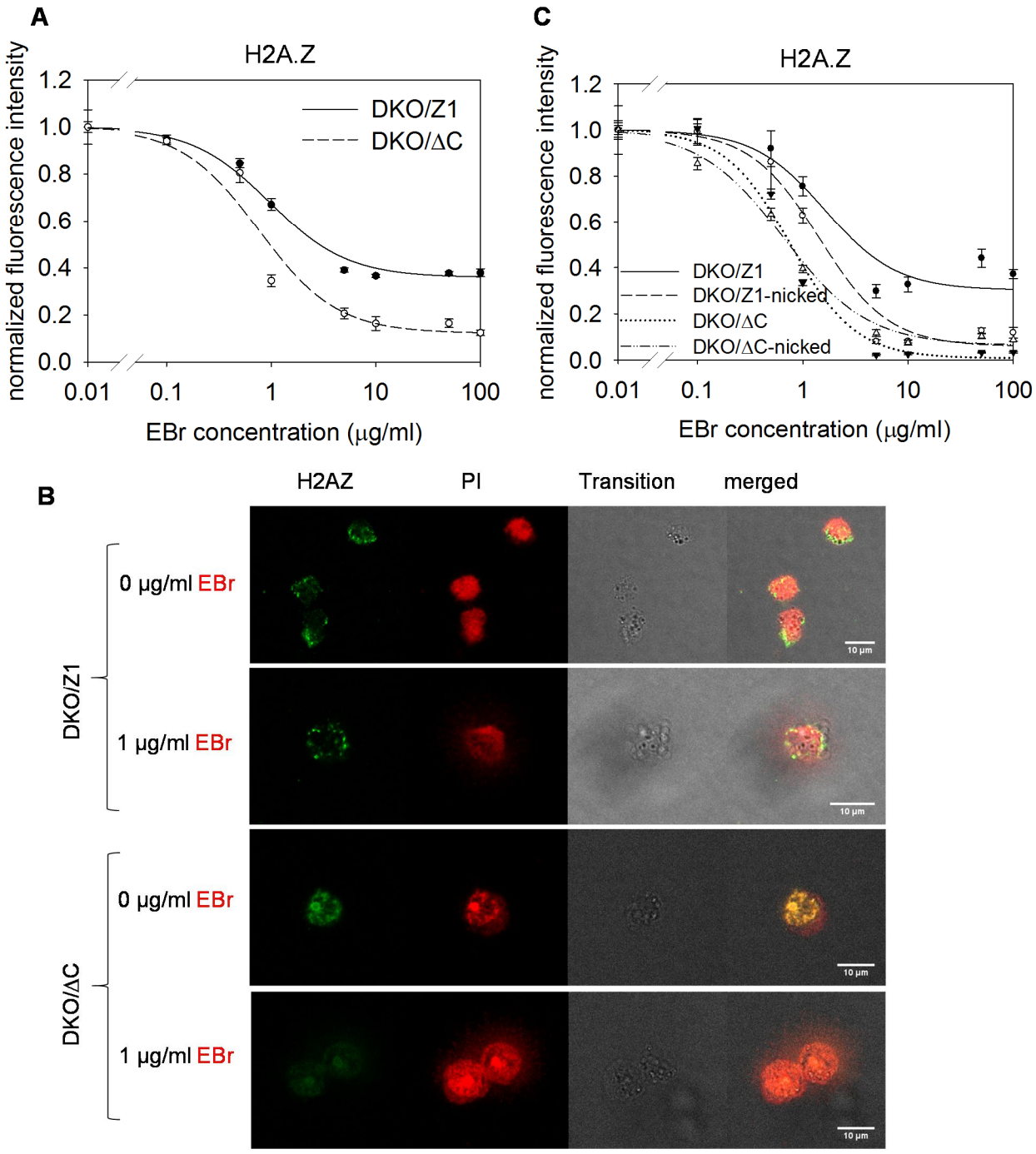

Figure 15: H2A.Z nucleosome sensitivity to the intercalator (EBr) is C-terminus dependent. **(A)** EBr elusion profiles of H2A.Z in DKO/ΔC and DKO/Z1 cells, in the presence of 750 mM NaCl. **(B)** Representative CLSM images of the samples from panel (A), showing the nuclear distribution of H2A.Z in the two cell lines, both untreated and treated with 1µg/ml EBr, in the presence of 750 mM NaCl. **(C)** EBr elution profiles of H2A.Z in DKO/ΔC and DKO/Z1 cells, with or without nickase pretreatment of the agarose-embedded nuclei. The elution curves refer to

G1 phase nuclei gated according to their DNA fluorescence intensity measured by LSC. The error bars representing the SEM of ~600 nuclei are shown.

To further validate our findings, I used another intercalator, Dox, an anthracyclin commonly employed in cancer chemotherapy [155]. Dox was particularly useful because of its property of facilitating nucleosome eviction without requiring the addition of salt, according to our previous experience[57], providing a clearer view of its effect on nucleosome stability in a near-physiological environment. The following experiments were performed using Dox at a concentration of 1 μM unless otherwise specified. This concentration is ~10x smaller than the peak serum cc. of the drug reached in cancer patients [156-158]. When H2A.Z nucleosome eviction was compared in the two DT40 cell lines, we found that the exposure to the intercalator Dox resulted in a higher degree of H2A.Z release in the nuclei prepared from tail-less H2A.Z cells (DKO/ΔC) compared to those obtained from control cells (DKO/Z1) (Fig. 16A) showing a similar effect to EBr. At the same time, the co-labeled H3K27me3-marked facultative heterochromatin exhibited similar behavior in both DKO/Z1 and DKO/ΔC nuclei (Fig. 16B). To further confirm these data, I investigated whether the higher level of H2A.Z elution in DKO/ΔC nuclei corresponds with a higher level of DNA binding by the intercalator, using biotin-labeled doxorubicin (Dox-Biotin) [153]. I first needed to determine if there was a difference in the amount of nucleosome-free DNA (i.e. nucleosome content) between the two cell lines. The agarose embedded nuclei were fixed with 4% paraformaldehyde prior to Dox-Biotin treatment then both Dox-Biotin binding and the amount of immunolabeled H3 were measured. The results showed that the intercalator-treated (Fig. 16C) and untreated (Fig. 16D) DKO/Z1 and DKO/ΔC cells have the same levels of nucleosome-free DNA and also they have similar nucleosome content. Thus, any difference we might see without fixation would reflect a differential effect of Dox-Biotin on the H2A.Z-nucleosomes of the two cell lines. Indeed, significantly more Dox-Biotin was bound to the DNA of the DKO/ΔC nuclei compared to the control (Fig. 16E, F). This demonstrated that the H2A.Z nucleosomes lacking the C-terminal tail are more readily susceptible to intercalator-induced eviction, confirming that the tail contributes to nucleosome stability.

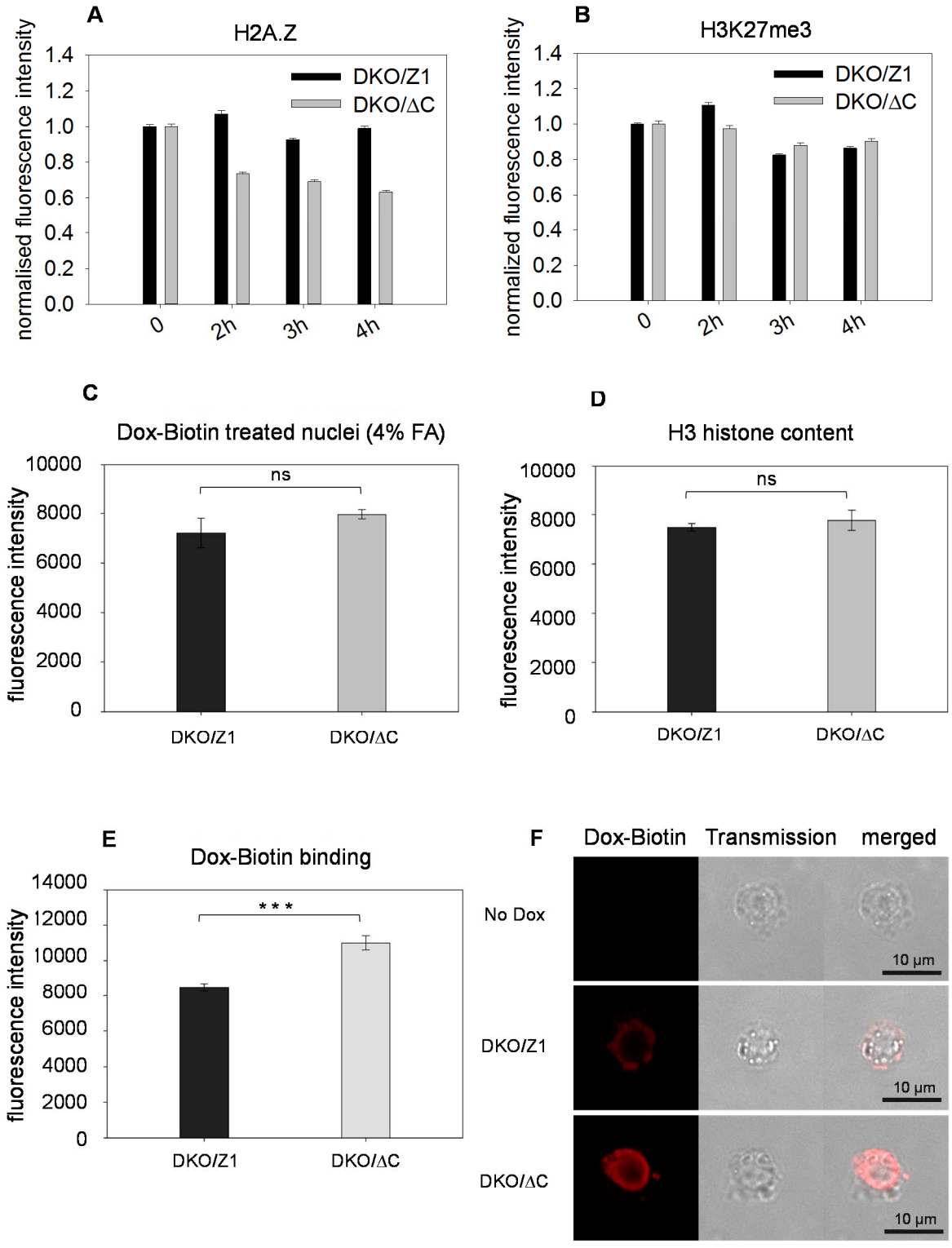

Figure 16: Histone eviction by Doxorubicin and its binding in DKO/ΔC compared to DKO/Z1 nuclei. (A) H2A.Z and **(B)** H3K27me3-containing nucleosomes remained in DKO/Z1

and DKO/ΔC nuclei, after Dox treatment (9 μM), measured in the same co-labeled sample as an internal control for each other. The mean fluorescence intensity of ~600 G1 phase nuclei gated according to their DNA content measured by LSC. The error bars representing the SEM values are shown. **(C)** Dox-Biotin binding in the nucleus of DKO/Z1 and DKO/ΔC cells after fixation with 4% paraformaldehyde before Dox-Biotin treatment (1 μM). ns: no significant difference (p= 0.1050). **(D)** The amount of immunolabeled H3 in the DKO/Z1 and DKO/ΔC nuclei. ns: no significant difference (p = 0.3227). **(E)** Comparison of Dox-Biotin binding to DNA in unfixed DKO/ΔC and DKO/Z1 nuclei. The columns represent the average immunofluorescence of nuclei quantified by LSC, utilizing labeled anti-biotin. Bar charts represent the mean fluorescence intensities, with error bars indicating the SD for 3 biological replicates. The significant difference represented as (*** p=0.0007). **(F)** Representative CLSM images showing Dox-Biotin within the nuclei of the cell line pairs. No Dox: intercalator-untreated DKO/Z1 nuclei**.** An unpaired t-test was used for statistical analysis (in panels C, D, and E).

2.2. The C-terminal H2A.Z tail binds to DNA in a superhelicity-dependent manner

The significant differences in the behavior of H2A.Z-containing nucleosomes in DKO/Z1 and DKO/ΔC nuclei in intercalator elution (Fig. 15), in intercalator binding (Fig. 16), and also in their response to nickase treatment ([159]; data not shown) raised the possibility that the H2A.Z C-terminal tail might bind to DNA in a superhelicity-dependent manner. To investigate this hypothesis, Fluorescence correlation spectroscopy (FCS) was used to assess the binding of the carboxyfluorescein-labeled tail peptide (CF-C9) to circular plasmid DNA in its different topological forms (superhelical and relaxed), prepared as described in Materials and Methods. Supercoiled, nicked (relaxed) and linearized plasmid DNA mixtures were run on a 1% agarose gel (Fig. 17A). The appropriate DNA bands were excised from the agarose gel, purified, and used for subsequent FCS measurements.

The diffusion constant *(D)* for both CF-C9 and CF-SCR (used as a negative control) peptides in solution as determined by FCS was around 200 $\mu m^2/s$ (Fig. 17B). In the presence of native plasmid DNA two diffusing components were observed: a fast component represented by the diffusion coefficients D_1 corresponding to freely diffusing CF-C9 and CF-SCR ($D_1 \sim$ 200 $\mu m^2/s$) (Fig. 17B) and a slow component represented by the diffusion coefficient D_2 ($D_2 \sim 3$ $\mu m^2/s$), which is interpreted as a complex formation (DNA-bound CF-C9) (Fig. 17C).

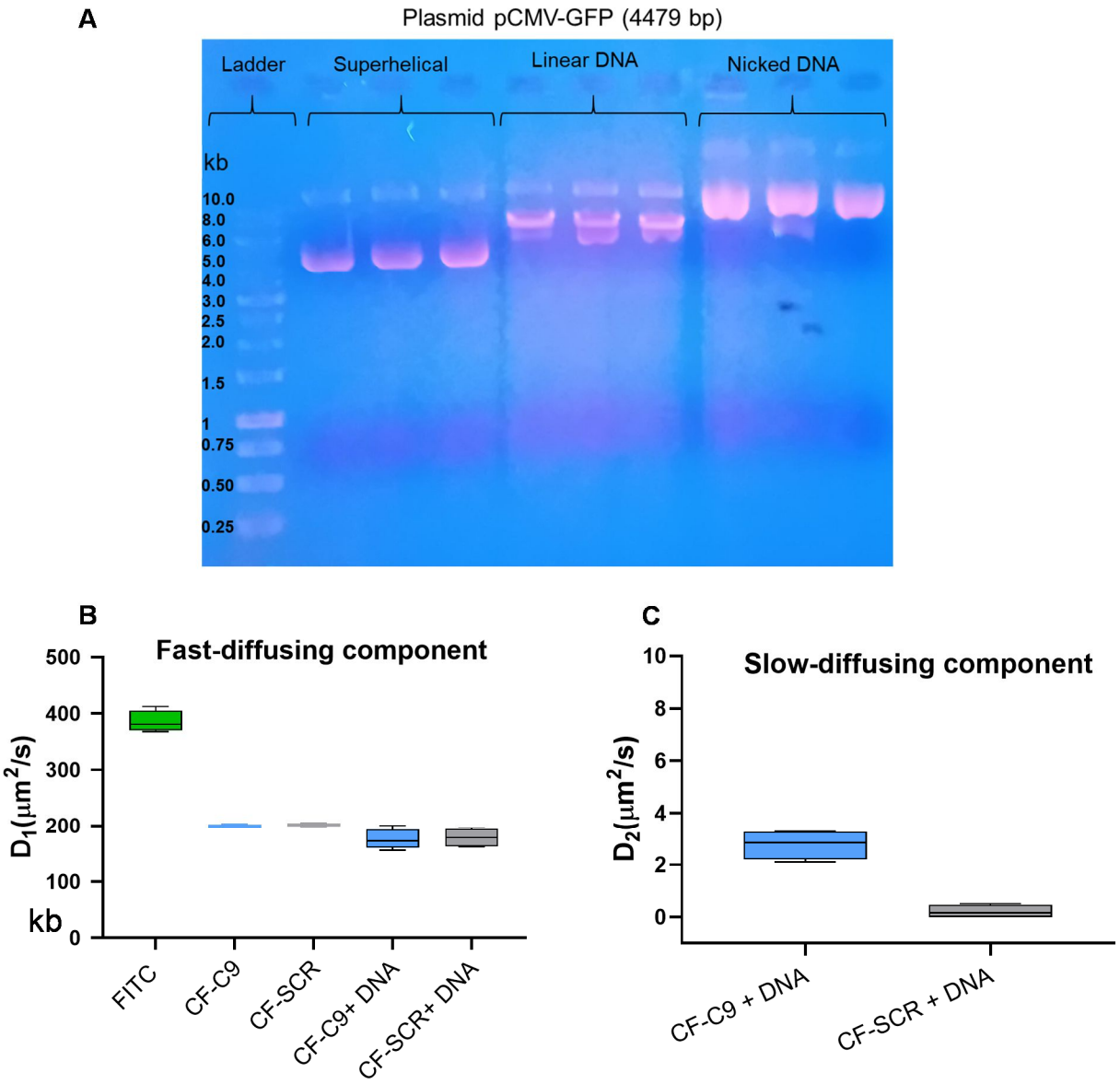

Figure 17: FCS characterization of fast- and slow-diffusing components in peptide–DNA complexes. (A) Agarose gel electrophoresis of plasmid DNA was performed by loading 1.5 µg mixtures containing equal amounts of nicked, linear, and supercoiled plasmid DNA into a 1% agarose gel. The different DNA bands are shown. **(B)** FCS analysis of the fast-moving component showing the diffusion coefficients *(D_1)* of FITC-labeled peptides (CF-C9 and CF-SCR) in solution, both in the presence and absence of plasmid DNA, as measured by FCS. **(C)** FCS analysis of the slow-diffusing component showing the diffusion coefficients *(D_2)* of the CF-C9 peptide when bound to plasmid DNA, as measured by FCS in solution. (The gel was overloaded with the samples to enable the preparation of sufficient amounts of the DNA fragments, what made the bands run slower than what is dictated by their true size).

The FCS results showed that CF-C9 preferentially bound to the supercoiled plasmid, unlike the control peptide (CF-SCR) (Fig. 18A, B). As expected, the fast diffusion constant *(D_1)* of the dye-labeled peptides (CF-C9 and CF-SCR) was lower than that of the fluorescent dye (FITC) alone (Fig. 18C), while the diffusion constant of the slow component *(D_2)* of CF-C9 in the presence of the Sh (Superhelical) plasmid was even lower (Fig. 18D).

The D value characterizing the motion of the center of mass of superhelical plasmids was found to be proportional to the -2.2 power of the plasmid length [160]; based on this model and on the *D* value of a 5.9 kb supercoiled plasmid determined by differential dynamic microscopy (0.44 $\mu m^2/s$), the predicted *D* value of our 4.48 kb supercoiled plasmid would be 0.81 $\mu m^2/s$. The FCS-determined D_2 of the slow component was ~2-3 $\mu m^2/s$ (Fig. 18D). Considering that the plasmid exhibits internal motion superimposed on the motion of the center of mass thereby increasing the apparent *D*, this value can be attributed to the motion of the DNA-bound CF-C9. As a conclusion, the CF-labeled nonapeptide representing the C-terminal end of H2A.Z preferentially binds to the superhelical plasmid DNA as compared with the relaxed plasmid, suggesting that the C-terminus of the native protein may also engage with the DNA in chromatin in a superhelicity-dependent manner.

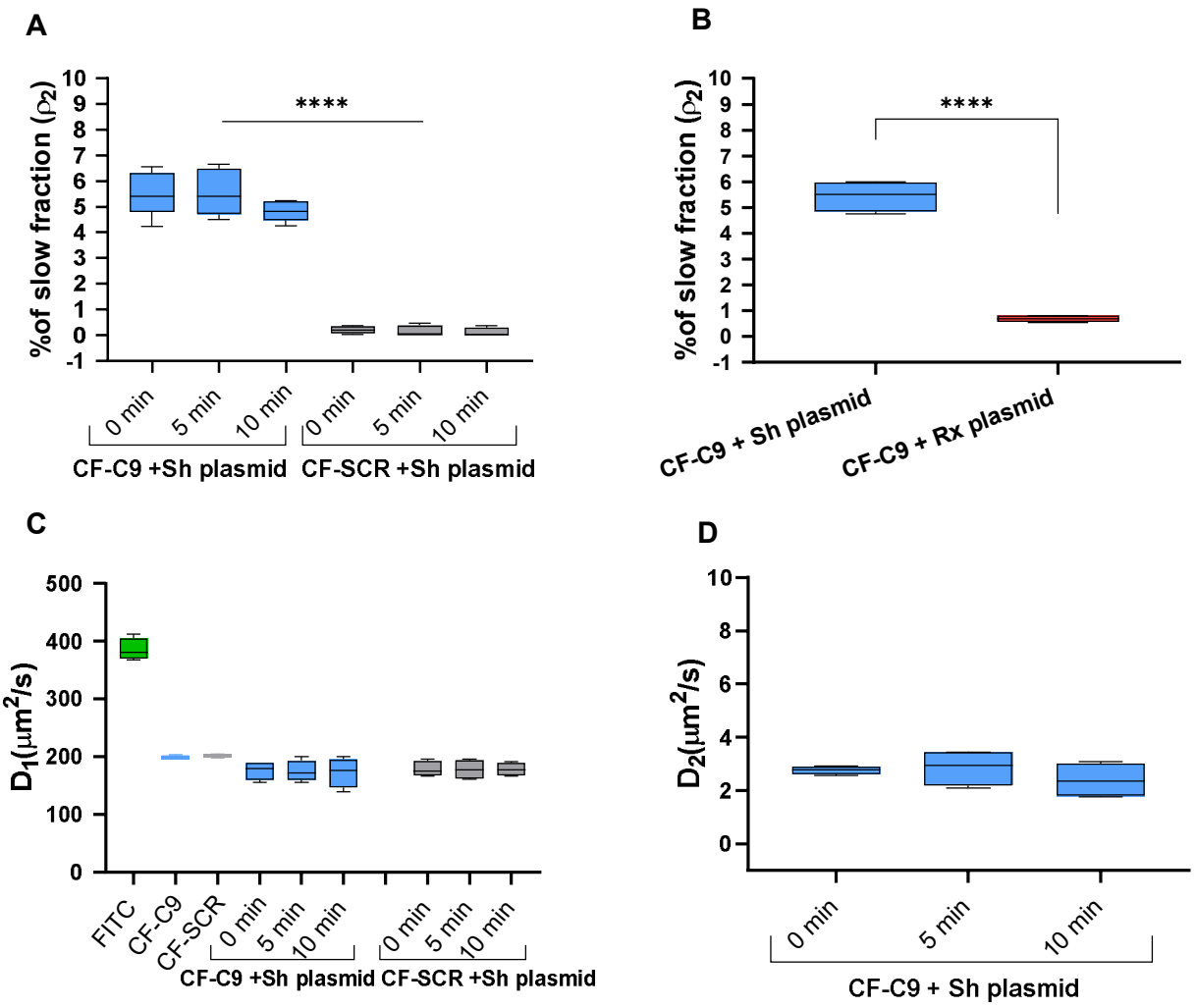

Figure 18: Measurement of CF-C9 binding to superhelical plasmid DNA by FCS. (A) The slow fraction *(ρ_2)* of CF-C9 and CF-SCR peptides mixed with superhelical (Sh) plasmid DNA. These peptides were incubated with the plasmid for 0 (measured immediately after addition), 5 and 10 minutes. The slow fraction *(ρ_2)* was determined from the autocorrelation function (ACF) fits and shown as a box-and-whisker plot. There is a significant difference between CF-C9+Sh and CF-SCR+Sh plasmids (*** p=0.0001). One-way ANOVA test was used for statistical analysis. **(B)** Comparison of the slow fraction *(ρ_2)* of CF-C9 incubated with superhelical (Sh) and incubated with relaxed (Rx) plasmid DNA. There is a significant difference between CF-C9+Sh and CF-C9+Rx plasmids (*** p=0.0001). Unpaired t test was used for statistical analyses. **(C)** Diffusion Coefficient D_1 corresponds to the fast-diffusing component, while **(D)** D_2 corresponds to the slow-diffusing component of panel A.

2.3. The effect of the C-terminal H2A.Z tail on cell proliferation

The superhelicity-dependent binding of the C-terminal H2A.Z tail to DNA, or its absence due to shielding e.g. when bound to a reader protein, may have significant biological importance. To address this possibility, I investigated the effect of the C-terminal tail on cell proliferation using cell growth assays. I compared the proliferation of DKO/Z1 and DKO/ΔC by counting cell numbers at different time points, immediately after splitting and at 24 h and 48 h of culture. At 24 h, DKO/ΔC cells displayed a significantly smaller cell count compared to the control DKO/Z1 cells. At 48 h, although both cells continued to proliferate, DKO/ΔC cells consistently showed lower cell numbers (Fig. 19A), suggesting an impaired proliferative capacity.

To confirm the difference between the growth rates, I compared the cell cycle distribution using flow cytometric measurement of their DNA content based on PI staining. The DNA distribution histograms revealed marked differences between the two cell lines. The truncation of the C-terminal H2A.Z tail in DKO/ΔC cells showed a smaller altered fraction of S, and G2/M cells compared to DKO/Z1 cells (Fig. 19B), indicating that the DKO/ΔC cells spend longer time in G1 implying an impaired cell cycle progression. To directly assess S-phase, I used the EdU (5-ethynyl-2′-deoxyuridine) incorporation assay. EdU is a specially derivatized thymidine analogue that is incorporated into DNA during active DNA replication, and its detection via click chemistry using a fluorescent azide allows the quantification of cells which are in S-phase during the period of EdU incubation [161]. In line with the cell counting and cell cycle analysis, when I compared these cells at 4h and 24h after splitting, I found that DKO/ΔC cells exhibited a significantly reduced fraction of EdU-positive cells (20.88%) relative to DKO/Z1 (40.41%) at 4h (Fig. 19C). At 24 h, although the percentage of EdU-positive cells increased in both cell lines, DKO/Z1 cells still showed a higher fraction (45.23%) relative to DKO/ΔC (36.48%) (Fig. 19D, E). This indicates that the absence of the C-terminal H2A.Z tail leads to a significant proliferation deficiency. This suggests that this histone variant domain is essential for cell cycle progression and proliferative capacity, confirming that the C-terminal H2A.Z tail contributes not only to chromatin organization but also to the biological behavior of the cells.

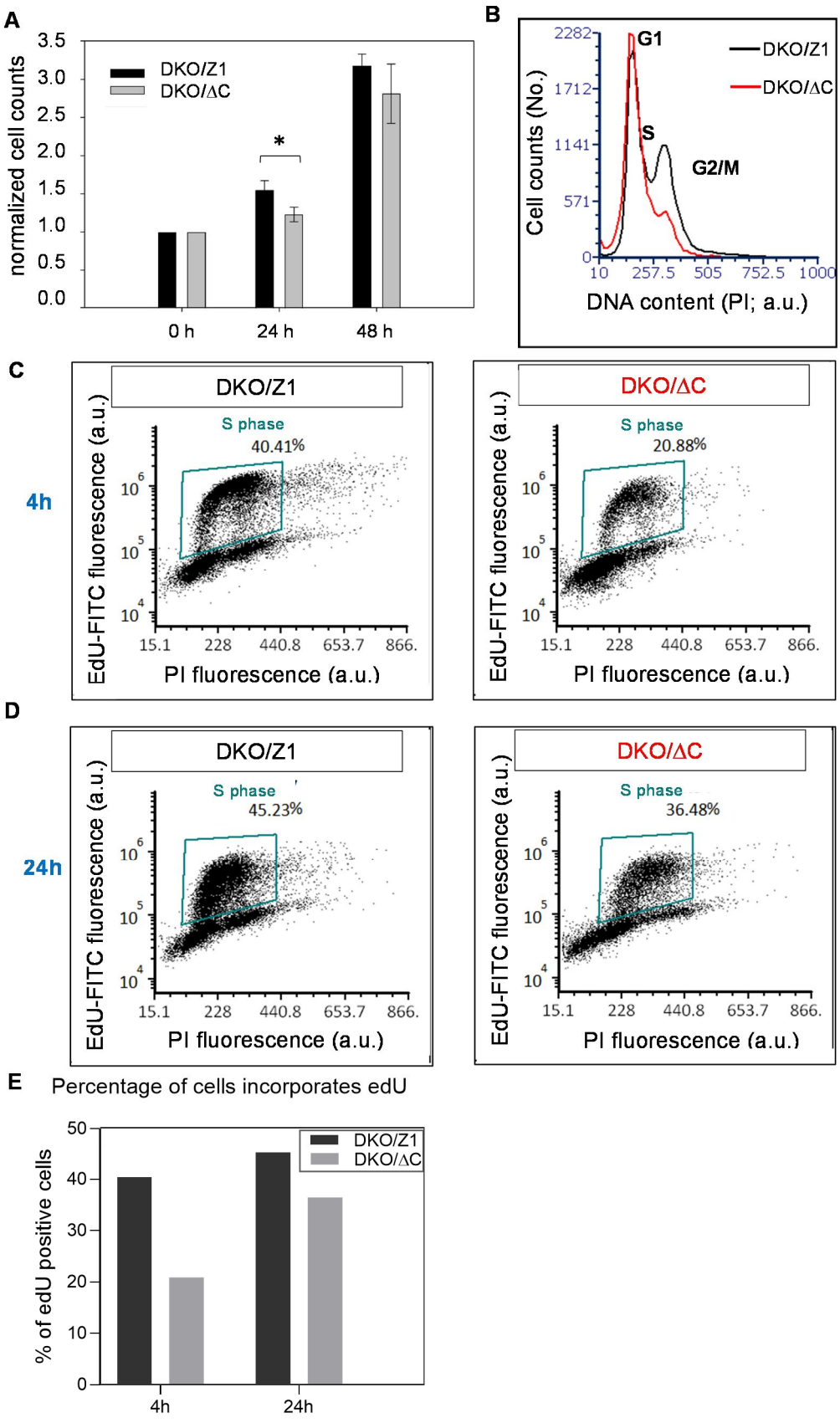
A
normalized cell counts
3.5
3.0
2.5
2.0
1.5
1.0
0.5
0.0
DKO/Z1
DKO/ΔC
*
0 h
24 h
48 h
B
Cell counts (No.)
2282
1712
1141
571
0
G1
S
G2/M
DKO/Z1
DKO/ΔC
10
257.5
505
752.5
1000
DNA content (PI; a.u.)
C
4h
DKO/Z1
S phase
40.41%
EdU-FITC fluorescence (a.u.)
PI fluorescence (a.u.)
15.1
228
440.8
653.7
866.
DKO/ΔC
S phase
20.88%
D
24h
DKO/Z1
S phase
45.23%
DKO/ΔC
S phase
36.48%
E
Percentage of cells incorporates edU
% of edU positive cells
50
40
30
20
10
0
DKO/Z1
DKO/ΔC
4h
24h

Figure 19: The effect of the lack of C-terminal H2A.Z tail on cell proliferation. (A) Normalized cell counts of DKO/ΔC and DKO/Z1 cells at different time points upon cell culturing. Error bars representing the SD of 3 independent experiments. There is a significant difference between DKO/Z1 and DKO/ΔC (* p=0.0234) **(B)** DNA distribution histograms of the cell pair obtained on day 0 of culturing. **(C)** Comparison of cell proliferation of DKO/Z1 and DKO/ΔC cells using the EdU incorporation assay 4h and **(D)** 24 h after splitting the cells using flow cytometry. (**E)** Percentage of cells incorporating EdU (utilizing the gates shown in panels C and D) after 4 h and 24 h of cell culturing before EdU addition.

DISCUSSION

Several independent lines of evidence show that the stability of H2A.Z-nucleosomes is dependent upon the C-terminal tail of the histone variant

To investigate the role of the unstructured C-terminal tail of H2A.Z in determining nucleosome stability, we examined the H2A.Z-nucleosomes in HeLa and melanoma nuclei and live cells, as well as in the nuclei of a DT40 cell line pair expressing either the full-length human H2A.Z1 (DKO/Z1) or its C-terminally truncated version (DKO/ΔC) [148]. These experiments were performed using the QINESIn assay developed in our lab [57], recording elution curves indicative of the off-rate of specific histones released from nucleosomes *in situ* upon exposure to salt (mainly the work of Dr. Imre László) and to intercalators (mainly my work).

The behavior of H2A.Z nucleosomes in HeLa under increasing concentrations of EBr, exhibited remarkable differences relative to H2A, H2A.X, or H3 containing nucleosomes. In particular, H2A.Z nucleosomes remained notably stable even at high EBr concentrations, suggesting resistance to superhelical alterations induced by the intercalator (Fig. 14A, B). The effect of H2A.Z C-terminal tail on nucleosome stability was also reproducible in the intercalator elution assay using the DT40 system. Nucleosomes containing full-length (DKO/Z1) or truncated H2A.Z C-terminal tail (DKO/ΔC) displayed distinct behaviors upon exposure to EBr, with or without nickase pretreatment (Fig. 15A, C), consistent with the salt elution data (Fig. 10). In this assay, the EBr was applied together with 750 mM NaCl solution, based on the titration of the salt concentration sufficient to allow EBr to destabilize nucleosomes described in our earlier publication [57], in line with the critical salt concentration where a major conformational change occurs in the nucleosomes involving mainly the dimers [162]. In contrast, the use of a different intercalator, Dox [153], does not require the addition of salt, as it is particularly effective in facilitating nucleosome eviction, according to our previous studies [57]. This property enabled the assessment of the impact of the H2A.Z C-terminal tail on nucleosome stability under near-physiological conditions, thereby validating our previous results from the EBr elution assay and confirming the tail dependent effect on nucleosome stability (Fig. 16A, B). These findings were further confirmed when I showed that the increased level of H2A.Z eviction upon C-terminal tail deletion in DKO/ΔC cells correlates with a higher level of DNA binding by Dox-Biotin (Fig. 16E, F).

Where does the tail bind in chromatin?

The observations involving the anthracyclin raised an important question: How do intercalators destabilize nucleosomes if they mainly bind to internucleosomal DNA, as shown in the case of Dox-Biotin [153]? Thus, although EBr or Dox can also intercalate within nucleosomal DNA, thereby altering its superhelicity [163] (Katalin Toth, DKFZ/UD; oral communication), since differences in Dox sensitivity between full-length and truncated C-terminal H2A.Z nucleosomes were observed at both low (1 µg/ml) (Fig. 16E) and high (9 µg/ml) (Fig. 16 A) Dox concentrations, we suggest that the tail binds to superhelical internucleosomal DNA. Since the plectonemic structure of the nucleosome-free DNA at the promoters resembles best the supercoiled plasmid of the FCS experiments, and because the superhelical density of the internucleosomal linker DNA is highly variable according to the twin-supercoil model [68], the primary target of the tail might be the promoter.

The mechanism of nucleosome destabilization by intercalators

The superhelicity of nucleosomal DNA meets the steric and topological requirements of its winding around the histone core more than once, approximately 1.6 times. When the DNA is negatively superhelical, the dynamic equilibrium between nucleosome formation and eviction favors nucleosome formation. When the DNA is relaxed by intercalation of planar DNA dyes (EBr or Dox) or relaxed by nicking, this winding is no longer supported by the favorable changes in free energy and entropy that accompany nucleosome formation in intact DNA, thereby disturbing the equilibrium. As a result, nucleosomes are more likely to dissociate, as the balance between the on-rate and off-rate of nucleosome formation shifts toward eviction.

Our FCS data revealed that the H2A.Z C-terminal tail (experimentally represented by the C9) binds to superhelical DNA; however, the exact binding sites in chromatin are yet to be determined. These possible interaction sites are illustrated in a graphical model (Fig. 20) considering potential binding sites in the internucleosomal linker DNA, nucleosomal DNA or DNA within nucleosome-free regions. Nucleosomal DNA, wound around the octamer core, has a toroidal superhelicity structure with varying twist values (toroid writhe), whereas DNA in nucleosome-free regions is typically plectonemic (plectonemic writhe) upon nucleosome eviction. In internucleosomal linker DNA, superhelicity changes dynamically during transcription of a particular chromatin loop (topological unit). If the C-terminal tail binds to linker DNA, this interaction would be

transcription-sensitive and preferentially target the underwound DNA (negatively supercoiled) regions, like those upstream of the RNA polymerase. At plectonemic, nucleosome-free regions (e.g. promoters), the tail could bind, unless the same regions get relaxed by topoisomerases or transient DNA breaks arising in any other plausible mechanism [164] would be expected to prevent tail binding. These dynamics offer an intriguing model for the behavior of H2A.Z-containing nucleosomes during transcription. Since the superhelical state of the plasmid DNA we used in our FCS resembles best the plectonemic structure that emerges following nucleosome eviction at the promoters, we favor this model, rather than models where the peptide would bind to the internucleosomal DNA or the DNA of the nucleosome that forms toroid rather than plectonemic supercoils.

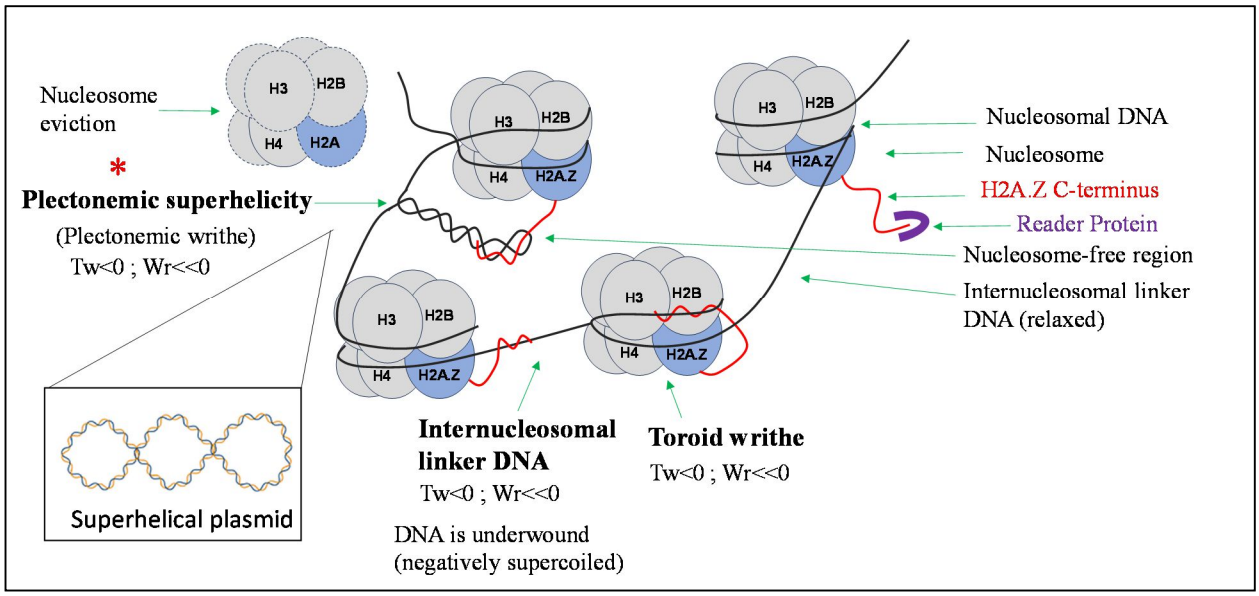

Figure 20: Graphical model illustrating the interaction sites where the C-terminal H2A.Z tail binds to DNA in a superhelicity dependent fashion.

The star (*) in the model demonstrates the alternative mechanistic explanation that appears to be most consistent with our observations on nucleosome stability, nuclear architecture, and chromatin accessibility.

Biological significance of the DNA superhelicity-dependent molecular interaction demonstrated

The general role of the C-terminal H2A.Z tail in overall chromatin architecture and nucleosome stability demonstrated under close-to-native conditions draws attention to its potential impact on

the biological behavior of cells. This view was supported by our cell proliferation studies, which revealed that deletion of the C-terminal tail led to altered cell cycle progression and a marked decrease in cell growth and proliferation (Fig. 19), consistent with previous studies [136]. This interaction may involve H2A.Z in the heterochromatic nucleosomes, while those in euchromatin, being prevented from the stabilizing interaction due to reader protein binding, would be allow the tail-independent stability-lowering effects of the variant become manifest [116].

Our results highlight the possibility that superhelicity-dependent interactions between DNA and certain histone tails may be exploited by the cell for regulatory functions. Although its role in gene regulation are generally accepted as of great significance [165], the concrete examples of experimental observations implying that the superhelical state of DNA could be sensed by a molecular interaction and potentially translated into regulatory cues are rare. One such example is the Far Upstream Element of the c-myc oncogene (FUSE) and its interaction of the regulatory protein FBP [166]. The superhelicity-dependent binding of H2A.Z to the DNA, substantiated in our work, may be a further example worthy of further investigations in this direction.

Limitations of our studies

Our working hypothesis and interpretational context are focused on the possible interactions between the C-terminus of H2A.Z and the fundamental chromatin constituents. However, there are various interacting partners conserved in evolution which may also contribute some of the phenomena observed in our studies. Among the known molecular partners interacting with the H2A.Z C-terminal tail, the histone chaperone ANP32E facilitates the removal of the H2A.Z–H2B dimer from chromatin [138], similarly to the Chz1 chaperone in *S. cerevisiae* [139]. ANP32E also prevents H2A.Z deposition at promoter regions in mouse fibroblasts [96], emphasizing the importance of the C-terminal tail mediated interactions in gene regulation and genome stability [136]. This interaction and the one involving PWWP2A [167] were the main known partnerships in the H2A.Z molecular landscape before our group's contributions to the field. Their possible role in the effects studied in our work has not been directly assessed.

Practical considerations

The sensitivity of the intercalator-elution approach to the presence or absence of a nonapeptide in the C-terminal tail of the histone variant demonstrated in our work suggests that the intercalator-based QINESIn assay could be applied to assess nucleosome stability in other similar experimental scenarios, maintaining conditions close-to-native experimental conditions.

The superhelicity-dependence of the binding of the labeled C9 peptide to DNA raises the possibility that the agent could be used as a detector of superhelical density, similarly to the psoralen technique currently used for this purpose. The possible advantages or disadvantages of such an application could be assessed only after the question whether the tail binds to the internucleosomal DNA, to plectonemic, nucleosome-free regions or to nucleosomal DNA will have been answered.

Conclusions

We have presented several independent lines of evidence demonstrating that the stability of H2A.Z-containing nucleosomes is dependent on the C-terminal tail. Multiple complementary assays, including EBr elution, Dox elution, and quantification of Dox-Biotin binding to DNA, consistently revealed decreased stability in nucleosomes lacking their C-terminal H2A.Z tail. Together with the previously reported salt-elution results, we provide four independent methodological approaches supporting the conclusion that the H2A.Z C-terminal tail has an essential role in nucleosome stability. These findings are also supported by the FCS data (Fig. 18), which validate the pivotal role of the C-terminal tail in stabilizing nucleosomes and reveal that the tail mediates molecular interactions through preferential binding to superhelical rather than relaxed DNA (Fig. 18B).

The findings my work contributed to fit the scenario of the three categories of H2A.Z nucleosomes identified: **(H2A.Zhc)**-stable nucleosomes in which the C-terminal tail binds to superhelical DNA; **(H2A.Zeu)**-less stable nucleosomes where the tail primarily interacts with molecular partners rather than DNA; and **(H2A.Zlmn)**-the most stable fraction, in which the tail establishes strong associations with the nuclear lamina.

Future directions of research

The prominent H3K9me3 signal, a marker of constitutive heterochromatin [45], was observed at the periphery in DKO/Z1 relative to DKO/ΔC nuclei, supporting a role for the C-terminal H2A.Z tail also in higher-order chromatin organization. On the other hand, these spectacular differences and changes upon addition of the C9 peptide to nuclei or live cells were accompanied by transitions in H2A.Z nucleosomal stability. Whether these tail-dependent effects are mechanistically connected or represent parallel but causally unrelated effects, is one of the important questions yet to be elucidated.

SUMMARY

Using an *in situ* assay of nucleosome stability called QINESIn, developed in our lab, recording elution curves indicative of the off-rate of specific histones released from nucleosomes *upon exposure to* salt or intercalator, I studied the stability of the nucleosomes containing the histone variant H2A.Z. The distinct stability features of H2A.Z nucleosome were found to be dependent on the C-terminal H2A.Z tail in the salt-elution format of QINESIn, which assesses intrinsic nucleosome stability. Moreover, the stability features of H2A.Z-nucleosomes could be modulated when we introduced a synthetic peptide resembling the C-terminal H2A.Z tail into live cells using a cyclodextrin-based procedure. These findings were further validated with an alternative approach, the intercalator-elution format of QINESIn, using the intercalating agents EBr and Dox, a assessing nucleosome stability by altering DNA superhelicity, rather than disrupting ionic and hydrogen bonds with salt. Importantly, the changes in DNA superhelicity naturally occur *in vivo* during e.g. transcriptional processes, suggesting that the differences in nucleosome stability detected by this assay may have direct biological significance. Using a DT40 cell line pair expressing either the full-length human H2A.Z1 or its C-terminally truncated version, we found that nucleosome stability is tail-dependent also through the spectacles of intercalator sensitivity. This conclusion was confirmed in experiments studying the binding of Dox-Biotin to DNA. Fluorescence correlation spectroscopy (FCS) also supported these findings, when I revealed that the H2A.Z-tail nonapeptide preferentially binds to supercoiled rather than relaxed-plasmid DNA. The DNA topology-dependent binding of the unstructured C-terminal tail of H2A.Z, by modulating nucleosome stability, may be functionally significant in various roles of the histone variant as shown in our cell proliferation studies. Our work demonstrates the interplay between DNA topology and nucleosome stability and opens new avenues for further studies on how it may be exploited by the cell for regulatory functions.

KEYWORDS

H2A.Z

C-terminal tail

Superhelicity

Nucleosome stability

QINESIn

FCS

DT40 cells

C9 peptide

REFERENCES

1. Paweletz N. Walther Flemming: pioneer of mitosis research. Nat Rev Mol Cell Biol 2001;**2**(1):72-5 doi: 10.1038/35048077.
2. Felsenfeld G, Groudine M. Controlling the double helix. Nature 2003;**421**(6921):448-53 doi: 10.1038/nature01411.
3. Kornberg RD, Lorch Y. Twenty-five years of the nucleosome, fundamental particle of the eukaryote chromosome. Cell 1999;**98**(3):285-94 doi: 10.1016/s0092-8674(00)81958-3.
4. Hou Z, Zhang P. In-cell chromatin structure by Cryo-FIB and Cryo-ET. Curr Opin Struct Biol 2025;**92**:103060 doi: 10.1016/j.sbi.2025.103060 [published Online First: 20250510].
5. Ambrosio S, Noviello A, Di Fusco G, et al. Interplay and Dynamics of Chromatin Architecture and DNA Damage Response: An Overview. Cancers (Basel) 2025;**17**(6) doi: 10.3390/cancers17060949 [published Online First: 20250311].
6. Hoencamp C, Rowland BD. Genome control by SMC complexes. Nat Rev Mol Cell Biol 2023;**24**(9):633-50 doi: 10.1038/s41580-023-00609-8 [published Online First: 20230525].
7. Baxter J, Aragon L. A model for chromosome condensation based on the interplay between condensin and topoisomerase II. Trends Genet 2012;**28**(3):110-7 doi: 10.1016/j.tig.2011.11.004 [published Online First: 20120110].
8. Parmar JJ, Woringer M, Zimmer C. How the Genome Folds: The Biophysics of Four-Dimensional Chromatin Organization. Annu Rev Biophys 2019;**48**:231-53 doi: 10.1146/annurev-biophys-052118-115638 [published Online First: 20190305].
9. Staynov DZ, Proykova YG. The sequentiallity of nucleosomes in the 30 nm chromatin fibre. FEBS J 2008;**275**(15):3761-71 doi: 10.1111/j.1742-4658.2008.06522.x [published Online First: 20080628].
10. Kruithof M, Chien FT, Routh A, Logie C, Rhodes D, van Noort J. Single-molecule force spectroscopy reveals a highly compliant helical folding for the 30-nm chromatin fiber. Nat Struct Mol Biol 2009;**16**(5):534-40 doi: 10.1038/nsmb.1590 [published Online First: 20090419].
11. Nikitina T, Norouzi D, Grigoryev SA, Zhurkin VB. DNA topology in chromatin is defined by nucleosome spacing. Sci Adv 2017;**3**(10):e1700957 doi: 10.1126/sciadv.1700957 [published Online First: 20171027].

12. Maeshima K, Matsuda T, Shindo Y, et al. A Transient Rise in Free Mg(2+) Ions Released from ATP-Mg Hydrolysis Contributes to Mitotic Chromosome Condensation. Curr Biol 2018;**28**(3):444-51 e6 doi: 10.1016/j.cub.2017.12.035 [published Online First: 20180118].
13. Maeshima K, Laemmli UK. A two-step scaffolding model for mitotic chromosome assembly. Dev Cell 2003;**4**(4):467-80 doi: 10.1016/s1534-5807(03)00092-3.
14. Rao SS, Huntley MH, Durand NC, et al. A 3D map of the human genome at kilobase resolution reveals principles of chromatin looping. Cell 2014;**159**(7):1665-80 doi: 10.1016/j.cell.2014.11.021 [published Online First: 20141211].
15. Dehingia B, Milewska M, Janowski M, Pekowska A. CTCF shapes chromatin structure and gene expression in health and disease. EMBO Rep 2022;**23**(9):e55146 doi: 10.15252/embr.202255146 [published Online First: 20220822].
16. Parelho V, Hadjur S, Spivakov M, et al. Cohesins functionally associate with CTCF on mammalian chromosome arms. Cell 2008;**132**(3):422-33 doi: 10.1016/j.cell.2008.01.011 [published Online First: 20080131].
17. Davidson IF, Peters JM. Genome folding through loop extrusion by SMC complexes. Nat Rev Mol Cell Biol 2021;**22**(7):445-64 doi: 10.1038/s41580-021-00349-7 [published Online First: 20210325].
18. Dixon JR, Selvaraj S, Yue F, et al. Topological domains in mammalian genomes identified by analysis of chromatin interactions. Nature 2012;**485**(7398):376-80 doi: 10.1038/nature11082 [published Online First: 20120411].
19. Dekker J, Mirny LA. The chromosome folding problem and how cells solve it. Cell 2024;**187**(23):6424-50 doi: 10.1016/j.cell.2024.10.026.
20. Kornberg RD. Chromatin structure: a repeating unit of histones and DNA. Science 1974;**184**(4139):868-71 doi: 10.1126/science.184.4139.868.
21. Olins AL, Olins D. 50th Anniversary of the Nucleosome Discovery: a Brief Essay. Postepy Biochem 2024;**70**(1):39-40 doi: 10.18388/pb.2021_542 [published Online First: 20240523].
22. Olins DE, Olins AL, Von Hippel PH. Model nucleoprotein complexes: studies on the interaction of cationic homopolypeptides with DNA. J Mol Biol 1967;**24**(2):157-76 doi: 10.1016/0022-2836(67)90324-5.

23. McGinty RK, Tan S. Nucleosome structure and function. Chem Rev 2015;**115**(6):2255-73 doi: 10.1021/cr500373h [published Online First: 20141212].
24. Pepenella S, Murphy KJ, Hayes JJ. Intra- and inter-nucleosome interactions of the core histone tail domains in higher-order chromatin structure. Chromosoma 2014;**123**(1-2):3-13 doi: 10.1007/s00412-013-0435-8 [published Online First: 20130831].
25. Ausio J, Dong F, van Holde KE. Use of selectively trypsinized nucleosome core particles to analyze the role of the histone "tails" in the stabilization of the nucleosome. J Mol Biol 1989;**206**(3):451-63 doi: 10.1016/0022-2836(89)90493-2.
26. Polach KJ, Lowary PT, Widom J. Effects of core histone tail domains on the equilibrium constants for dynamic DNA site accessibility in nucleosomes. J Mol Biol 2000;**298**(2):211-23 doi: 10.1006/jmbi.2000.3644.
27. Luger K, Mader AW, Richmond RK, Sargent DF, Richmond TJ. Crystal structure of the nucleosome core particle at 2.8 A resolution. Nature 1997;**389**(6648):251-60 doi: 10.1038/38444.
28. Hergeth SP, Schneider R. The H1 linker histones: multifunctional proteins beyond the nucleosomal core particle. EMBO Rep 2015;**16**(11):1439-53 doi: 10.15252/embr.201540749 [published Online First: 20151015].
29. Zhang R, Erler J, Langowski J. Histone Acetylation Regulates Chromatin Accessibility: Role of H4K16 in Inter-nucleosome Interaction. Biophys J 2017;**112**(3):450-59 doi: 10.1016/j.bpj.2016.11.015 [published Online First: 20161206].
30. Tang D, Kang R, Zeh HJ, Lotze MT. The multifunctional protein HMGB1: 50 years of discovery. Nat Rev Immunol 2023;**23**(12):824-41 doi: 10.1038/s41577-023-00894-6 [published Online First: 20230615].
31. Orsetti A, van Oosten D, Vasarhelyi RG, et al. Structural dynamics in chromatin unraveling by pioneer transcription factors. Biophys Rev 2024;**16**(3):365-82 doi: 10.1007/s12551-024-01205-6 [published Online First: 20240704].
32. Panday A, Grove A. Yeast HMO1: Linker Histone Reinvented. Microbiol Mol Biol Rev 2017;**81**(1) doi: 10.1128/MMBR.00037-16 [published Online First: 20161130].
33. Bosire R, Nanasi P, Jr., Imre L, et al. Intercalation of small molecules into DNA in chromatin is primarily controlled by superhelical constraint. PLoS One 2019;**14**(11):e0224936 doi: 10.1371/journal.pone.0224936 [published Online First: 20191120].

34. Clapier CR, Cairns BR. The biology of chromatin remodeling complexes. Annu Rev Biochem 2009;**78**:273-304 doi: 10.1146/annurev.biochem.77.062706.153223.
35. Mueller-Planitz F, Klinker H, Becker PB. Nucleosome sliding mechanisms: new twists in a looped history. Nat Struct Mol Biol 2013;**20**(9):1026-32 doi: 10.1038/nsmb.2648.
36. Clapier CR, Iwasa J, Cairns BR, Peterson CL. Mechanisms of action and regulation of ATP-dependent chromatin-remodelling complexes. Nat Rev Mol Cell Biol 2017;**18**(7):407-22 doi: 10.1038/nrm.2017.26 [published Online First: 20170517].
37. Yan L, Wang L, Tian Y, Xia X, Chen Z. Structure and regulation of the chromatin remodeller ISWI. Nature 2016;**540**(7633):466-69 doi: 10.1038/nature20590 [published Online First: 20161205].
38. Karl LA, Peritore M, Galanti L, Pfander B. DNA Double Strand Break Repair and Its Control by Nucleosome Remodeling. Front Genet 2021;**12**:821543 doi: 10.3389/fgene.2021.821543 [published Online First: 20220112].
39. Li B, Carey M, Workman JL. The role of chromatin during transcription. Cell 2007;**128**(4):707-19 doi: 10.1016/j.cell.2007.01.015.
40. Krajewski WA. Histone Modifications, Internucleosome Dynamics, and DNA Stresses: How They Cooperate to "Functionalize" Nucleosomes. Front Genet 2022;**13**:873398 doi: 10.3389/fgene.2022.873398 [published Online First: 20220428].
41. Millan-Zambrano G, Burton A, Bannister AJ, Schneider R. Histone post-translational modifications - cause and consequence of genome function. Nat Rev Genet 2022;**23**(9):563-80 doi: 10.1038/s41576-022-00468-7 [published Online First: 20220325].
42. Kalashnikova AA, Porter-Goff ME, Muthurajan UM, Luger K, Hansen JC. The role of the nucleosome acidic patch in modulating higher order chromatin structure. J R Soc Interface 2013;**10**(82):20121022 doi: 10.1098/rsif.2012.1022 [published Online First: 20130227].
43. Santos-Rosa H, Schneider R, Bannister AJ, et al. Active genes are tri-methylated at K4 of histone H3. Nature 2002;**419**(6905):407-11 doi: 10.1038/nature01080 [published Online First: 20020911].
44. Cao R, Wang L, Wang H, et al. Role of histone H3 lysine 27 methylation in Polycomb-group silencing. Science 2002;**298**(5595):1039-43 doi: 10.1126/science.1076997 [published Online First: 20020926].

45. Lachner M, O'Carroll D, Rea S, Mechtler K, Jenuwein T. Methylation of histone H3 lysine 9 creates a binding site for HP1 proteins. Nature 2001;**410**(6824):116-20 doi: 10.1038/35065132.

46. Ahmad K, Henikoff S. Histone H3 variants specify modes of chromatin assembly. Proc Natl Acad Sci U S A 2002;**99 Suppl 4**(Suppl 4):16477-84 doi: 10.1073/pnas.172403699 [published Online First: 20020812].

47. Lewis TS, Sokolova V, Jung H, Ng H, Tan D. Structural basis of chromatin regulation by histone variant H2A.Z. Nucleic Acids Res 2021;**49**(19):11379-91 doi: 10.1093/nar/gkab907.

48. Redon C, Pilch D, Rogakou E, Sedelnikova O, Newrock K, Bonner W. Histone H2A variants H2AX and H2AZ. Curr Opin Genet Dev 2002;**12**(2):162-9 doi: 10.1016/s0959-437x(02)00282-4.

49. Jung H, Sokolova V, Lee G, Stevens VR, Tan D. Structural and Biochemical Characterization of the Nucleosome Containing Variants H3.3 and H2A.Z. Epigenomes 2024;**8**(2) doi: 10.3390/epigenomes8020021 [published Online First: 20240527].

50. Weischet WO, Tatchell K, Van Holde KE, Klump H. Thermal denaturation of nucleosomal core particles. Nucleic Acids Res 1978;**5**(1):139-60 doi: 10.1093/nar/5.1.139.

51. Yager TD, McMurray CT, van Holde KE. Salt-induced release of DNA from nucleosome core particles. Biochemistry 1989;**28**(5):2271-81 doi: 10.1021/bi00431a045.

52. Gloss LM, Placek BJ. The effect of salts on the stability of the H2A-H2B histone dimer. Biochemistry 2002;**41**(50):14951-9 doi: 10.1021/bi026282s.

53. Greil W, Igo-Kemenes T, Zachau HG. Nuclease digestion in between and within nucleosomes. Nucleic Acids Res 1976;**3**(10):2633-44 doi: 10.1093/nar/3.10.2633.

54. Killian JL, Li M, Sheinin MY, Wang MD. Recent advances in single molecule studies of nucleosomes. Curr Opin Struct Biol 2012;**22**(1):80-7 doi: 10.1016/j.sbi.2011.11.003 [published Online First: 20111213].

55. Burgos-Bravo F, Tong AB, Li C, et al. FACT weakens the nucleosomal barrier to transcription and preserves its integrity by forming a hexasome-like intermediate. Mol Cell 2025;**85**(11):2097-109 e8 doi: 10.1016/j.molcel.2025.05.002 [published Online First: 20250523].

56. Pang B, Qiao X, Janssen L, et al. Drug-induced histone eviction from open chromatin contributes to the chemotherapeutic effects of doxorubicin. Nat Commun 2013;**4**:1908 doi: 10.1038/ncomms2921.

57. Imre L, Simandi Z, Horvath A, et al. Nucleosome stability measured in situ by automated quantitative imaging. Sci Rep 2017;**7**(1):12734 doi: 10.1038/s41598-017-12608-9 [published Online First: 20171006].

58. Lipfert J, Klijnhout S, Dekker NH. Torsional sensing of small-molecule binding using magnetic tweezers. Nucleic Acids Res 2010;**38**(20):7122-32 doi: 10.1093/nar/gkq598 [published Online First: 20100712].

59. Teves SS, Weber CM, Henikoff S. Transcribing through the nucleosome. Trends Biochem Sci 2014;**39**(12):577-86 doi: 10.1016/j.tibs.2014.10.004.

60. Babokhov M, Hibino K, Itoh Y, Maeshima K. Local Chromatin Motion and Transcription. J Mol Biol 2020;**432**(3):694-700 doi: 10.1016/j.jmb.2019.10.018 [published Online First: 20191102].

61. Benjamin LR, Chung HJ, Sanford S, Kouzine F, Liu J, Levens D. Hierarchical mechanisms build the DNA-binding specificity of FUSE binding protein. Proc Natl Acad Sci U S A 2008;**105**(47):18296-301 doi: 10.1073/pnas.0803279105 [published Online First: 20081117].

62. Bowman GD, Poirier MG. Post-translational modifications of histones that influence nucleosome dynamics. Chem Rev 2015;**115**(6):2274-95 doi: 10.1021/cr500350x [published Online First: 20141126].

63. Lorch Y, Maier-Davis B, Kornberg RD. Mechanism of chromatin remodeling. Proc Natl Acad Sci U S A 2010;**107**(8):3458-62 doi: 10.1073/pnas.1000398107 [published Online First: 20100208].

64. Fierz B. Dynamic Chromatin Regulation from a Single Molecule Perspective. ACS Chem Biol 2016;**11**(3):609-20 doi: 10.1021/acschembio.5b00832 [published Online First: 20151125].

65. Happel N, Doenecke D. Histone H1 and its isoforms: contribution to chromatin structure and function. Gene 2009;**431**(1-2):1-12 doi: 10.1016/j.gene.2008.11.003 [published Online First: 20081114].

66. Kaczmarczyk A, Meng H, Ordu O, Noort JV, Dekker NH. Chromatin fibers stabilize nucleosomes under torsional stress. Nat Commun 2020;**11**(1):126 doi: 10.1038/s41467-019-13891-y [published Online First: 20200108].

67. Wang JC. Helical repeat of DNA in solution. Proc Natl Acad Sci U S A 1979;**76**(1):200-3 doi: 10.1073/pnas.76.1.200.

68. Liu LF, Wang JC. Supercoiling of the DNA template during transcription. Proc Natl Acad Sci U S A 1987;**84**(20):7024-7 doi: 10.1073/pnas.84.20.7024.

69. Pommier Y, Nussenzweig A, Takeda S, Austin C. Human topoisomerases and their roles in genome stability and organization. Nat Rev Mol Cell Biol 2022;**23**(6):407-27 doi: 10.1038/s41580-022-00452-3 [published Online First: 20220228].

70. Kaczmarczyk A, Allahverdi A, Brouwer TB, Nordenskiold L, Dekker NH, van Noort J. Single-molecule force spectroscopy on histone H4 tail-cross-linked chromatin reveals fiber folding. J Biol Chem 2017;**292**(42):17506-13 doi: 10.1074/jbc.M117.791830 [published Online First: 20170830].

71. Mihardja S, Spakowitz AJ, Zhang Y, Bustamante C. Effect of force on mononucleosomal dynamics. Proc Natl Acad Sci U S A 2006;**103**(43):15871-6 doi: 10.1073/pnas.0607526103 [published Online First: 20061016].

72. Higgins NP, Vologodskii AV. Topological Behavior of Plasmid DNA. Microbiol Spectr 2015;**3**(2) doi: 10.1128/microbiolspec.PLAS-0036-2014.

73. Muskhelishvili G, Travers A. The regulatory role of DNA supercoiling in nucleoprotein complex assembly and genetic activity. Biophys Rev 2016;**8**(Suppl 1):5-22 doi: 10.1007/s12551-016-0237-3 [published Online First: 20161119].

74. Verma SC, Qian Z, Adhya SL. Architecture of the Escherichia coli nucleoid. PLoS Genet 2019;**15**(12):e1008456 doi: 10.1371/journal.pgen.1008456 [published Online First: 20191212].

75. Bettotti P, Visone V, Lunelli L, Perugino G, Ciaramella M, Valenti A. Structure and Properties of DNA Molecules Over The Full Range of Biologically Relevant Supercoiling States. Sci Rep 2018;**8**(1):6163 doi: 10.1038/s41598-018-24499-5 [published Online First: 20180418].

76. Deweese JE, Osheroff MA, Osheroff N. DNA Topology and Topoisomerases: Teaching a "Knotty" Subject. Biochem Mol Biol Educ 2008;**37**(1):2-10 doi: 10.1002/bmb.20244.

77. Sogo JM, Stahl H, Koller T, Knippers R. Structure of replicating simian virus 40 minichromosomes. The replication fork, core histone segregation and terminal structures. J Mol Biol 1986;**189**(1):189-204 doi: 10.1016/0022-2836(86)90390-6.

78. Kouzine F, Gupta A, Baranello L, et al. Transcription-dependent dynamic supercoiling is a short-range genomic force. Nat Struct Mol Biol 2013;**20**(3):396-403 doi: 10.1038/nsmb.2517 [published Online First: 20130217].

79. Yu H, Droge P. Replication-induced supercoiling: a neglected DNA transaction regulator? Trends Biochem Sci 2014;**39**(5):219-20 doi: 10.1016/j.tibs.2014.02.009 [published Online First: 20140314].

80. Gartenberg MR, Wang JC. Positive supercoiling of DNA greatly diminishes mRNA synthesis in yeast. Proc Natl Acad Sci U S A 1992;**89**(23):11461-5 doi: 10.1073/pnas.89.23.11461.

81. Racko D, Benedetti F, Dorier J, Stasiak A. Transcription-induced supercoiling as the driving force of chromatin loop extrusion during formation of TADs in interphase chromosomes. Nucleic Acids Res 2018;**46**(4):1648-60 doi: 10.1093/nar/gkx1123.

82. Kreienbaum C, Paasche LW, Hake SB. H2A.Z's 'social' network: functional partners of an enigmatic histone variant. Trends Biochem Sci 2022;**47**(11):909-20 doi: 10.1016/j.tibs.2022.04.014 [published Online First: 20220520].

83. Matsuda R, Hori T, Kitamura H, Takeuchi K, Fukagawa T, Harata M. Identification and characterization of the two isoforms of the vertebrate H2A.Z histone variant. Nucleic Acids Res 2010;**38**(13):4263-73 doi: 10.1093/nar/gkq171 [published Online First: 20100318].

84. Bonisch C, Schneider K, Punzeler S, et al. H2A.Z.2.2 is an alternatively spliced histone H2A.Z variant that causes severe nucleosome destabilization. Nucleic Acids Res 2012;**40**(13):5951-64 doi: 10.1093/nar/gks267 [published Online First: 20120329].

85. West MH, Bonner WM. Histone 2A, a heteromorphous family of eight protein species. Biochemistry 1980;**19**(14):3238-45 doi: 10.1021/bi00555a022.

86. Bonisch C, Hake SB. Histone H2A variants in nucleosomes and chromatin: more or less stable? Nucleic Acids Res 2012;**40**(21):10719-41 doi: 10.1093/nar/gks865 [published Online First: 20120921].

87. Lai WKM, Pugh BF. Understanding nucleosome dynamics and their links to gene expression and DNA replication. Nat Rev Mol Cell Biol 2017;**18**(9):548-62 doi: 10.1038/nrm.2017.47 [published Online First: 20170524].

88. Yin X, Zeng D, Liao Y, Tang C, Li Y. The Function of H2A Histone Variants and Their Roles in Diseases. Biomolecules 2024;**14**(8) doi: 10.3390/biom14080993 [published Online First: 20240812].

89. Park YJ, Dyer PN, Tremethick DJ, Luger K. A new fluorescence resonance energy transfer approach demonstrates that the histone variant H2AZ stabilizes the histone octamer within the nucleosome. J Biol Chem 2004;**279**(23):24274-82 doi: 10.1074/jbc.M313152200 [published Online First: 20040313].

90. Thambirajah AA, Dryhurst D, Ishibashi T, Li A, Maffey AH, Ausio J. H2A.Z stabilizes chromatin in a way that is dependent on core histone acetylation. J Biol Chem 2006;**281**(29):20036-44 doi: 10.1074/jbc.M601975200 [published Online First: 20060517].

91. Chen Z, Gabizon R, Brown AI, et al. High-resolution and high-accuracy topographic and transcriptional maps of the nucleosome barrier. Elife 2019;**8** doi: 10.7554/eLife.48281 [published Online First: 20190731].

92. Fan JY, Gordon F, Luger K, Hansen JC, Tremethick DJ. The essential histone variant H2A.Z regulates the equilibrium between different chromatin conformational states. Nat Struct Biol 2002;**9**(3):172-6 doi: 10.1038/nsb767.

93. Henikoff S. Labile H3.3+H2A.Z nucleosomes mark 'nucleosome-free regions'. Nat Genet 2009;**41**(8):865-6 doi: 10.1038/ng0809-865.

94. Jin C, Zang C, Wei G, et al. H3.3/H2A.Z double variant-containing nucleosomes mark 'nucleosome-free regions' of active promoters and other regulatory regions. Nat Genet 2009;**41**(8):941-5 doi: 10.1038/ng.409 [published Online First: 20090726].

95. Hu G, Cui K, Northrup D, et al. H2A.Z facilitates access of active and repressive complexes to chromatin in embryonic stem cell self-renewal and differentiation. Cell Stem Cell 2013;**12**(2):180-92 doi: 10.1016/j.stem.2012.11.003 [published Online First: 20121220].

96. Murphy KE, Meng FW, Makowski CE, Murphy PJ. Genome-wide chromatin accessibility is restricted by ANP32E. Nat Commun 2020;**11**(1):5063 doi: 10.1038/s41467-020-18821-x [published Online First: 20201008].

97. Wen Z, Zhang L, Ruan H, Li G. Histone variant H2A.Z regulates nucleosome unwrapping and CTCF binding in mouse ES cells. Nucleic Acids Res 2020;**48**(11):5939-52 doi: 10.1093/nar/gkaa360.

98. Cole L, Kurscheid S, Nekrasov M, et al. Multiple roles of H2A.Z in regulating promoter chromatin architecture in human cells. Nat Commun 2021;**12**(1):2524 doi: 10.1038/s41467-021-22688-x [published Online First: 20210505].

99. Sarcinella E, Zuzarte PC, Lau PN, Draker R, Cheung P. Monoubiquitylation of H2A.Z distinguishes its association with euchromatin or facultative heterochromatin. Mol Cell Biol 2007;**27**(18):6457-68 doi: 10.1128/MCB.00241-07 [published Online First: 20070716].

100. Ryan DP, Tremethick DJ. The interplay between H2A.Z and H3K9 methylation in regulating HP1alpha binding to linker histone-containing chromatin. Nucleic Acids Res 2018;**46**(18):9353-66 doi: 10.1093/nar/gky632.

101. Punzeler S, Link S, Wagner G, et al. Multivalent binding of PWWP2A to H2A.Z regulates mitosis and neural crest differentiation. EMBO J 2017;**36**(15):2263-79 doi: 10.15252/embj.201695757 [published Online First: 20170623].

102. Link S, Spitzer RMM, Sana M, et al. PWWP2A binds distinct chromatin moieties and interacts with an MTA1-specific core NuRD complex. Nat Commun 2018;**9**(1):4300 doi: 10.1038/s41467-018-06665-5 [published Online First: 20181016].

103. Mao Z, Pan L, Wang W, et al. Anp32e, a higher eukaryotic histone chaperone directs preferential recognition for H2A.Z. Cell Res 2014;**24**(4):389-99 doi: 10.1038/cr.2014.30 [published Online First: 20140311].

104. Alatwi HE, Downs JA. Removal of H2A.Z by INO80 promotes homologous recombination. EMBO Rep 2015;**16**(8):986-94 doi: 10.15252/embr.201540330 [published Online First: 20150703].

105. Malone HA, Roberts CWM. Chromatin remodellers as therapeutic targets. Nat Rev Drug Discov 2024;**23**(9):661-81 doi: 10.1038/s41573-024-00978-5 [published Online First: 20240716].

106. Jostes S, Vardabasso C, Dong J, et al. H2A.Z chaperones converge on E2F target genes for melanoma cell proliferation. Genes Dev 2024;**38**(7-8):336-53 doi: 10.1101/gad.351318.123 [published Online First: 20240521].

107. Faast R, Thonglairoam V, Schulz TC, et al. Histone variant H2A.Z is required for early mammalian development. Curr Biol 2001;**11**(15):1183-7 doi: 10.1016/s0960-9822(01)00329-3.

108. Jackson JD, Gorovsky MA. Histone H2A.Z has a conserved function that is distinct from that of the major H2A sequence variants. Nucleic Acids Res 2000;**28**(19):3811-6 doi: 10.1093/nar/28.19.3811.

109. Colino-Sanguino Y, Clark SJ, Valdes-Mora F. The H2A.Z-nucleosome code in mammals: emerging functions. Trends Genet 2022;**38**(5):516 doi: 10.1016/j.tig.2022.02.004 [published Online First: 20220226].

110. Diegmuller F, Leers J, Hake SB. The "Ins and Outs and What-Abouts" of H2A.Z: A tribute to C. David Allis. J Biol Chem 2025;**301**(2):108154 doi: 10.1016/j.jbc.2025.108154 [published Online First: 20250104].

111. Cheema MS, Good KV, Kim B, et al. Deciphering the Enigma of the Histone H2A.Z-1/H2A.Z-2 Isoforms: Novel Insights and Remaining Questions. Cells 2020;**9**(5) doi: 10.3390/cells9051167 [published Online First: 20200508].

112. Mylonas C, Lee C, Auld AL, Cisse, II, Boyer LA. A dual role for H2A.Z.1 in modulating the dynamics of RNA polymerase II initiation and elongation. Nat Struct Mol Biol 2021;**28**(5):435-42 doi: 10.1038/s41594-021-00589-3 [published Online First: 20210510].

113. Day DS, Zhang B, Stevens SM, et al. Comprehensive analysis of promoter-proximal RNA polymerase II pausing across mammalian cell types. Genome Biol 2016;**17**(1):120 doi: 10.1186/s13059-016-0984-2 [published Online First: 20160603].

114. Adelman K, Lis JT. Promoter-proximal pausing of RNA polymerase II: emerging roles in metazoans. Nat Rev Genet 2012;**13**(10):720-31 doi: 10.1038/nrg3293.

115. Skene PJ, Hernandez AE, Groudine M, Henikoff S. The nucleosomal barrier to promoter escape by RNA polymerase II is overcome by the chromatin remodeler Chd1. Elife 2014;**3**:e02042 doi: 10.7554/eLife.02042 [published Online First: 20140415].

116. Weber CM, Ramachandran S, Henikoff S. Nucleosomes are context-specific, H2A.Z-modulated barriers to RNA polymerase. Mol Cell 2014;**53**(5):819-30 doi: 10.1016/j.molcel.2014.02.014.

117. Brunelle M, Nordell Markovits A, Rodrigue S, Lupien M, Jacques PE, Gevry N. The histone variant H2A.Z is an important regulator of enhancer activity. Nucleic Acids Res 2015;**43**(20):9742-56 doi: 10.1093/nar/gkv825 [published Online First: 20150828].

118. Valdes-Mora F, Gould CM, Colino-Sanguino Y, et al. Acetylated histone variant H2A.Z is involved in the activation of neo-enhancers in prostate cancer. Nat Commun 2017;**8**(1):1346 doi: 10.1038/s41467-017-01393-8 [published Online First: 20171107].

119. Dalvai M, Bellucci L, Fleury L, Lavigne AC, Moutahir F, Bystricky K. H2A.Z-dependent crosstalk between enhancer and promoter regulates cyclin D1 expression. Oncogene 2013;**32**(36):4243-51 doi: 10.1038/onc.2012.442 [published Online First: 20121029].

120. Yang Y, Dai Z, Dai X. Insights into active intragenic enhancers. Biochem Biophys Res Commun 2019;**515**(3):423-28 doi: 10.1016/j.bbrc.2019.05.160 [published Online First: 20190531].

121. Dhillon N, Oki M, Szyjka SJ, Aparicio OM, Kamakaka RT. H2A.Z functions to regulate progression through the cell cycle. Mol Cell Biol 2006;**26**(2):489-501 doi: 10.1128/MCB.26.2.489-501.2006.

122. Tsai CH, Chen YJ, Yu CJ, et al. SMYD3-Mediated H2A.Z.1 Methylation Promotes Cell Cycle and Cancer Proliferation. Cancer Res 2016;**76**(20):6043-53 doi: 10.1158/0008-5472.CAN-16-0500 [published Online First: 20160828].

123. Vardabasso C, Gaspar-Maia A, Hasson D, et al. Histone Variant H2A.Z.2 Mediates Proliferation and Drug Sensitivity of Malignant Melanoma. Mol Cell 2015;**59**(1):75-88 doi: 10.1016/j.molcel.2015.05.009 [published Online First: 20150604].

124. Yang HD, Kim PJ, Eun JW, et al. Oncogenic potential of histone-variant H2A.Z.1 and its regulatory role in cell cycle and epithelial-mesenchymal transition in liver cancer. Oncotarget 2016;**7**(10):11412-23 doi: 10.18632/oncotarget.7194.

125. Long H, Zhang L, Lv M, et al. H2A.Z facilitates licensing and activation of early replication origins. Nature 2020;**577**(7791):576-81 doi: 10.1038/s41586-019-1877-9 [published Online First: 20191225].

126. Xu Y, Ayrapetov MK, Xu C, Gursoy-Yuzugullu O, Hu Y, Price BD. Histone H2A.Z controls a critical chromatin remodeling step required for DNA double-strand break repair. Mol Cell 2012;**48**(5):723-33 doi: 10.1016/j.molcel.2012.09.026 [published Online First: 20121030].

127. Gursoy-Yuzugullu O, Ayrapetov MK, Price BD. Histone chaperone Anp32e removes H2A.Z from DNA double-strand breaks and promotes nucleosome reorganization and DNA

repair. Proc Natl Acad Sci U S A 2015;**112**(24):7507-12 doi: 10.1073/pnas.1504868112 [published Online First: 20150601].

128. Banaszynski LA, Allis CD, Lewis PW. Histone variants in metazoan development. Dev Cell 2010;**19**(5):662-74 doi: 10.1016/j.devcel.2010.10.014.
129. Chang M, Sun L, Liu X, Sun W, You X. Association of common variants in H2AFZ gene with schizophrenia and cognitive function in patients with schizophrenia. J Hum Genet 2015;**60**(10):619-24 doi: 10.1038/jhg.2015.89 [published Online First: 20150806].
130. Gretzinger TL, Tyagi M, Fontaine CJ, et al. Fetal alcohol spectrum disorder (FASD) affects the hippocampal levels of histone variant H2A.Z-2. Biochem Cell Biol 2019;**97**(4):431-36 doi: 10.1139/bcb-2018-0240 [published Online First: 20190103].
131. Shen T, Ji F, Wang Y, Lei X, Zhang D, Jiao J. Brain-specific deletion of histone variant H2A.z results in cortical neurogenesis defects and neurodevelopmental disorder. Nucleic Acids Res 2018;**46**(5):2290-307 doi: 10.1093/nar/gkx1295.
132. Su L, Xia W, Shen T, et al. H2A.Z.1 crosstalk with H3K56-acetylation controls gliogenesis through the transcription of folate receptor. Nucleic Acids Res 2018;**46**(17):8817-31 doi: 10.1093/nar/gky585.
133. Stefanelli G, Makowski CE, Brimble MA, et al. The histone chaperone Anp32e regulates memory formation, transcription, and dendritic morphology by regulating steady-state H2A.Z binding in neurons. Cell Rep 2021;**36**(7):109551 doi: 10.1016/j.celrep.2021.109551.
134. Buchanan L, Durand-Dubief M, Roguev A, et al. The Schizosaccharomyces pombe JmjC-protein, Msc1, prevents H2A.Z localization in centromeric and subtelomeric chromatin domains. PLoS Genet 2009;**5**(11):e1000726 doi: 10.1371/journal.pgen.1000726 [published Online First: 20091113].
135. Suto RK, Clarkson MJ, Tremethick DJ, Luger K. Crystal structure of a nucleosome core particle containing the variant histone H2A.Z. Nat Struct Biol 2000;**7**(12):1121-4 doi: 10.1038/81971.
136. Wang AY, Aristizabal MJ, Ryan C, Krogan NJ, Kobor MS. Key functional regions in the histone variant H2A.Z C-terminal docking domain. Mol Cell Biol 2011;**31**(18):3871-84 doi: 10.1128/MCB.05182-11 [published Online First: 20110726].

137. Schuldiner M, Collins SR, Thompson NJ, et al. Exploration of the function and organization of the yeast early secretory pathway through an epistatic miniarray profile. Cell 2005;**123**(3):507-19 doi: 10.1016/j.cell.2005.08.031.

138. Obri A, Ouararhni K, Papin C, et al. ANP32E is a histone chaperone that removes H2A.Z from chromatin. Nature 2014;**505**(7485):648-53 doi: 10.1038/nature12922 [published Online First: 20140122].

139. Wang Y, Liu S, Sun L, et al. Structural insights into histone chaperone Chz1-mediated H2A.Z recognition and histone replacement. PLoS Biol 2019;**17**(5):e3000277 doi: 10.1371/journal.pbio.3000277 [published Online First: 20190520].

140. Bosire R, Fadel L, Mocsar G, et al. Doxorubicin impacts chromatin binding of HMGB1, Histone H1 and retinoic acid receptor. Sci Rep 2022;**12**(1):8087 doi: 10.1038/s41598-022-11994-z [published Online First: 20220516].

141. Imre L, Niaki EF, Bosire R, et al. Nucleosome destabilization by polyamines. Arch Biochem Biophys 2022;**722**:109184 doi: 10.1016/j.abb.2022.109184 [published Online First: 20220405].

142. Imre L, Nanasi P, Jr., Benhamza I, et al. Epigenetic modulation via the C-terminal tail of H2A.Z. Nat Commun 2024;**15**(1):9171 doi: 10.1038/s41467-024-53514-9 [published Online First: 20241024].

143. Kimura H, Cook PR. Kinetics of core histones in living human cells: little exchange of H3 and H4 and some rapid exchange of H2B. J Cell Biol 2001;**153**(7):1341-53 doi: 10.1083/jcb.153.7.1341.

144. Vamosi G, Damjanovich S, Szollosi J, Vereb G. Measurement of molecular mobility with fluorescence correlation spectroscopy. Curr Protoc Cytom 2009;**Chapter 2**:Unit2 15 doi: 10.1002/0471142956.cy0215s50.

145. Widengren J, Rigler R, Mets U. Triplet-state monitoring by fluorescence correlation spectroscopy. J Fluoresc 1994;**4**(3):255-8 doi: 10.1007/BF01878460.

146. Widengren J, Rigler R. Fluorescence correlation spectroscopy as a tool to investigate chemical reactions in solutions and on cell surfaces. Cell Mol Biol (Noisy-le-grand) 1998;**44**(5):857-79.

147. Culbertson CT, Jacobson SC, Michael Ramsey J. Diffusion coefficient measurements in microfluidic devices. Talanta 2002;**56**(2):365-73 doi: 10.1016/s0039-9140(01)00602-6.

148. Kusakabe M, Oku H, Matsuda R, et al. Genetic complementation analysis showed distinct contributions of the N-terminal tail of H2A.Z to epigenetic regulations. Genes Cells 2016;**21**(2):122-35 doi: 10.1111/gtc.12327 [published Online First: 20160111].

149. Ueda H, Ou D, Endo T, Nagase H, Tomono K, Nagai T. Evaluation of a sulfobutyl ether beta-cyclodextrin as a solubilizing/stabilizing agent for several drugs. Drug Dev Ind Pharm 1998;**24**(9):863-7 doi: 10.3109/03639049809088532.

150. Petiti J, Revel L, Divieto C. Standard Operating Procedure to Optimize Resazurin-Based Viability Assays. Biosensors (Basel) 2024;**14**(4) doi: 10.3390/bios14040156 [published Online First: 20240326].

151. Olmsted J, 3rd, Kearns DR. Mechanism of ethidium bromide fluorescence enhancement on binding to nucleic acids. Biochemistry 1977;**16**(16):3647-54 doi: 10.1021/bi00635a022.

152. Ijas H, Shen B, Heuer-Jungemann A, et al. Unraveling the interaction between doxorubicin and DNA origami nanostructures for customizable chemotherapeutic drug release. Nucleic Acids Res 2021;**49**(6):3048-62 doi: 10.1093/nar/gkab097.

153. Yu Z, Spiegel J, Melidis L, et al. Chem-map profiles drug binding to chromatin in cells. Nat Biotechnol 2023;**41**(9):1265-71 doi: 10.1038/s41587-022-01636-0 [published Online First: 20230123].

154. Kolbeck PJ, Tisma M, Analikwu BT, Vanderlinden W, Dekker C, Lipfert J. Supercoiling-dependent DNA binding: quantitative modeling and applications to bulk and single-molecule experiments. Nucleic Acids Res 2024;**52**(1):59-72 doi: 10.1093/nar/gkad1055.

155. Neefjes J, Gurova K, Sarthy J, Szabo G, Henikoff S. Chromatin as an old and new anticancer target. Trends Cancer 2024;**10**(8):696-707 doi: 10.1016/j.trecan.2024.05.005 [published Online First: 20240601].

156. He H, Liu C, Wu Y, Zhang X, Fan J, Cao Y. A Multiscale Physiologically-Based Pharmacokinetic Model for Doxorubicin to Explore its Mechanisms of Cytotoxicity and Cardiotoxicity in Human Physiological Contexts. Pharm Res 2018;**35**(9):174 doi: 10.1007/s11095-018-2456-8 [published Online First: 20180709].

157. Harahap Y, Ardiningsih P, Corintias Winarti A, Purwanto DJ. Analysis of the Doxorubicin and Doxorubicinol in the Plasma of Breast Cancer Patients for Monitoring the Toxicity of Doxorubicin. Drug Des Devel Ther 2020;**14**:3469-75 doi: 10.2147/DDDT.S251144 [published Online First: 20200825].

158. Conley BA, Egorin MJ, Whitacre MY, Carter DC, Zuhowski EG, Van Echo DA. Phase I and pharmacokinetic trial of liposome-encapsulated doxorubicin. Cancer Chemother Pharmacol 1993;**33**(2):107-12 doi: 10.1007/BF00685327.

159. Benhamza I, Imre L, Yu Z, et al. H2A.Z-nucleosomes are stabilized by the superhelicity-dependent DNA binding of the C-terminal tail of the histone variant. Nucleus 2025;**16**(1):2557113 doi: 10.1080/19491034.2025.2557113 [published Online First: 20250909].

160. Smrek J, Garamella J, Robertson-Anderson R, Michieletto D. Topological tuning of DNA mobility in entangled solutions of supercoiled plasmids. Sci Adv 2021;**7**(20) doi: 10.1126/sciadv.abf9260 [published Online First: 20210512].

161. Chehrehasa F, Meedeniya AC, Dwyer P, Abrahamsen G, Mackay-Sim A. EdU, a new thymidine analogue for labelling proliferating cells in the nervous system. J Neurosci Methods 2009;**177**(1):122-30 doi: 10.1016/j.jneumeth.2008.10.006 [published Online First: 20081018].

162. Bohm V, Hieb AR, Andrews AJ, et al. Nucleosome accessibility governed by the dimer/tetramer interface. Nucleic Acids Res 2011;**39**(8):3093-102 doi: 10.1093/nar/gkq1279 [published Online First: 20101221].

163. McMurray CT, van Holde KE. Binding of ethidium to the nucleosome core particle. 1. Binding and dissociation reactions. Biochemistry 1991;**30**(23):5631-43 doi: 10.1021/bi00237a001.

164. Wu HY, Shyy SH, Wang JC, Liu LF. Transcription generates positively and negatively supercoiled domains in the template. Cell 1988;**53**(3):433-40 doi: 10.1016/0092-8674(88)90163-8.

165. Corless S, Gilbert N. Effects of DNA supercoiling on chromatin architecture. Biophys Rev 2016;**8**(Suppl 1):51-64 doi: 10.1007/s12551-016-0242-6 [published Online First: 20161114].

166. Kouzine F, Sanford S, Elisha-Feil Z, Levens D. The functional response of upstream DNA to dynamic supercoiling in vivo. Nat Struct Mol Biol 2008;**15**(2):146-54 doi: 10.1038/nsmb.1372 [published Online First: 20080113].

167. Ponne S, Chinnadurai RK, Kumar R, et al. PWWP2A/B: Prominent players in the proteomic landscape. Gene 2025;**942**:149245 doi: 10.1016/j.gene.2025.149245 [published Online First: 20250112].

AUTHORS CONTRIBUTION

Although the data obtained from the salt-elution format of QINESIn, which assesses intrinsic nucleosome stability, clearly demonstrated the effect of the H2A.Z C-terminal tail on nucleosome stability and nuclear architecture, these data (Dr. Laszlo Imre's work) were not entirely convincing as to the biological significance of the observations since the assay involved exposure of chromatin to high salt concentrations. Therefore, in my work I sought to examine whether this tail dependency persists under more physiological conditions. To this end, I employed an alternative approach, the intercalator-elution format of QINESIn, in which DNA intercalating agents such as EBr [151] and Dox challenge nucleosomal structure by altering DNA superhelicity, rather than disrupting ionic and hydrogen bonds with salt [154]. The intercalator-induced elution has been shown to be more sensitive than the salt-induced format of QINESIn [57], providing an independent and importantly, a biologically relevant means of assessing nucleosome stability.

Regarding the FCS studies, when the binding of C9 to reconstituted nucleosomes was tested, those data (Dr. Péter Nánási's work) revealed nucleosomal binding but no direct DNA binding. However, because linear DNA was used in those experiments ([142]; data not shown), an interaction between C9 and superhelical DNA could not be excluded.

The following figures were done by Dr. Laszlo Imre: Figure 10, Figure 13 (panels B, C, D, E), Figure 14, Fig 16 (Panels A, B).

ACKNOWLEDGEMENTS

A Ph.D. is the culmination of years of learning, passion, and persistence. It represents not only extensive study but also a profound journey of growth, discovery, patience, and transformation—a path that tested my limits and deepened my understanding of both knowledge and life. I am profoundly grateful to God for blessing me with health, strength, and grace that have sustained me through every stage of this work. Throughout this journey, I have been privileged to encounter many people whose guidance, and support have profoundly shaped my academic and personal growth. While it is impossible to name everyone, their contributions have left an indelible mark on this achievement.

I am deeply grateful to my supervisor, Prof. Gábor Szabó, for giving me the chance to join his lab. I greatly appreciate his invaluable guidance, availability, patience, and insight throughout this journey. My deep thanks also go to my co-supervisor, Dr. György Vámosi, for helping me understand and perform the biophysical techniques, as well as for his continuous support. Thank you both for believing in me and offering me this chance when opportunities were scarce — your support truly changed my path, and I will never forget that. I also would like to extend my sincere thanks to the Head of Department, Prof. Dr. Panyi György, for allowing me to pursue my Ph.D. studies in the Department of Biophysics and Cell Biology.

My sincere gratitude goes to my colleagues, Dr. László Imre, Dr. Péter Nánási, Dr. Rosevalentine Bosire, and Pialy Sen, from whom I learned many techniques and greatly benefited from their experience and insightful discussions. I also wish to express my deep appreciation to our lab assistant, Ms. Adél Nagy Vezendiné, for consistently providing all the reagents and cells needed for my experiments.

I also extend my gratitude to my beloved family. To my dear parents, my mother Louazna and my father Abdelhafid, for their prayers, support, and high expectations, which motivated me keep going in my academic journey. Special thanks to my dear husband, Dr. Abdennour**,** whose constant love, support, encouragement, and understanding have been my greatest strength. And to my little princess, my daughter Amira, for her love and positive energy that accompanied me each and every day of this journey. To my dear sisters, Fatima, Meriam, Zineb, Rahma, and Batoul; my dear brothers, Mohammed, Ramzi, and Abderahim; and my husband's family and parents, Nadia and Yassin, for their unwavering love, and encouragement.

I thank my friends who made my stay in Debrecen truly worthwhile: Sara, Bannen, Latifa, Razan, Zahra, Alaa, and Hiba, for being a family away from home. I am also grateful to my dear friends in Algeria, Imen, Somaya, Souad, Loubna, and Sakina—for their support across the distance.

I am immensely grateful to our collaborators who either shared their knowledge or materials to make my research complete. They include Dr. Katalin Tóth (DKFZ, Heidelberg), Dr. Masahiko Harata (Sendai, Japan), Zutao Yu (Cambridge University, UK)

I dedicate this work to the soul of my grandmother, Hania, who passed away during my Ph.D. journey and had been waiting for this moment—may she rest in paradise.

PUBLICATION LIST

UNIVERSITY AND NATIONAL LIBRARY
UNIVERSITY OF DEBRECEN
H-4002 Egyetem tér 1, Debrecen
Phone: +3652/410-443, email: publikaciok@lib.unideb.hu

Registry number: DEENK/558/2025.PL
Subject: PhD Publication List

Candidate: Ibtissem Benhamza
Doctoral School: Doctoral School of Molecular Cellular and Immune Biology

List of publications related to the dissertation

1. **Benhamza, I.**, Imre, L., Yu, Z., Nánási, P. P. i., Sen, P., Enyedi, K. N., Goda, K., Vámosi, G., Szabó, G.: H2A.Z-nucleosomes are stabilized by the superhelicity-dependent DNA binding of the C-terminal tail of the histone variant.
   Nucleus. 16 (1), 1-14, 2025.
   DOI: http://dx.doi.org/10.1080/19491034.2025.2557113
   IF: 4.5 (2024)
2. Imre, L., Nánási, P. P. i., **Benhamza, I.**, Enyedi, K. N., Mocsár, G., Bosire, R., Hegedűs, É., Niaki, E. F., Csóti, Á., Darula, Z., Csősz, É., Póliska, S., Scholtz, B., Mező, G., Bacsó, Z., Timmers, H. T. M., Kusakabe, M., Balázs, M., Vámosi, G., Ausio, J., Cheung, P., Tóth, K., Tremethick, D., Harata, M., Szabó, G.: Epigenetic modulation via the C-terminal tail of H2A.Z.
   Nat Comms. 15 (1), 1-21, 2024.
   DOI: http://dx.doi.org/10.1038/s41467-024-53514-9
   IF: 15.7

Total IF of journals (all publications): 20,2
Total IF of journals (publications related to the dissertation): 20,2

The Candidate's publication data submitted to the Tudóstér have been validated by DEENK on the basis of the Journal Citation Report (Impact Factor) database.

29 October, 2025

DEBRECENI EGYETEM * Egyetemi és Nemzeti Könyvtár *